Numerical Simulation of Hydrodynamic Forces on Riverine and Coastal Bridges Subjected to Extreme Weather Events

by

Fahad Pervaiz

Presented to the Faculty of the Graduate School of
The University of Texas at Arlington in Partial Fulfillment
of the Requirements for the Degree of

Doctor of Philosophy

The University of Texas at Arlington
December 2022

This dissertation is a dedication to my family, all the talented but striving individuals, and all the unaided flood victims.

Acknowledgments

I want to thank my supervising professor, Dr. Michelle A. Hummel, for constantly motivating and encouraging me and for her invaluable advice during my doctoral studies. I would like to thank my academic advisors, Dr. Habib Ahmari, Dr. Nick Fang, and Dr. Ankit Aggarwal, for their interest in my research and for taking the time to serve on my dissertation committee. I appreciate their time and work, especially for helping me recognize any blind spots I may have overlooked.

I also want to thank the Texas Department of Transportation (TxDOT) for supporting my doctoral studies through RTI 0-7068. I acknowledge the assistance UTA OIT and TACC support staff provided in running numerical simulations on the HPC. I especially want to thank Dr. Ajay B Harish from the University of Manchester and Dr. Kuanshi Zhong from Stanford University for their interest in my research and for sharing sample OpenFOAM and OpenSEES codes for CFD and structural response modeling, as well as for the helpful conversations and invaluable remarks. I would also like to thank Dr. Sangri-Yi from UC Berkeley for her time and help in running quoFEM and OpenSEES. I thank Imran Kabir and Max Dean from Dr. Habib Ahmari's research group for sharing their experimental datasets. I also want to thank Dr. Simon Chao and Bhupendra Raj Acharya for their insightful conversations and for providing bridge drawings for numerical modeling.

I also want to thank my colleagues Klaus, Nahal, Kasra, Arif, Junaid, Hussain, Hasnain, Farhad, and Saman for our time together. For the little things which helped throughout the courses and semester projects. I am grateful to all the teachers who taught me during my years in school, first in Pakistan, then in Netherlands and Norway, and finally in the United States.

Finally, I want to express my deep gratitude to my mother and wife for their sacrifice, encouragement, and patience.

December 7, 2022

Abstract

Numerical Simulation of Hydrodynamic Forces on Riverine and Coastal Bridges Subjected to Extreme Weather Events

Fahad Pervaiz, Ph.D.

The University of Texas at Arlington, 2022

Supervising Professor: Michelle A. Hummel

Recent bridge failures due to hurricane-generated storm surges and riverine flood events have highlighted the vulnerability of bridge infrastructure to extreme hydrodynamic loading. In addition to posing an immediate risk to human life, bridge failures can hinder evacuation planning and emergency response efforts. Changes in flood frequency and intensity due to climate change and urbanization may alter the hydrodynamic conditions along urban streams, further stressing bridge infrastructure designed based on historical flow conditions. As a result, quantifying the structural response and stability of bridges under current and future hydrodynamic conditions is crucial to improving transportation safety and efficiency.

This dissertation advances the transportation community's research needs by developing validated computational frameworks to improve the assessment of hydrodynamic impacts on bridges in riverine and coastal areas. In particular, the presented research evaluates the impacts of climate change and urbanization on bridge vulnerability to riverine flood events to support regional transportation asset management; quantifies hydrodynamic loading conditions on a range of bridge superstructures to inform the design of failure

countermeasures; and develops a probabilistic framework that combines hydrodynamic modeling, structural analysis, and uncertainty quantification to improve risk assessment of coastal bridges subjected to surge and wave loading. These contributions are critical in the design and evaluation of safe and cost-effective bridge structures.

The vulnerability of bridge infrastructure to riverine flood events is projected to increase due to changes in precipitation intensity and land use. Most previous assessments of changing vulnerability to high-flow events use empirical hydrologic approaches with simplifying assumptions about bridge and channel geometry. They do not model local hydraulic conditions experienced by bridges or consider spatially explicit projections of land use change. The first part of this dissertation improves upon these past studies by developing a physically-based, spatially-explicit framework to evaluate the impacts of urbanization and climate change on bridges. The framework combines future precipitation and land use projections with hydrologic and hydraulic modeling to simulate water surface elevations and velocities at stream-crossing bridges, allowing for a location-specific estimate of flow conditions. The framework is applied to bridges in Harris County, Texas, to assess the vulnerability of regional bridge infrastructure to high-flow events and to prioritize maintenance, retrofitting, and replacement efforts. The findings highlight the importance of applying hydraulic models that incorporate channel and bridge geometry, as hydrologic modeling alone cannot accurately predict impacts on bridges.

Following the quantification of flow conditions (e.g., water surface elevation and velocity) at riverine bridges, formal assessment of the resulting hydrodynamic loading on bridge structures is needed to determine the potential for failure. In previous studies, the stability of bridges during flood events has been studied using scaled physical experiments and numerical modeling. However, these studies are typically limited to a constrained set of bridge geometries due to cost and time restrictions, and no studies have applied numerical simulations on full-scale bridges to investigate the scaling impacts. The second

part of this dissertation applies scaled and full-scale computational fluid dynamics (CFD) modeling to calculate hydrodynamic forces on typical Texas Department of Transportation bridge superstructures and to evaluate potential scaling effects. The results allow for an assessment of how hydrodynamic loads vary with inundation depth, flow velocity, and bridge geometry and can be used to determine the resisting details necessary to ensure adequate bridge performance for flood-durable designs.

Bridges located in coastal areas may be subjected to waves and surges during coastal storm events. Despite this recognized vulnerability, there is not yet a comprehensive and computationally efficient tool to evaluate hydrodynamic loading and structural response of bridges during coastal storm events while also accounting for uncertainty. The third part of this dissertation investigates surge and wave loading on coastal bridges and develops fragility curves to inform probabilistic bridge failure during hurricane events. The developed framework couples CFD modeling of hydrodynamic loading using wave conditions observed during Hurricane Ike, finite element modeling (FEM) of bridge structural response, and quantification of uncertainty in structural response based on variations in hydrodynamic conditions and material properties. The findings highlight the hydrodynamic conditions and material properties that most significantly influence bridge stability and can thus aid in determining potential bridge vulnerability during hurricane hazards.

Overall, these analyses provide critical information about the flow conditions affecting bridges, the resulting hydrodynamic forces experienced by bridge structures, and the implications for bridge reliability in riverine and coastal systems. The findings of this study can be used to design bridges to withstand adverse hydrodynamic forces and overturning moments during extreme weather events, as well as to determine whether current design standards for bridges are adequate or may require improvement.

Table of Contents

List of Figures

List of Tables

CHAPTER 1

Introduction

Flooding is a severe hazard to communities worldwide, causing loss of life, damage to homes and businesses, and disruptions to major infrastructure systems [8, 9]. In the U.S. alone, 36 billion-dollar flood events with damages over $1 billion occurred between 1980 and 2021, causing approximately $168 billion in total damages [10]. The potential implications on critical infrastructure systems, such as transportation networks that connect our communities and offer access and evacuation routes in times of emergency, are particularly concerning. Bridges that span rivers or coastal embayments may be more vulnerable to damage and failure due to their proximity to flood hazard zones [11, 12]. Hence, quantifying a bridge's exposure, structural response, and stability during and after flooding events is essential to ensuring roadway safety [13, 14].

1.1 Bridge Infrastructure Vulnerability

Bridges are an important part of the nation's transportation network. There are over 600,000 bridges in the U.S., of which 80% span inland and coastal waterways [15, 16]. Bridge failure during flood events may occur for multiple reasons, including (1) high-velocity flows that cause scouring upstream of bridge piers, which can compromise the integrity of the foundation, (2) excessive loading due to high riverine water levels, turbulent flows, and debris, which can cause partial displacement, shearing, or overturning of the bridge deck, and (3) wave-induced loading on bridge decks that can exceed the bridge capacity, resulting in unseating of the deck [17, 18]. Local flow conditions and bridge geometry both influence the severity of these effects.

In recent decades, several notable bridge failures have occurred in the U.S. In 1994, approximately 500 bridges in Georgia were damaged due to scouring and overtopping during Tropical Storm Alberto [19, 20]. In 2005, Hurricane Katrina and its associated storm surge caused damage to approximately 45 bridges in Alabama, Louisiana, and Mississippi, including the Interstate 10 (I-10) bridge over Lake Pontchartrain in Louisiana and the US-90 bridge over Bay St. Louis in Mississippi [21]. The subsequent repairs for the I-10 bridge took 20 days and required a total investment of $5.8 million [21]. The US-90 bridge experienced such extensive damage that it required complete replacement, costing an estimated $267 million [22]. Several years later, during Hurricane Ike in 2008, 53 bridges were damaged due to hydraulic-induced failures. Rollover Pass Bridge at Bolivar Peninsula near Galveston, Texas, collapsed due to a 15-ft storm surge and 5-ft waves. Emergency repairs were completed in six days following the event and cost $6.5 million [23]. More recently, bridges over the Blanco and Llano Rivers in Texas collapsed during flood events in 2015 and 2018, respectively [24]. Reported reconstruction costs were $17.3 million for the Llano River bridge [25] and $900,000 for the Blanco River bridge [26].

As these events highlight, bridge damage or failure requires a substantial investment for repair and replacement and can lead to extended disruptions to the transportation network. Thus, there is a critical need to better understand the hydrodynamic loads experienced by bridges during flood events to improve the assessment of failure mechanisms and to inform the design of countermeasures that enhance bridge safety and reliability [24, 27, 23, 28].

1.2 Changing Future Conditions

The frequency and severity of flood events are projected to increase in many areas in the future due to the effects of climate change [29, 30, 31]. As the atmosphere warms, the water vapor capacity of the air increases. Air with higher moisture content can produce

more intense precipitation when a storm system forms [32, 33]. Global climate models indicate that, across the U.S., extreme precipitation events with a return period of five years or higher are projected to be two to three times more likely by the end of the century [34]. Rainfall associated with hurricanes, which are often the drivers of the most extreme precipitation along the Gulf and Southeast Atlantic coasts, is also projected to intensify by 8–17% in the 21st century [34]. Since 1979, the probability of a tropical cyclone becoming a major hurricane (category three or higher) has increased globally by approximately 8% every decade [35]. A study of Hurricane Harvey, which made landfall in Texas in August 2017, found that the observed precipitation had a 1% probability of occurrence in the historical period (1981–2000) compared to a 6% probability in 2017 [36]. The study further concluded that the probability of occurrence would increase to 18% by the end of the century due to human-caused climate change.

At the same time that extreme precipitation is intensifying, urbanization and expanding development in many communities are increasing the imperviousness of inland and coastal watersheds [37], leading to reduced infiltration capacity and increased runoff to streams [38, 39]. According to the U.S. Census Bureau, the population of the United States expanded from 148 to 338 million between 1950 and 2022, and it is expected to increase to 458 million by 2050 [4]. This population increase is likely to result in even more impervious surfaces unless significant policy changes related to land use, development density, and stormwater management are implemented [40, 41]. Ultimately, more intense precipitation and expanding urbanization may produce higher water levels and velocities in waterways, posing a threat to riverine and coastal bridges and increasing the vulnerability of the nation's transportation infrastructure.

1.3 Research Questions

This dissertation aims to improve the prediction of the potential magnitude of hydrodynamic forces on bridges during extreme events to support design, maintenance, and retrofitting efforts that reduce future bridge failures. To accomplish this, the following research questions are explored:

- How will peak flows and hydraulic conditions experienced by bridges change over this century due to urbanization and climate change?
- What are the critical hydrodynamic conditions that can cause bridge failures during flood events?
- How do time-varying hydrodynamic conditions and uncertainties in material parameters affect risk assessment for bridges subjected to coastal storm events?

1.4 Approach and Methods

To address these research questions, hydrologic and hydraulic models (i.e., HEC-HMS and HEC-RAS) were used in combination with geospatial tools to quantify flow conditions at stream-crossing bridges under current and future scenarios that included projected changes in land use and precipitation intensity. Commercial and open-source computational fluid dynamics (CFD) modeling solvers (i.e., ANSYS Fluent and OpenFOAM) were used to compute the resulting hydrodynamic forces on bridge structures based on modeled flow conditions. A finite element model (FEM), OpenSEES, was used to simulate bridge response to hydrodynamic loading. Statistical models, including quoFEM and Sofixtic, were used to conduct a reliability analysis of coastal bridges subjected to surge and wave loading. The analysis frameworks developed in this dissertation provide a comprehensive set of tools to evaluate bridge vulnerability and response under extreme hydrodynamic loading and can be applied to any transportation system where adequate data is available to characterize local flow conditions and the existing bridge inventory.

1.5 Dissertation Outline

Chapter 2 of this dissertation analyzes current and future riverine flow parameters in watersheds in Harris County, Texas, by applying hydrologic and hydraulic modeling. Outputs from the models are used to evaluate how bridge vulnerability to extreme hydrodynamic conditions may change due to climate change and urbanization. The developed framework can be used to prioritize bridges for maintenance, retrofit, or replacement. Results from this chapter inform the numerical modeling of hydrodynamic forces on bridges (Chapter 3).

Chapter 3 quantifies the magnitude of hydrodynamic forces on bridge decks under a range of flow conditions using CFD modeling and evaluates the feasibility of using scaled-model experiments to predict conditions at full-scale bridges using similitude theory. Flow parameters are extracted from the hydrologic and hydraulic modeling from Chapter 2 and are representative of flow conditions in the vicinity of bridge structures in Texas. The results can be used to assess the effectiveness of the Texas Department of Transportation's current countermeasures (e.g., shear keys and ear walls) for resisting hydrodynamic forces and overturning moments during floods. The results can also inform decision making and improve bridge infrastructure design and construction to withstand flood impacts, protect public safety, and reduce flood-related economic and societal impacts.

Chapter 4 assesses probabilistic failure risk for coastal bridges subjected to surge and wave loading through the application of an integrated modeling framework that couples hydrodynamic modeling of coastal water levels and velocities, CFD modeling of resulting forces, and finite element modeling of structural response. The integrated framework also allows for incorporating uncertainty in hazard magnitude and bridge material properties when determining structural response. The results provide insight into parameters that most strongly influence bridge failure and should thus be carefully considered in bridge vulnerability analysis.

Finally, Chapter 5 summarizes the conclusions of this dissertation and discusses the implications for bridge vulnerability assessment and transportation planning.

CHAPTER 2

Effects of Climate Change and Urbanization on Bridge Flood Vulnerability: A Regional Assessment for Harris County, Texas

2.1 Abstract

The failure of stream-crossing bridges during flood events can endanger human life, impede evacuation planning and emergency response efforts, and cause long-term disruptions to transportation systems and local and regional economies. Expanding urban development and changing precipitation patterns due to climate change can increase the frequency and intensity of high-flow conditions at bridge locations, potentially exacerbating flood-related damages. Thus, there is a critical need to evaluate how shifts in extreme precipitation and continued urban growth will affect peak flows and hydraulic conditions experienced by bridges. This study applies hydrologic and hydraulic modeling to investigate the individual and combined effects of climate change and urbanization on the magnitude of peak discharge, bridge freeboard encroachment, and flow velocity at stream-crossing bridge locations in 19 watersheds of Harris County, Texas. The developed framework provides a screening tool to assess the vulnerability of regional bridge infrastructure to high-flow events and to prioritize maintenance, retrofitting, and replacement efforts. The model results demonstrate that peak flows during a 2% annual exceedance probability event can increase by up to 43% by 2100 when considering the combined impacts of climate change and urbanization, with changes in precipitation generally contributing more than changes in land use. In 16 of the 19 studied watersheds, the 1% annual exceedance probability event is projected to occur at least twice as frequently by 2100. Across the region, an additional 43 bridges experience loss of freeboard due to the effects of urbanization

and climate change, while notable increases in flow velocity ($\geq$10%) are observed at 107 bridge locations, nine of which are considered scour critical. Overall, the results of this study show that climate change and urbanization will influence the hydraulic conditions at bridge locations and, therefore, should be carefully accounted for in the design, operation, and maintenance of bridge infrastructure in the future.

2.2 Introduction

Flooding poses a serious threat to communities across the globe, leading to loss of life, damage to homes and businesses, and disruptions to critical infrastructure systems. In the U.S. alone, 36 flood events with damages over $1 billion occurred between 1980 and 2021, causing approximately $168 billion in total damages [10]. Rainfall intensity is projected to increase in many locations in the future [42, 43], which could exacerbate flooding issues in areas with aging stormwater infrastructure designed based on historical data [44]. In addition, urbanization and expanding development in floodplains have increased the exposure of people and infrastructure, leading to greater potential for damage [37]. New development often results in the loss of pervious surfaces, which reduces the infiltration capacity of land areas and can lead to increased runoff to streams, further exacerbating flooding [38, 39].

Riverine flooding is a particular concern for stream-crossing roadway bridges [45, 46], which comprise an important part of the surface transportation network. High riverine water levels can overtop bridge decks, leading to inundation of the roadway and temporary loss of serviceability [47]. Excessive hydraulic loading due to elevated water levels and velocities can compromise the structural integrity of bridges and may lead to bridge collapse, posing a threat to personal safety and resulting in extended disruptions to personal and commercial mobility [17, 48]. Bridge overtopping or failure can also hinder evacuation and emergency response efforts during extreme events [49]. Recent flood events have

highlighted this vulnerability [50], including storms in 2015 and 2018 that caused bridge collapses in Texas over the Blanco and Llano Rivers, respectively [24].

Past studies have suggested that impacts to bridge infrastructure due to urbanization and more intense rainfall could be substantial. In a national-scale study of bridge vulnerability to climate change, [51] applied an empirical rainfall-runoff model to determine peak flows in over 2,000 watersheds based on future precipitation projections derived from global climate models (GCMs). They estimated that more than 100,000 bridges in the U.S. could be vulnerable to climate change based on scour potential, with associated adaptation costs of $140 to $250 billion. In another study of bridge infrastructure in Montgomery County, Maryland, [52] used precipitation estimates from GCMs combined with an empirical hydrologic analysis to determine the change in return period of flows impacting bridges of various roadway classifications. They found that future changes in precipitation frequency will cause a reduction in the return period at which bridges are impacted, with local roads experiencing greater vulnerability than highways. While these and other past studies (e.g., [53, 54]) provide insight into the potential for future impacts on bridges, they generally apply top-down, empirical hydrologic approaches and make simplifying assumptions about bridge and channel geometry. They also do not consider spatially explicit projections of land use change. As a result, these analyses can be viewed as initial estimates of vulnerability but may not be sufficient to inform local-level risk assessments or adaptation planning efforts.

To address the need for locally relevant information on future bridge vulnerability to climate change and urbanization, this study develops a physically-based, spatially-explicit framework that combines projections of future precipitation and land use with hydrologic and hydraulic modeling to simulate water surface elevations and velocities at stream-crossing bridges in Harris County, Texas. Model outputs are used to assess the loss of freeboard (i.e., the clearance between a bridge's low chord elevation and the design flood

elevation) and increased scour potential at bridge locations under future scenarios. The results of this study allow for an evaluation of bridge susceptibility to flood impacts on a county-wide scale and highlight which drivers of future flood hazards are most critical. The framework presented here can be applied to other local or regional studies of bridge infrastructure to support transportation planning and design.

2.3 Study Area

Harris County is located along the Texas coast and is the third-most populous and one of the fastest growing counties in the U.S. [55]. Between 1990 and 2020, its population grew by 76%, spurring extensive new development, and the county is expected to experience future population growth of 59% over the next 30 years [4]. Approximately 7% of Texas' bridges are located in Harris County [5]. The area is vulnerable to both riverine and coastal flooding driven by intense, short-duration thunderstorms, slower-moving frontal systems, and tropical cyclones. Low topography, poorly-draining soils, and an extensive network of bayous and streams increase the risk of flooding for residents and critical infrastructure systems [56]. Observational data since 1880 reveals that rainfall intensity for the 1% annual exceedance probability (AEP) event has increased by 12–22% in the greater Houston area [57], and recent flood events have had devastating impacts in the county, such as those observed during Hurricanes Harvey and Ike [58, 59]. Various studies have projected continued increases in extreme precipitation intensity across parts of Texas [60, 61] and the Southern Great Plains [34]. Given the chronic flooding concerns faced by the region, as well as the projected increases in population and rainfall intensity, Harris County presents a valuable case study to examine future flood impacts on bridge infrastructure.

This study focuses on 19 Harris County watersheds (Figure 2.1) located within the Galveston Bay-San Jacinto hydrologic unit code (HUC) 4 subregion. The watersheds range in size from 39 km^2 to 1,000 km^2 and together are home to a population of 4.3 million

residents (Table 2.1) [3, 4]. Ten of the 19 watersheds are highly urbanized, with greater than 50% developed area. There are a total of 629 bridges along the main-stem rivers in these watersheds [5].

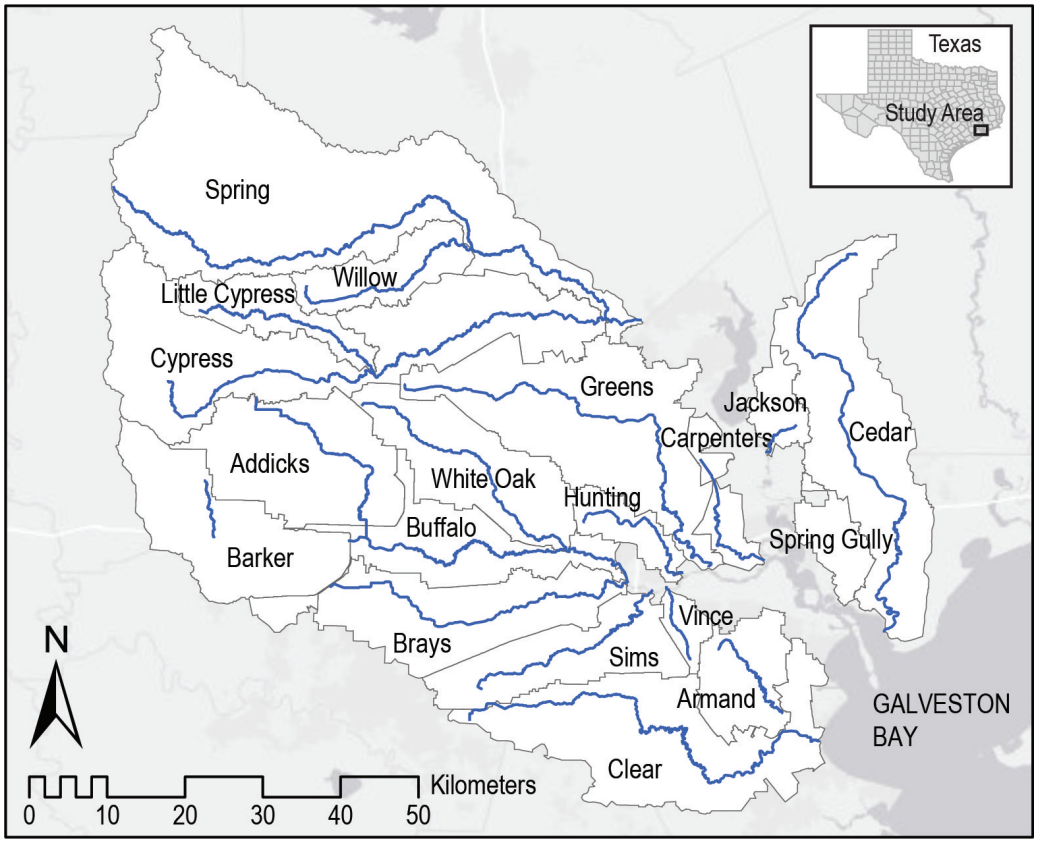

Fig. 2.1. Map of Harris County watersheds.

Table 2.1. Watersheds analyzed for this study along with their characteristics. Sources: [3, 4, 5].

Watershed	Area (km^2)	Population (1,000)	Total Bridges	Scour-Critical Bridges	Average ADT (1,000 vehicles/day)
Addicks Reservoir	360	390	14	-	5
Armand Bayou	153	133	7	-	9
Barker Reservoir	334	113	10	-	1
Brays Bayou	334	767	74	4	11
Buffalo Bayou	264	506	65	1	17
Carpenters Bayou	80	71	24	-	8
Cedar Bayou	515	43	14	-	1
Clear Creek	521	194	26	-	7
Cypress Creek	692	453	39	2	17
Greens Bayou	546	608	75	12	10
Hunting Bayou	80	76	53	-	9
Jackson Bayou	67	19	5	-	1
Little Cypress Creek	135	45	12	-	2
Sims Bayou	243	298	56	-	8
Spring Gully	85	66	18	-	5
Spring Creek	1,000	58	20	1	4
Vince Bayou	39	89	21	-	9
White Oak Bayou	287	465	76	5	10
Willow Creek	145	77	20	-	3

2.4 Methods

This section summarizes the approach for evaluating bridge vulnerability to loss of freeboard and scour due to high-flow events. The analysis framework is also illustrated in Figure 2.2. First, a hydrologic model was applied to estimate peak flows within each watershed. Before running the hydrologic model, the impact of urbanization was incorporated by adjusting the impervious area within each watershed based on current and projected future land use land cover (LULC). The effects of climate change were included by altering the magnitude of hourly rainfall depths based on projected changes in extreme precipitation. Peak discharges from the hydrologic model were then used as boundary conditions in a hydraulic model to simulate flow velocities and water surface elevations at bridge locations

within each watershed. This information was used to evaluate the vulnerability of Harris County bridges during high-flow events. The following subsections provide more details for each step.

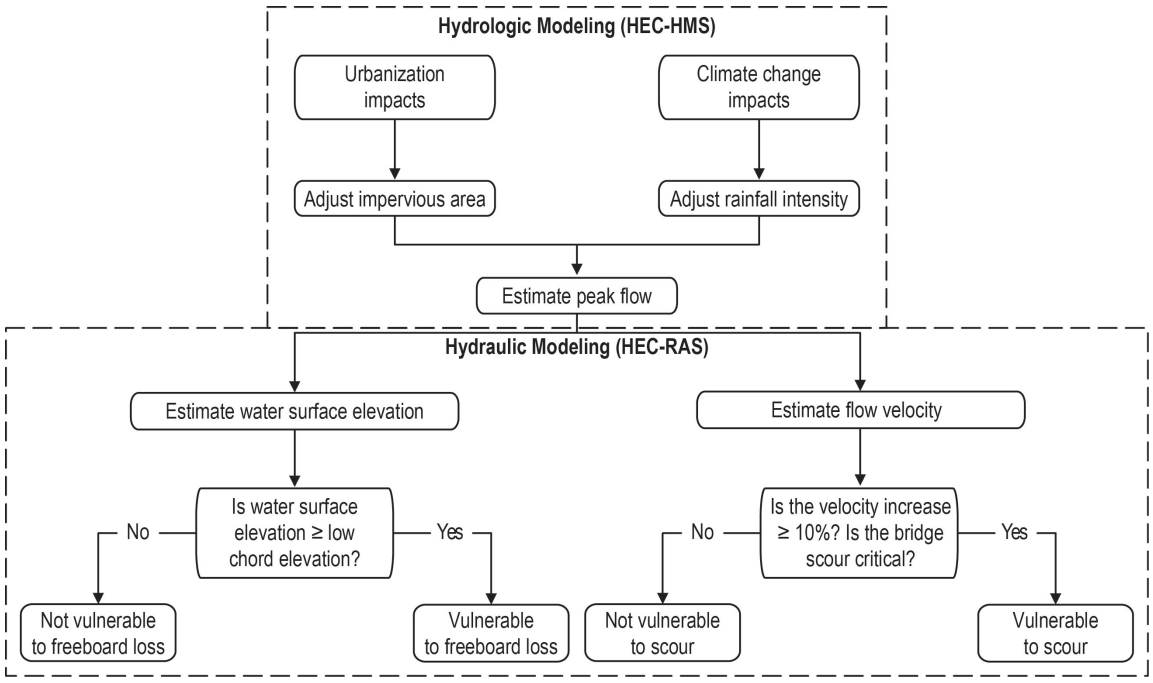

Fig. 2.2. Framework to evaluate bridge vulnerability due to high-flow events.

2.4.1 Data Acquisition

Spatially explicit, 250-m resolution projections of future LULC developed by the U.S. Geological Survey's FOREcasting SCEnarios of Land-use Change (FORE-SCE) modeling framework [1] were used to represent future urbanization in 2050 and 2100. These projections are based on A1B, A2, B1, and B2 emissions scenarios developed by the Intergovernmental Panel on Climate Change and used in their third and fourth assessment reports [62]. Example LULC maps for the A1B emissions scenario are shown in Figure 2.3. In these maps, all urban classes (i.e., low-intensity residential, high-intensity residential, recreational, commercial, industrial, and transportation) from the National

Land Cover Database were aggregated into one developed class [1], which was assumed to represent the percent imperviousness in each watershed. The maximum and minimum imperviousness projections in each watershed across the four emissions scenarios (Table 2.2) were used as upper and lower bounds for the urbanization analysis.

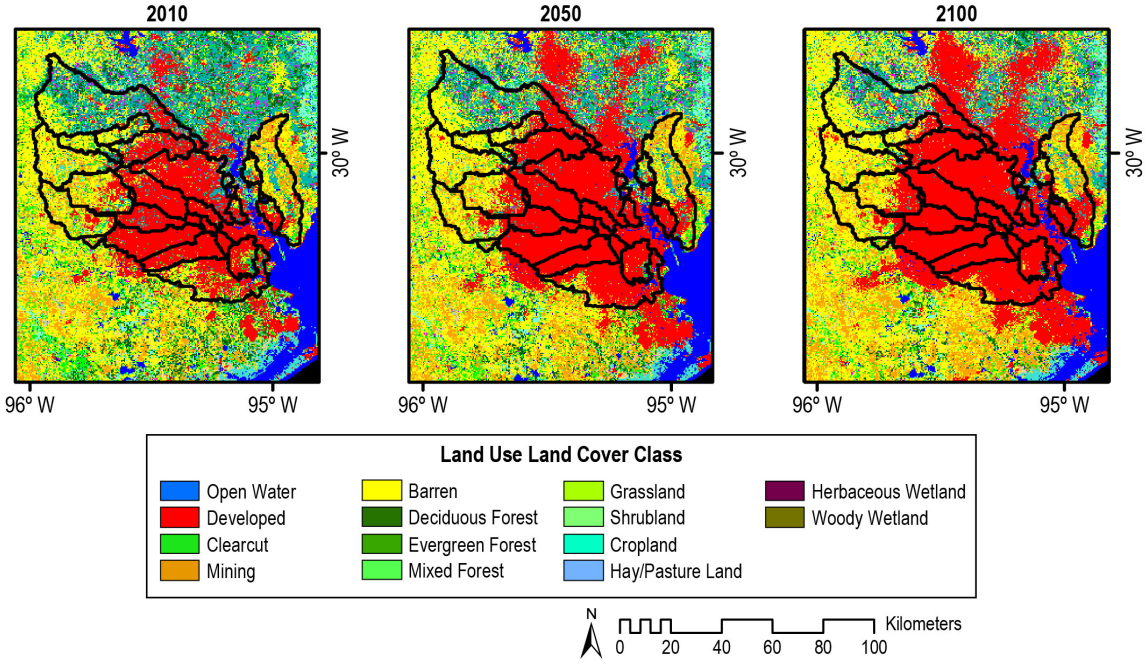

Fig. 2.3. Land use land cover projections for Harris County. Data used to generate the maps was obtained from [1].

Projections for the percent increase in daily 20-year extreme rainfall in the Southern Great Plains in 2050 and 2100 from [34] were used to represent the effects of climate change. These projections were developed by applying the LOcally Constructed Analogs (LOCA) approach to downscale GCM data [63]. Results from high and low emissions scenarios were used as upper and lower bounds for precipitation changes, resulting in increases of 9–13% in 2050 and 12–20% in 2100. These ranges were assumed to apply across three AEP rainfall events considered in this analysis: 2% AEP, 1% AEP, and 0.2% AEP.

Table 2.2. Imperviousness projections for Harris County watersheds. Source: [1].

Watershed	Imperviousness (%)					
	2010		2050		2100	
	Min	Max	Min	Max	Min	Max
Addicks	22	23	28	33	27	40
Armand	53	55	66	80	69	88
Barker	13	14	15	18	16	22
Brays	95	95	97	98	98	99
Buffalo	82	83	86	89	87	91
Carpenters	45	48	56	75	59	87
Cedar	8	9	10	17	11	25
Clear	53	55	66	80	69	88
Cypress	27	29	36	40	37	44
Greens	79	80	90	94	91	98
Hunting	94	95	98	99	98	99
Jackson	15	15	15	18	14	24
Little Cypress	4	4	5	6	9	11
Sims	92	92	97	99	98	100
Spring Gully	61	63	70	81	73	89
Spring	11	11	14	18	15	21
Vince	99	99	99	100	100	100
White Oak	88	89	93	97	94	99
Willow	11	12	21	32	23	42

13 scenarios were simulated to assess the individual and combined impacts of climate change and urbanization (Table 2.3). The base scenario (2010) consisted of existing LULC and historical rainfall intensities derived from the hydrologic models used for this study (see next section). Six mid-century (2050) scenarios were simulated based on the minimum and maximum changes in LULC (U^- and U^+), the minimum and maximum changes in rainfall intensity (P^- and P^+), and the combined minimum and maximum LULC and precipitation intensity (U^-P^- and U^+P^+). The same six scenarios were also simulated using LULC and precipitation projections for the end-of-century (2100) time frame.

Table 2.3. Scenarios considered for precipitation and urbanization analyses.

Year	Scenario	Precipitation Change (%)	LULC Change
2010	Base	-	-
2050	U^-	-	min
	U^+	-	max
	P^-	9	-
	P^+	13	-
	U^-P^-	9	min
	U^+P^+	13	max
2100	U^-	-	min
	U^+	-	max
	P^-	12	-
	P^+	20	-
	U^-P^-	12	min
	U^+P^+	20	max

2.4.2 Hydrologic and Hydraulic Modeling

Existing, calibrated hydrologic and hydraulic models were obtained from the Harris County Flood Control District (HCFCD) for the 19 watersheds considered in this study [3]. The models were developed as part of the Federal Emergency Management Agency's (FEMA) Flood Insurance Studies (FISs) to delineate floodplains and utilize the Hydrologic Engineering Center's Hydrological Modeling System (HEC-HMS) and River Analysis System (HEC-RAS) software.

The HCFCD HEC-HMS models for each watershed were used to determine the peak discharges for each scenario. The models included hydrologic elements (e.g., sub-basin, reach, junction, reservoir, diversion, source, and sink) and their connectivity to represent water movement through the watersheds [64]. The Green and Ampt loss method [65] was used to calculate rainfall losses from the sub-basins. The direct runoff from excess precipitation was calculated using the Clark unit hydrograph transform method [66], and the Modified Puls routing method [67, 68] was used to predict flow at the outlet. For this study, the effect of urbanization was modeled by changing the Green and Ampt impervious area at the sub-basin scale based on the FORE-SCE LULC maps. The effects of future

precipitation were modeled by increasing the hourly rainfall depth inputs by the percentages listed in Table 2.3.

The HCFCD HEC-RAS models were used to quantify flow depth and velocities at stream-crossing bridge locations. The models included detailed channel and bridge geometry and Manning's roughness values along the mainstem of the primary stream in each watershed [69]. For this study, peak discharges obtained from the HEC-HMS models for each scenario were assigned as discharge boundary conditions to represent upstream and tributary inflows in the HEC-RAS models. All models were run using steady flow analysis.

2.4.3 Bridge Vulnerability Assessment

At each of the 629 bridge locations across the 19 watersheds, the water surface elevation and flow velocity were extracted from the HEC-RAS models at the cross-section just upstream of the bridge. The water surface elevations were compared with the bridge low-chord elevations to evaluate vulnerability to loss of freeboard. Bridges were considered vulnerable if the water level was greater than or equal to the low-chord elevation, indicating the point when total loss of freeboard occurs and hydrodynamic forces begin to impact the bridge superstructure. Average daily traffic (ADT) counts for each bridge were extracted from the Texas Department of Transportation's (TxDOT) bridge inventory [5] to evaluate the criticality of impacted bridges based on traffic volumes. Three ADT categories are considered here: low (<1,000), moderate (1,000–5,000), and high (>5,000).

Flow velocities were compared between the future scenarios (2050 and 2100) and the 2010 scenario to calculate the percent change in velocity at each bridge location. In addition, scour ratings were extracted from TxDOT's bridge inventory [5]. Scour ratings range from 0–9, with ratings of 0–3 indicating major foundation exposure (scour critical), 4–5 indicating moderate foundation exposure, six indicating that no scour evaluation has

been conducted, and 7–9 indicating minimal foundation exposure. Scour ratings are based either on observed scour depths measured during physical inspections or on calculated scour depths determined through a scour analysis that accounts for flow velocities and water surface elevations during design floods (e.g., using the guidance in the Federal Highway Administration's (FHWA) Hydraulic Engineering Circular No. 18 or the TxDOT Scour Evaluation Guide) [70, 71]. For this study, bridges rated 0–3 that also experienced a flow velocity increase of ≥10% were identified as vulnerable due to the combined influence of pre-existing foundation exposure and higher flow velocities.

2.5 Results

The modeled changes in peak flow, freeboard loss, and flow velocity are presented below. The results for the 2% AEP are discussed throughout, as this is the event with the highest probability of occurrence of the three AEP events studied. Results for the 1% AEP and 0.2% AEP events are summarized in Appendix A.

2.5.1 Changes in Peak Flow

The percent increase in peak flow at the outlets of Harris County watersheds for the 2% AEP rainfall event is summarized in Figure 2.4. The results for the 1% and 0.2% AEP events are shown in Figures A.1 and A.2. Values shown are the averages of the minimum and maximum projections for the urbanization (U^- and U^+), precipitation (P^- and P^+), and combined (U^-P^- and U^+P^+) scenarios. At the county scale, peak flow increases by an average of 2% in 2050 and 3% in 2100 compared to 2010 under the urbanization scenario. The larger increase between 2010 and 2050 reflects that urbanization is projected to be more rapid in the first half of the century but slow after 2050. Willow Creek, which is minimally developed under the baseline scenario (Table 2.2) but is projected to experience a 10–20% increase in imperviousness concentrated near the downstream end of the watershed by 2050 (Figure 2.3) and an additional 2–10% increase by 2100, shows the most significant

increase in peak flow due to urbanization, ranging from 14% higher in 2050 to 19% higher in 2100. Other watersheds experience smaller increases in peak flow, with a maximum increase of 9% in Cypress Creek by 2100. As with Willow Creek, Cypress Creek has low imperviousness under the baseline scenario but is projected to see moderate increases in development (10–15%) by 2100, mostly near the watershed outlet. Several watersheds with low projected changes in imperviousness (≤10%), including Barker Reservoir, Brays Bayou, Vince Bayou, and White Oak Bayou, do not experience significant peak flow increases due to urbanization in 2050 or 2100.

For the precipitation scenario, peak flow increases by 11% in 2050 and 15% in 2100 on average across all watersheds. Little Cypress Creek, a headwater tributary of Cypress Creek, and Willow Creek, a headwater tributary of Spring Creek, experience the most significant changes in peak flow, increasing by 20% and 16%, respectively, in 2050 and 29% and 23%, respectively, in 2100. When urbanization and precipitation are combined, peak flow increases by 13% in 2050 and 18% in 2100 on average. Willow Creek, which experiences the largest increase in peak flow due to urbanization and the second largest increase due to precipitation, also experiences the most significant increase in peak flow under the combined scenario, increasing by 29% in 2050 and 43% in 2100. Increases in peak flow greater than 20% are also observed in Cypress Creek and Little Cypress Creek by 2050 and in Addicks Reservoir, Carpenters Bayou, and Clear Creek by 2100.

Changes in the magnitude and frequency of discharge events due to urbanization and precipitation can influence the adequacy and expected performance level of bridge infrastructure. For example, if a bridge is designed to pass a 2% AEP event based on historical observations, but the magnitude of the 2% AEP event continues to increase due to climate change, the bridge may no longer perform as desired. To assess the potential for changes in flood frequency in Harris County watersheds, the percent difference between the 2% AEP peak discharge in 2050 or 2100 and the 1% AEP peak discharge in 2010 was

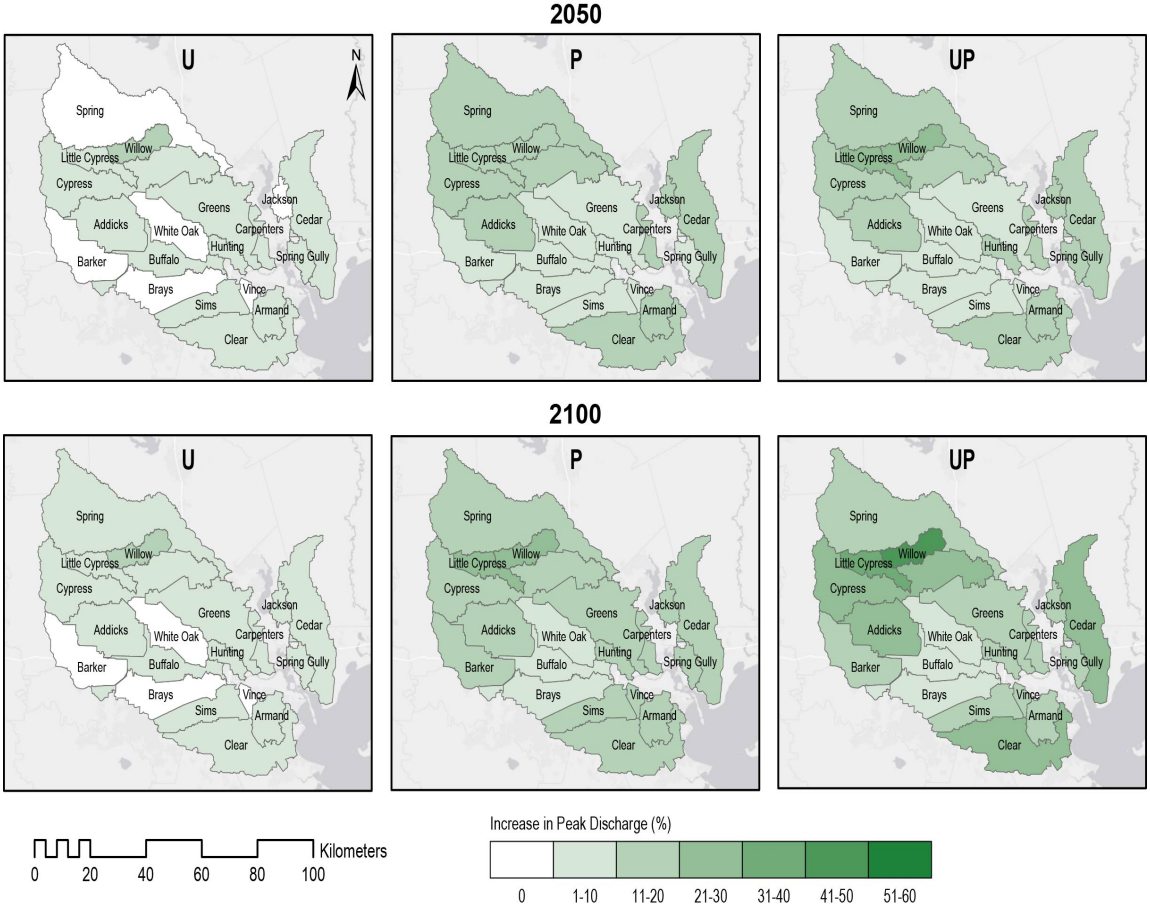

Fig. 2.4. Increase in peak discharge for 2% AEP event.

calculated for each scenario (Table 2.4). The values in the table show where the magnitude of the 2% AEP peak flow in 2050 or 2100 equals (zero values) or exceeds (positive values) the 1% AEP peak flow for the 2010 scenario. In 2050, this change in frequency occurs in Carpenters Bayou, Clear Creek, Cypress Creek, Hunting Bayou, and Willow Creek for the U^+P^+ scenario. In 2100, the U^+, P^+, U^-P^-, and U^+P^+ scenarios all cause increases in the 2% AEP magnitude that equal or exceed the 2010 1% AEP magnitude. This change in frequency occurs only for Willow Creek in the U^+ scenario and Willow Creek and Cypress Creek in the U^-P^- scenario. The impacts are most substantial for the P^+ and U^+P^+ scenarios, which affect 16 of the 19 watersheds. The largest impact is observed in Willow Creek,

where the magnitude of the 2% AEP peak discharge for the U^+P^+ scenario is 26% higher than the 1% AEP peak discharge for the 2010 scenario.

Table 2.4. Percent difference between 2050 or 2100 2% annual exceedance probability (AEP) peak discharge and 2010 1% AEP peak discharge.

Watershed	2050	2100			
	U^+P^+	U^+	P^+	U^-P^-	U^+P^+
Addicks	-	-	2	-	8
Armand	-	-	3	-	5
Barker	-	-	-	-	-
Brays	-	-	1	-	1
Buffalo	-	-	-	-	-
Carpenters	0	-	3	-	8
Cedar	-	-	1	-	7
Clear	1	-	3	-	9
Cypress	4	-	3	2	10
Greens	-	-	2	-	3
Hunting	0	-	3	-	5
Jackson	-	-	3	-	4
Little Cypress	-	-	1	-	5
Sims	-	-	2	-	3
Spring	-	-	-	-	-
Spring Gully	-	-	3	-	4
Vince	-	-	3	-	3
White Oak	-	-	1	-	2
Willow	10	2	3	3	26

2.5.2 Impacts on Bridges

Figure 2.5 shows the increase (referenced to the 2010 base scenario) in the number of bridges in each watershed that experience a complete loss of freeboard (i.e., water levels equal or exceed the bridge low chord elevation) for the 2% AEP event. The results for the 1% and 0.2% AEP events are shown in Figures A.3 and A.4. Overall, 233 bridges are susceptible to loss of freeboard under the 2010 base scenario. With urbanization, the number of vulnerable bridges increases by nine in 2050 and 11 in 2100. Urbanization

has the greatest impact in Buffalo Bayou, affecting three additional bridges, but it also impacts Carpenters Bayou, Clear Creek, Cypress Creek, and Greens Bayou. The effects of increased precipitation are larger and more widespread, causing 30 more bridges to become vulnerable in 2050 and 38 in 2100. These impacts are spread across 11 watersheds, with the largest impacts in Buffalo Bayou, Sims Bayou, and Vince Bayou. When combined, urbanization and precipitation result in 32 more vulnerable bridges in 2050 and 43 in 2100, impacting the same 11 watersheds as the precipitation-only scenarios. In 2050, Buffalo Bayou experiences the greatest increase in vulnerability, with seven additional bridges affected. By 2100, Sims Bayou is affected the most, with eight additional bridges impacted. Countywide, the increase in vulnerable bridges between 2010 and 2050 is three to five times greater than the subsequent increase from 2050 to 2100, reflecting the larger projected increases in urbanization and precipitation intensity in the first half of the century.

For all scenarios except the 2050 urbanization scenario, 50% or more of the additional bridges impacted by freeboard loss have high (>5,000) ADT (Table 2.5). 35–56% of bridges impacted under future scenarios have moderate (1,000–5,000) ADT and 0–13% have low (<1,000) ADT. However, the moderate ADT category experiences the highest percent increase in bridges vulnerable to freeboard loss, increasing from 52 to 67 bridges (29%) by 2100 for the combined urbanization and precipitation scenario, as compared to 15% for high ADT and 18% for low ADT.

Table 2.5. Number of bridges (2010) or increase in number of bridges (2050 and 2100) with loss of freeboard by average daily traffic (ADT) count.

Counts	2010	2050			2100		
	Baseline	U	P	UP	U	P	UP
<1000	28	0	3	4	0	4	5
1000-5000	52	5	12	12	5	14	15
>5000	153	4	15	16	6	20	23
Total	233	9	30	32	11	38	43

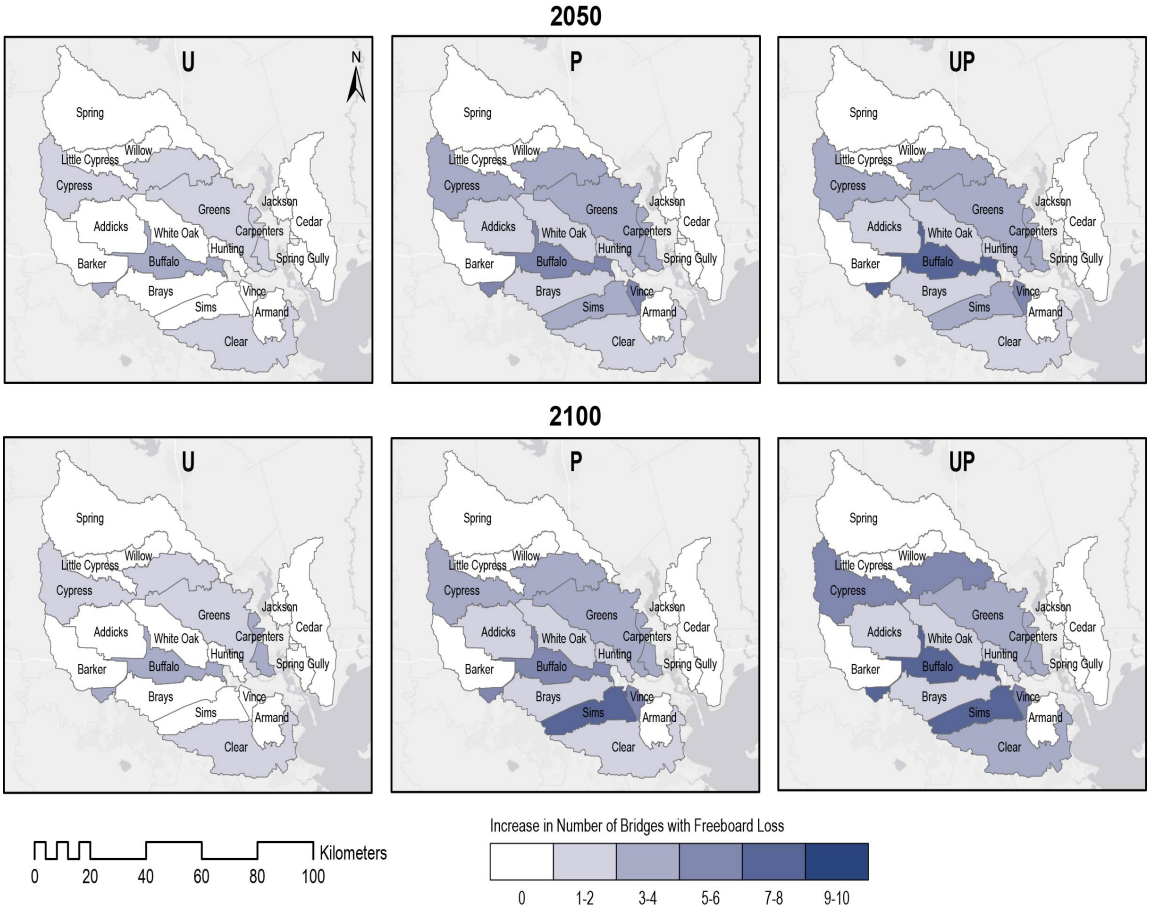

Fig. 2.5. Increase in number of bridges with freeboard loss for 2% AEP event.

An increase in flow velocity due to changes in discharge can also pose a risk to bridge structures, especially those that are classified as scour critical. The number of bridges in each watershed where velocity increases by ≥10% is shown for the 2% AEP event in Figure 2.6. The results for the 1% and 0.2% AEP events are shown in Figures A.5 and A.6. The scour ratings of bridges with ≥10% increase in velocity are summarized in Table 2.6, and the locations of scour-critical bridges (scour ratings 0–3) are also indicated in Figure 2.6. For the urbanization scenario, a total of four bridges in three different watersheds are impacted by a velocity increase ≥10% in 2050. These bridges are classified as having either minimal (scour ratings 7–9) or moderate (scour ratings 4–5) foundation exposure, but none

are scour critical. In 2100, 11 bridges are impacted due to urbanization, but again none are assessed as scour critical. Increased precipitation causes more widespread impacts, affecting a total of 43 bridges (three of which are scour critical) in 2050 and 90 bridges (seven of which are scour critical) in 2100. These impacts are noted across all watersheds except Hunting Bayou and Barker Reservoir. Cypress Creek and Buffalo Bayou see the largest impacts, with 16 and 15 bridges, respectively, experiencing a velocity increase of ≥10% by 2100. The combined scenario exhibits similar patterns as the precipitation-only scenario, with 66 bridges (five of which are scour critical) impacted in 2050 and 107 bridges (nine of which are scour critical) in 2100. Cypress Creek and Buffalo Bayou once again have the largest number of impacted bridges (20 each by 2100). For all scenarios except the 2050 urbanization scenario, the majority of bridges impacted by velocity increases ≥10% are rated as having moderate foundation exposure.

Table 2.6. Number of bridges (2010) or increase in number of bridges (2050 and 2100) by TxDOT scour rating.

Scour Rating	2010	2050			2100		
	Baseline	U	P	UP	U	P	UP
0–3	25	0	3	5	0	7	9
4–5	314	2	25	37	7	48	54
6	1	0	1	1	0	1	1
7–9	289	2	14	23	4	34	43
Total	629	4	43	66	11	90	107

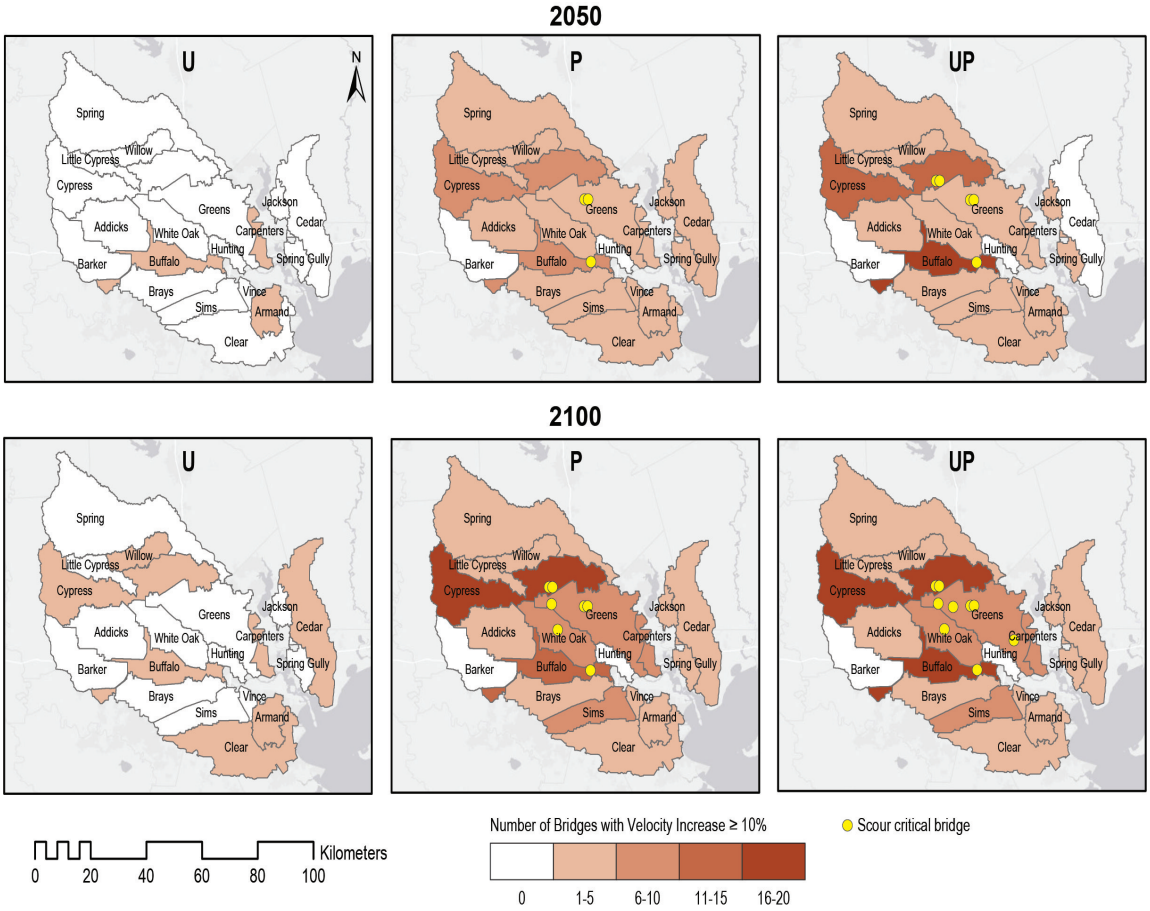

Fig. 2.6. Number of bridges with velocity increase ≥10% for 2% AEP event.

2.6 Discussion

The results of the hydrologic modeling indicate that the combined effects of urbanization and changes in precipitation intensity can lead to large increases (as high as 43%) in peak flows across Harris County watersheds. Six of the 19 watersheds experience an increase in peak flow of greater than 20% for the 2% AEP event. These six watersheds have low to moderate imperviousness (4–54%) under the 2010 baseline condition and experience moderate increases in imperviousness (6–25%) by 2100. However, the observed increase in peak flow magnitude is driven primarily by changes in extreme precipitation rather than changes in LULC. In fact, the average climate-driven increase in peak flow

is more than four times higher than the average increase due to urbanization. Variations in the magnitude of peak flow increases across watersheds may be driven by a variety of watershed characteristics, including the available storage area, topography, number of diversions, and spatial distribution of LULC.

In many Harris County watersheds, peak flows that previously occurred once every 100 years on average could occur at least twice as frequently by the end of the century. As the frequency and magnitude of peak flows change over the 21st century, bridges spanning waterways could experience flow events exceeding their hydraulic design criteria, potentially leading to an increased prevalence of flood-driven disruptions and unanticipated hydraulic loads. Given that the increases in peak flow and resulting impacts to bridges are generally greater from 2010 to 2050 than from 2050 to 2100, there is an immediate need to incorporate future projections into current transportation planning efforts to address potential impacts by mid-century.

By coupling hydrologic and hydraulic modeling, this analysis provides greater insight into potential mechanisms for bridge vulnerability than previous studies, which used peak flow increase as a proxy for vulnerability without considering local flow conditions at bridge locations (e.g., [51]). The importance of hydraulic modeling can be readily observed by comparing the spatial pattern of peak flow increases determined from hydrologic modeling (Figure 2.4) with the patterns of freeboard loss and velocity increases determined from hydraulic modeling (Figures 2.5 and 2.6). For example, although Willow Creek exhibits the largest increase in peak flow (43%) due to urbanization and increased precipitation by 2100, no additional bridges in the watershed experience loss of freeboard, and only two bridges (neither of which are considered scour critical) experience a velocity increase $\geq$10%. Thus, while flow increases are large, the existing bridge infrastructure appears to be adequate to handle the additional flow. In contrast, Buffalo Bayou experiences a more moderate increase in peak flow (9%), but this results in seven additional bridges experiencing loss

of freeboard and twenty bridges (one of which is scour critical) experiencing a velocity increase ≥10%. From a regional planning perspective, Buffalo Bayou, which has the highest average ADT among all watersheds, would thus be a higher priority for bridge vulnerability assessment than Willow Creek.

Changes in water levels due to increases in urbanization and precipitation intensity lead to a 14% increase in the number of bridges impacted by loss of freeboard for the 2% AEP event by 2050 and an 18% increase by 2100. Given that the majority of these bridges have high ADT, overtopping or structural damage due to hydraulic loading at these bridges could cause greater traffic disruptions due to their high usage. Even at low and moderate ADT bridges, which experience higher percent increases in freeboard loss, flood-related disruptions can cause delays and limit mobility, particularly if alternative routes are not available. Although beyond the scope of this study, dynamic traffic modeling could be applied in the future to assess how a disruption at one or multiple bridges would impact travel times and delays throughout the regional transportation network. Insights derived from such modeling could be especially applicable for emergency response or evacuation planning.

The findings of this study provide an initial assessment of locations where future changes in urbanization and precipitation may increase velocity and scour potential. Of the bridges that experience a velocity increase of ≥10% under the combined urbanization and precipitation scenario, 64% are rated as having major or moderate foundation exposure in 2050 and 59% in 2100. Existing issues with foundation exposure at these bridges could be exacerbated by higher-velocity flows and undermine bridge stability. Although a formal scour analysis would be needed to determine the critical velocity increase and resulting effects at each bridge location, the presented approach can be used to prioritize bridges for inspection and further evaluation, thus providing a useful screening tool for transportation managers. Future work could assess scour potential in more detail using guidance in

FWHA's Hydraulic Engineering Circular No. 18 or the TxDOT Scour Evaluation Guide [70, 71].

The presented framework for bridge vulnerability assessment can be utilized by agencies and jurisdictions responsible for managing transportation infrastructure, including TxDOT, Harris County, or the City of Houston, to identify potentially vulnerable bridges and prioritize mitigation activities. This framework is transferable to other jurisdictions where hydrologic and hydraulic models exist or can be developed, such as the many municipalities in the U.S. where FEMA floodplain studies have been conducted using such models. The input data required to analyze future scenarios of climate change and urbanization can leverage national-scale studies and datasets such as the ones used here, and bridge data can be extracted from the National Bridge Inventory [72] or state-specific datasets.

Several additional limitations could be addressed through follow-on studies. Although this study considered each watershed individually, changes observed in upstream watersheds can propagate downstream, potentially leading to larger increases in peak flows, water surface elevations, and velocities in other watersheds. The development of a combined model of interconnected watersheds would provide more insight into the propagation of upstream flood peaks and the resulting impacts on bridges downstream. Secondly, while this study quantifies water levels and velocities at bridge locations, it does not account for the structural condition of each bridge, which will ultimately determine the potential for failure during high-flow events. Once bridges are identified as being vulnerable to loss of freeboard or increased flow velocities using the presented approach, subsequent analyses of hydraulic loading and structural response could inform decisions about maintenance, retrofitting, or replacement.

2.7 Conclusions

This study presents a regional screening tool to assess the impacts of climate change and urbanization on stream-crossing bridges in Harris County, Texas. The framework improves upon previous studies by applying both hydrologic and hydraulic models to simulate local flow conditions at bridge locations based on meteorological inputs and land use in the contributing watersheds. The findings suggest that projected changes in precipitation have a larger impact on peak flows than projected changes in urbanization. In addition, bridge vulnerability to loss of freeboard or increased flow velocity due to higher peak flows is observed across all of the 19 watersheds studied. Increases in peak flows and resulting impacts to bridges are projected to be greater from 2010 to 2050 than from 2050 to 2100, highlighting the importance of incorporating climate non-stationarity and changes in urbanization into current bridge design and hydraulic analysis guidelines to address potential impacts by mid-century. Overall, outputs from the presented bridge vulnerability assessment approach can assist decision-makers in identifying potentially vulnerable bridges and prioritizing maintenance, retrofitting, or replacement efforts that reduce susceptibility to expected climate change and urbanization. Furthermore, the hydraulic and hydrodynamic parameters from this chapter were used as the boundary conditions in the numerical modeling of bridge superstructures subjected to flood loading in Chapter 3.

CHAPTER 3

Analysis of Hydrodynamic Loading on Riverine Bridges in Texas Using Computational Fluid Dynamics Modeling

3.1 Abstract

Hurricane-generated storm surges and riverine flood events may partially or completely inundate bridges, resulting in hydrodynamic loading that can significantly influence structural reliability. Therefore, there is a critical need for improved hydrodynamic force prediction on bridges to guide the design of countermeasures that increase stability and resistance to failure. In past research, scaled physical and computational experiments were used to investigate the stability of bridges subjected to severe flooding and debris loading. Because of cost and time constraints, these investigations are often confined to limited flow conditions and deck geometries, and application to full-scale bridge models is absent from the literature. To address these gaps in knowledge, this study applied scaled and full-scale computational fluid dynamics (CFD) modeling to quantify potential hydrodynamic forces on bridges. Flow parameters from Chapter 2 were used to represent modeled hydraulic conditions in the vicinity of bridge structures in Texas. The results suggest that scaling effects are minimal, even when applying results from a 1:50 scaled model to characterize forces on full-scale bridge decks. In addition, CFD modeling revealed numerous variables that affect the hydrodynamic force coefficients, including the bridge geometry and flow field around the deck. The findings of this study can be used to develop more thorough bridge design standards than those specified by the American Association of State Highway and Transportation Officials (AASHTO) load-and-resistance factor design (LRFD) guidelines, which assume constant values for force and moment coefficients regardless of

flow conditions, and can inform the design of countermeasures to hydraulic loading on bridges.

3.2 Introduction

Functioning transportation systems, including roadways and bridges, are crucial to a community's economic growth and mobility [73]. However, aging infrastructure and changing environmental conditions make transportation networks more vulnerable to natural disasters and floods [45, 74]. Bridges spanning inland and coastal waterways, which make up 80% of the bridge inventory in the U.S., may be particularly vulnerable to flood events [15, 16]. High riverine and coastal water levels, turbulent flows, waves, and debris associated with flood events can cause inundation of bridge decks, extreme loading on structures, and scouring around piers [75, 76]. This can lead to impaired performance or failure and hinder evacuation and emergency response efforts following extreme events [77, 17]. Past studies of bridge collapses in the U.S. between 1980–2014 found that hydraulic-induced failures are the leading cause of bridge failure [78, 79, 80]. Therefore, adequate estimation of hydrodynamic loading on riverine bridges is critical for optimizing design, evaluating vulnerability, and strengthening the resiliency of transportation systems [81].

A primary step in evaluating the vulnerability of riverine bridges to flooding is the quantification of hydraulic loading on bridge structures. Recent advancements in high-performance computing and the availability of reliable commercial and open-source computational fluid dynamics (CFD) software (e.g., ANSYS Fluent, Flow-3D, Star-CCM+, OpenFOAM) have enabled the use of numerical simulations to investigate hydraulic forces on inundated bridges under a range of flow conditions [13, 17, 82, 83] and debris loading [84, 73]. Such simulations are often coupled with physical model experiments conducted in a laboratory flume to validate the numerical results, either through load comparisons or

by comparing modeled flow fields with those observed using particle image velocimetry (PIV) techniques [13, 81]. Comparisons between physical experiments and numerical models have shown varying levels of agreement in these studies, highlighting the need for improved assessment of model validity.

Due to cost and time constraints and limits of the laboratory environment, past studies of flood loading on bridges are typically limited to scaled bridge models and focus on a constrained number of flood events and deck geometries. When translating the resulting force estimates to a full-scale bridge geometry, there is the potential for scaling effects, which are discrepancies caused by unequal force ratios between the prototype and the model [85]. Scaling effects can be reduced by maintaining dynamic similarity [86], meaning that the Froude and Reynolds numbers are consistent between the prototype and the model [87]. For example, [88] investigated the effects of scaling on drag, lift, and moment coefficients for bridge models of various scales in a laboratory environment using Froude number similitude and observed no variation in force and moment coefficients, demonstrating that these are independent of the model scale. [82] performed CFD modeling using ANSYS Fluent to evaluate the effects of scaling on hydrodynamic force coefficients using Froude number similitude. A range of bridge deck models up to five times larger than those typically used in the laboratory was considered, although the largest model was still eight times smaller than a full-scale bridge. The researchers concluded that the force coefficients did not show any scaling effect across a range of submergence ratios [82]. However, to the authors' knowledge, the potential to observe scaling effects when translating results to a full-scale bridge deck has not yet been investigated numerically, given the computational constraints associated with CFD modeling.

Transportation agencies often require countermeasures to resist hydrodynamic loading on bridge decks and reduce the potential for flood-induced failure. [89] discusses measures for ensuring bridge stability against storm surges, which include force mitigation

and force accommodation. The force mitigation measures include (a) increasing vertical clearance, preferably over 11.8 in (0.3 m) above the 100-year event wave crest line, (b) using open or sacrificial parapets, (c) venting air-trapping cells, (d) using diaphragms with large openings, (e) using continuous spans, and (f) using solid or voided slab bridges to reduce buoyancy forces [90]. Similarly, the Texas Department of Transportation (TxDOT) has developed design guidelines to mitigate the impacts of flood events on bridge structures. For example, the TxDOT Bridge Design Manual requires the use of countermeasures (i.e., shear keys) on bridges spanning waterways if (a) the 1% Annual Exceedance Probability (AEP) water surface elevation is within 4 ft of the bridge low chord or (b) the bridge crosses a tidally influenced waterway [5]. Several past studies have used numerical modeling approaches to evaluate the effectiveness of countermeasures at increasing bridge stability or reducing hydrodynamic forces applied on bridge superstructures [75, 91, 92, 93]. These studies suggest that strengthening pier-deck connections, streamlining bridge geometry, and venting entrapped air can reduce the failure potential for bridges [75, 91]. Although previous researchers suggested many countermeasures to resist the hydrodynamic loading on bridge decks, the efficacy of these countermeasures in resisting the range of potential flow conditions observed in real riverine systems is still understudied.

Given the current gaps in knowledge regarding flood loading on riverine bridges, this study applies CFD modeling of bridge decks to assess potential hydrodynamic forces on different types of bridges for a range of waterways in Texas. The goals of this study are to (1) assess the ability of two commonly used CFD software programs, ANSYS Fluent and OpenFOAM, to capture observed flow conditions through a model intercomparison; (2) evaluate the potential for scaling effects when translating scaled model results to full-scale bridge geometries; and (3) develop more detailed force and moment coefficient estimates that span a range of bridge geometries and are reflective of flow conditions observed in

riverine systems to evaluate the efficacy of existing designs in mitigating potential bridge failure.

3.3 Methods

Flow parameters obtained from hydraulic models (Chapter 2) and as-built drawings of bridges spanning Texas waterways were used to define boundary conditions in the CFD modeling. Scaled numerical modeling was used to compare the results of ANSYS Fluent and OpenFOAM CFD solvers with physical modeling for numerical model validation and selection. The validated model was subsequently utilized to perform scaled and full-scale numerical modeling and to evaluate the scaling effects associated with hydrodynamic force coefficients. The performance of 1:50 scaled bridge models with different geometries and debris loading conditions was examined under a range of flow conditions.

3.3.1 Identification of Flow Parameters

Flow parameters were identified from existing Hydrologic Engineering Center's River Analysis System (HEC-RAS) models of Texas creeks obtained from the City of Austin and the Harris County Flood Control District [94, 3] and were utilized to define the boundary conditions in the numerical modeling. These models were created as part of FEMA's Flood Insurance Studies (FISs) to identify regulatory floodplains. The hydraulic parameters of 43 creeks and about 900 stream-crossing bridges in Harris and Travis counties were collected from these models. In addition, as-built drawings provided by TxDOT with project-specific hydraulic analyses for 83 bridges were also utilized. Parameters of interest included water surface elevation, flow depth, channel velocity, Froude number (Fr), and bridge elevation. These parameters were used to assess typical flow regimes in the vicinity of bridges.

3.3.2 Physical Modeling

The impacts of flood forces on bridges were examined by Dr. Habib Ahmari, Dr. Imran Kabir, and Max Dean from the UTA Department of Civil Engineering in a laboratory environment using scaled physical models. The experimental team calculated hydrodynamic force and moment coefficients for a Tx-28 I-girder bridge model with an 8-m deck width for Fr = 0.2 under a range of inundation ratios (h^* = 0.25–2.5) [95, 96]. The results of their experiments were used in this analysis to compare with and validate the numerical modeling results.

3.3.3 Computational Fluid Dynamics Modeling

The numerical modeling of hydrodynamic forces on bridge superstructures was conducted using ANSYS Fluent and OpenFOAM CFD solvers. With accuracy and computational cost in mind, the effects of several critical modeling parameters, including the length of the numerical flume and the computational mesh size, were investigated using a sensitivity analysis. An inter-model comparison between OpenFOAM and ANSYS Fluent was performed to select the preferred solver for the scaled and full-scale bridge models. To be consistent with the physical modeling, a scale of 1:50 was used for model validation and inter-model comparison under Fr similarity. Following the selection of the numerical model, the performance of scaled models with I-girder, box beam, and slab beam structures was examined. The scaling effects of hydrodynamic force coefficients were also explored by comparing force and moment coefficients from scaled and full-scale modeling.

3.3.3.1 Bridge Models

Four typical TxDOT bridges were chosen for CFD modeling, including two I-girder bridges (Tx-28 and Tx-54), one box beam bridge (5B-28), and one slab beam bridge (5SB-15). The dimensions of each bridge model are shown in Figure 3.1. Full-scale CFD modeling with deck widths of 8 m and 14 m, respectively, was performed to assess the

effect of deck width. The effect of different debris configurations (i.e., flat plate and wedge shape) was also assessed. The configuration and dimensions of debris shapes were adopted from [96].

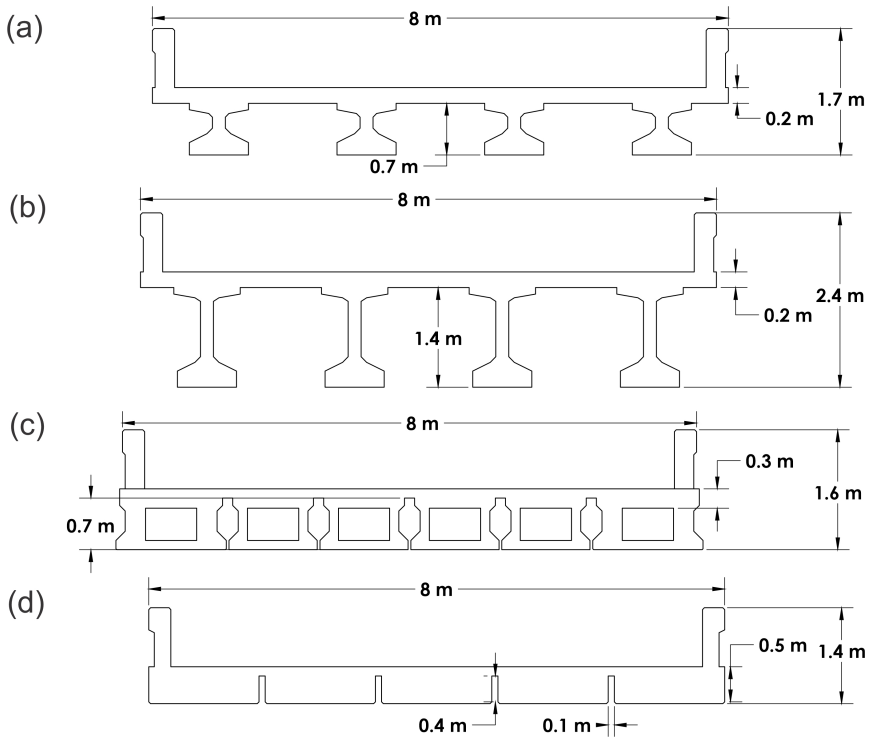

Fig. 3.1. Full-scale bridge model dimensions for (a) Tx-28, (b) Tx-54, (c) 5B-28, and (d) 5SB-15 geometries.

3.3.3.2 Numerical Flume

A smaller numerical flume is preferred for computational efficiency. However, the flume length upstream of the bridge should be long enough to generate a fully turbulent boundary layer. As a rule of thumb, the flume length should be at least 20 times the water depth [17]. To check the effect of the flume length on hydrodynamic forces, scaled open channel flow models were constructed with different upstream lengths in both ANSYS Fluent and OpenFOAM solvers. All simulations were run for a scaled Tx-28 bridge with

an 8-m deck at $h^* = 2.5$ and $Fr = 0.2$. Based on this analysis, it was determined that the flume length had no significant impact on the computed hydrodynamic forces (Tables 3.1 and 3.2).

Table 3.1. Effect of upstream flume length on hydrodynamic force coefficients using OpenFOAM for a scaled Tx-28 bridge deck with $Fr = 0.2$ and $h^* = 2.5$.

Distance (m)	$\mathbf{C_D}$	$\mathbf{C_L}$	$\mathbf{C_M}$
4.35	3.18	-0.82	0.0071
3.35	3.15	-0.79	0.0069
2.35	3.11	-0.78	0.0065

Table 3.2. Effect of upstream flume length on hydrodynamic force coefficients using ANSYS Fluent for a scaled Tx-28 bridge deck with $Fr = 0.2$ and $h^* = 2.5$.

Distance (m)	$\mathbf{C_D}$	$\mathbf{C_L}$	$\mathbf{C_M}$
4.35	1.85	-0.49	-0.035
3.35	1.78	-0.45	-0.033
2.35	1.73	-0.41	-0.029

To ensure consistency with the standard practice that the upstream length is at least 20 times the water depth, an upstream flume length of 217 m was chosen for all full-scale numerical models. The height of the numerical flume was set to 23 m. The full-scale flume dimensions are shown in Figure 3.2. The dimensions of the scaled models were set according to the chosen scale (1:50).

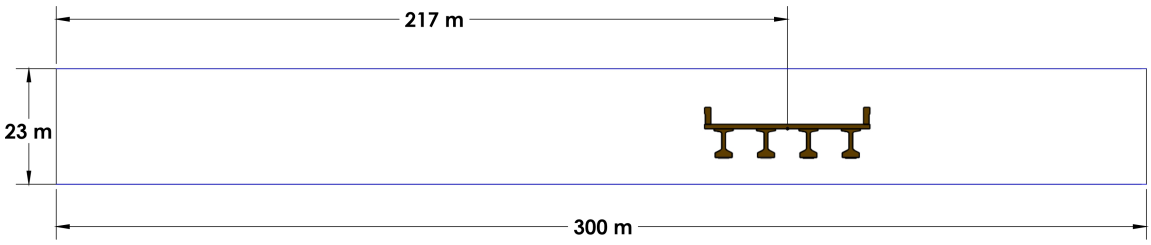

Fig. 3.2. Geometry of numerical flume.

3.3.3.3 Meshing

In CFD modeling, an appropriate mesh geometry and size must be selected to achieve accurate results while balancing the required computational cost. For the OpenFOAM model, a hexahedral mesh was selected because the mesh generation could be automated using a high-performance computing (HPC) system [97]. For ANSYS Fluent, a simpler tetrahedral mesh was used because the mesh generation was confined to a local machine, which limited the computational power [98]. A mesh convergence study was conducted for both models to determine the optimum mesh size. The results of the mesh convergence study are shown in Tables 3.3 and 3.4. Based on the results, a three-dimensional hexahedral grid system with 817,924 cells was generated in OpenFOAM using blockMesh and snappyHexMesh dictionaries. In ANSYS Fluent, a three-dimensional tetrahedral grid system with 10,338,500 cells was generated using the included meshing software. The number of cells for the scaled and full-scale models was the same. Mesh quality metrics, including minimum orthogonal quality, aspect ratio, and skewness, were carefully examined before the initialization of the numerical models. In both CFD solvers, the meshing near the bridge was kept more refined for capturing the boundary layer and complex flow behavior around the bridge. The mesh distributions around the bridge for both OpenFOAM and ANSYS Fluent are shown in Figure 3.3.

Table 3.3. Grid convergence using OpenFOAM for a scaled Tx-28 bridge deck with Fr = 0.2 and h^* = 2.5.

Elements	Drag (N)	% Diff.	Lift (N)	% Diff.	Moment (Nm)	% Diff.
3,205,038	1.34	2.46	-2.10	-2.34	-0.0013	8.33
817,924	1.31	9.17	-2.15	-7.66	-0.0012	26.32
204,512	1.20	20.85	-2.33	-17.93	-0.0010	41.16
63,608	0.99	-	-2.84	-	-0.0007	-

Table 3.4. Grid convergence using ANSYS Fluent for a scaled Tx-28 bridge deck with Fr = 0.2 and h^* = 2.5.

Elements	Drag (N)	% Diff.	Lift (N)	% Diff.	Moment (Nm)	% Diff.
18,431,220	2.32	0.26	1.19	0.41	-0.0352	0.05
13,969,321	2.30	0.58	1.18	0.78	-0.0352	0.22
10,338,500	2.28	1.88	1.17	2.48	-0.0351	0.39
7,324,765	2.19	2.80	1.14	13.64	-0.0350	5.52
5,732,575	2.07	1.93	1.31	5.23	-0.0331	0.93
4,793,222	1.99	-	1.38	-	-0.0328	-

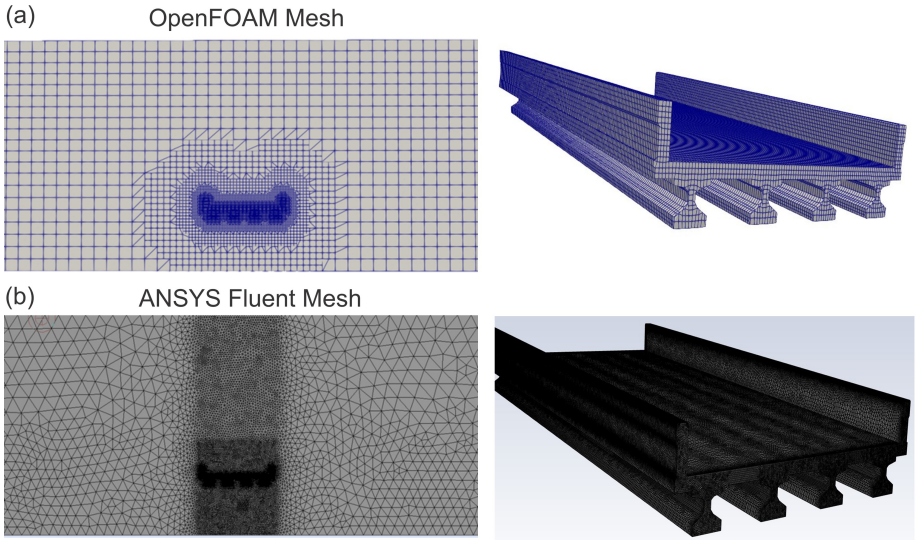

Fig. 3.3. Mesh distribution around the bridge for (a) OpenFOAM and (b) ANSYS Fluent.

3.3.3.4 Boundary Conditions and Solution Methods

The boundary conditions in both CFD solvers were kept the same and are shown in Figure 3.4. A uniform velocity with constant water depth was defined at the inlet based

on the chosen Fr. The pressure on the domain's topside was set to atmospheric pressure. At the outlet, an open channel boundary condition with constant water depth was defined. The channel bed and bridge were defined as no-slip walls with a default roughness. The simulations were completed using the volume of fluid (VOF) multiphase model [99, 100] and $K\omega$-SST turbulence model [101]. The main reason for using the VOF model is its accuracy in tracking the air-water interface while conserving fractional fluid volume [102]. Because the $K\omega$-SST turbulence model operates well in situations involving separation flows and adverse pressure gradients and produces more accurate drag and lift coefficient results, it was chosen for the simulations. In the turbulence model, the near-wall treatment of the standard wall function was enabled.

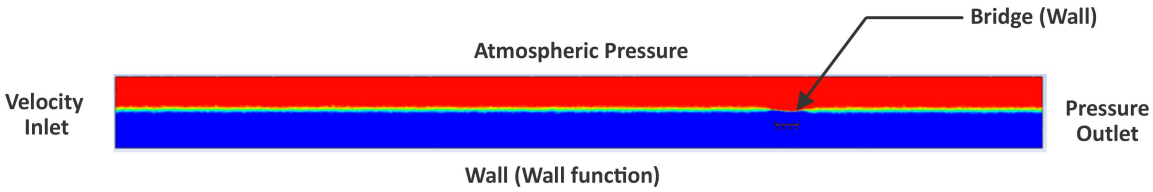

Fig. 3.4. Boundary conditions of numerical simulations.

Divergence in the numerical simulations can be caused by several factors, such as large mesh size, conservative under-relaxation factors, and complex flow physics [103, 104]. Furthermore, if the time step is too large compared to the grid cell size, numerical smearing may occur, leading to numerical instability and, in some cases, divergence [98]. To avoid issues with divergence, the time step for the ANSYS Fluent simulations was set to 0.005 seconds based on the Courant number criteria, which should be less than 1 to ensure the stability of the numerical models. For OpenFOAM, the time step was adjustable according to the maximum Courant number in the simulation. The Semi-Implicit Method for Pressure Linked Equations (SIMPLE) scheme [105] was chosen to couple pressure and velocity because it is more computationally efficient than the other schemes, such as the

Pressure-Implicit Split-Operator (PISO) scheme [13]. To discretize momentum, turbulent kinetic energy, and turbulent dissipation rate, a second-order upwind scheme [106] was utilized. The under-relaxation factor for pressure was set to 0.30, and the under-relaxation factors for the other terms (density, momentum, turbulent kinetic energy, and specific dissipation rate) were set to 0.70 to achieve better convergence.

The run time for the simulations was chosen based on the flow time at which the drag, lift, and overturning moment coefficients had reasonably converged in order to ensure accurate results. The convergence for the OpenFOAM and ANSYS Fluent simulations are shown in Figures 3.5 and 3.6. In this study, hexahedral mesh was used in OpenFOAM, which tends to take longer to converge than tetrahedral mesh. As a result, the simulations were run for 40 seconds in ANSYS Fluent and 200 seconds in OpenFOAM. The average value of the last 5 seconds was utilized to smooth out small fluctuations in the drag, lift, and moment coefficients.

The operating pressure was specified to be atmospheric pressure (101,325 Pascal). The gravitational acceleration in the vertical direction was set to -9.81 m/s^2, and the operational density was set as 1.23 kg/m^3. A flat, open channel initialization method was used to initiate the solution from the inlet. After obtaining solution convergence, the results were post-processed and analyzed. All simulations were run on HPC systems at the Texas Advanced Computing Center (TACC) and UT Arlington (UTA). The node specifications for the TACC and UTA systems are shown in Table 3.5. One simulation on TACC's HPC took 48 hours with five nodes, while one simulation on UTA's HPC took 60 hours with two nodes.

Table 3.5. Compute node specifications.

HPC	RAM	Cores	Threads	Processor
UTA	512 GB	22	44	Intel(R) Xeon(R) CPU E5-2699 v4
TACC	96 GB	68	272	Intel Xeon Phi 7250 (Knights Landing)

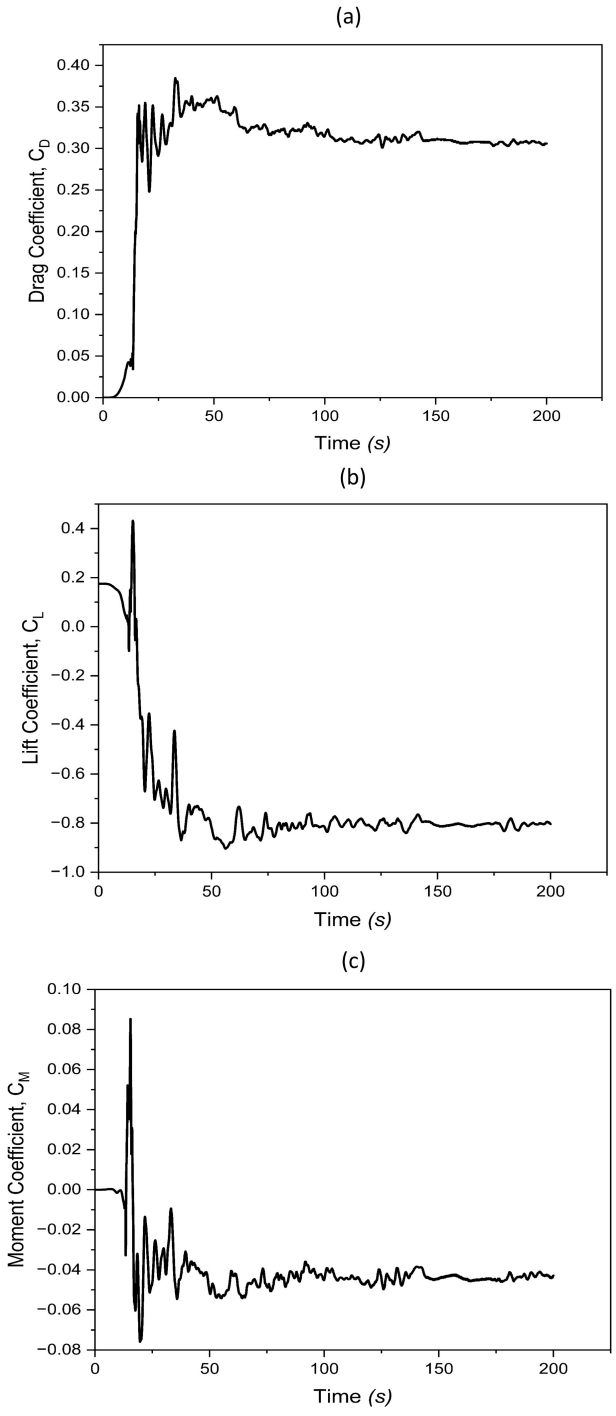

Fig. 3.5. Convergence for (a) drag, (b) lift, and (c) moment coefficients in OpenFOAM for a full-scale box-beam bridge deck with Fr = 0.9 and h^* = 2.5.

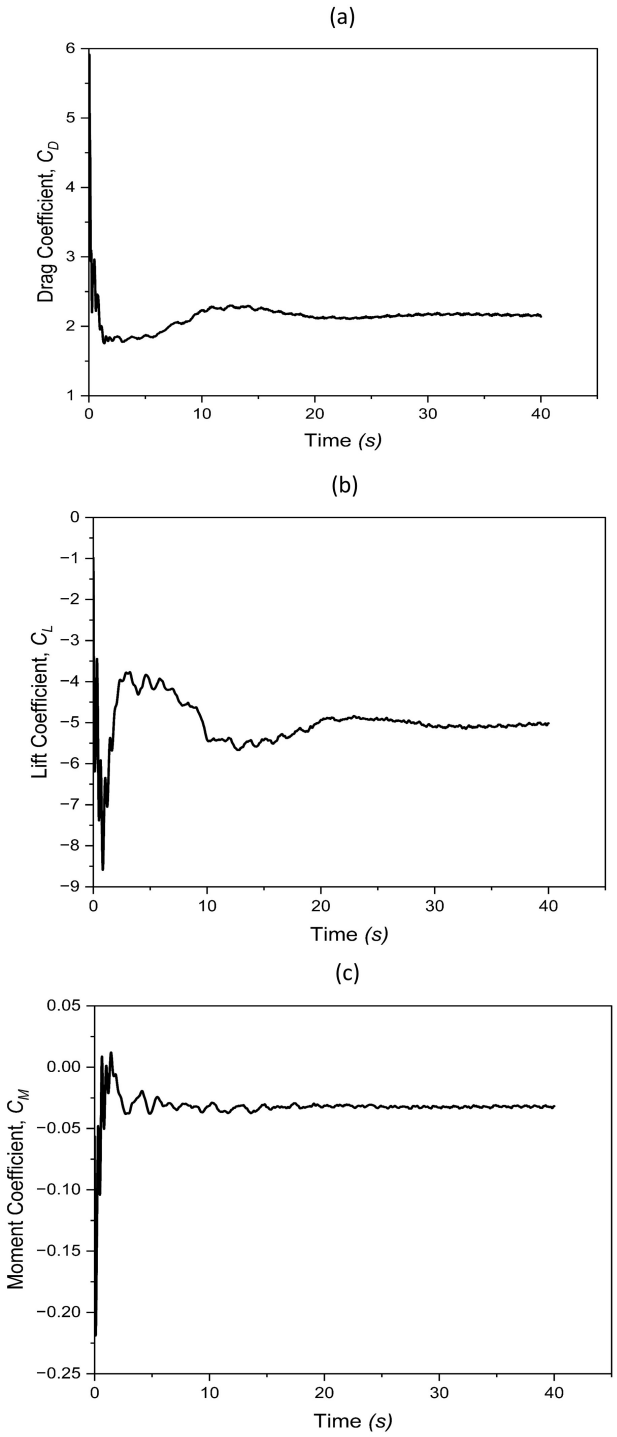

Fig. 3.6. Convergence for (a) drag, (b) lift, and (c) moment coefficients in ANSYS Fluent for a full-scale box-beam bridge deck with Fr = 0.9 and h^* = 2.5.

3.4 Results

3.4.1 Flow Parameters

Tables 3.6 and 3.7 summarize the flow parameters for 2%, 1%, and 0.2% AEP events extracted from the Harris County and Travis County HEC-RAS models, including channel velocity, flow depth in the channel, Fr, and water depth above the bridge low chord. Also included are the number and percent of bridges along each modeled creek/stream at which the water surface in the channel reaches or exceeds the elevation of the low chord of the bridge. Note that bridges are designed for a specific AEP storm and thus are expected to be impacted by flooding during higher return period events. In Harris County, maximum velocities in the vicinity of bridges vary from 14.5 ft/s for the 2% AEP to 17.4 ft/s for the 0.2% AEP, with associated water depths above low chord of 15.8 ft to 20.0 ft. Maximum flow depths in the channel vary from 48.3 ft for the 2% AEP to 56.8 ft for the 0.2% AEP. In Travis County, maximum velocities in the vicinity of bridges vary from 20.2 ft/s for the 2% AEP to 26.9 ft/s for the 0.2% AEP, with associated water depths above low chord of 15.4 ft to 23.9 ft. Maximum flow depths in the channel vary from 34.6 ft for the 2% AEP to 44.8 ft for the 0.2% AEP. Based on this analysis, the critical flow condition in Texas creeks was determined to be $Fr = 0.9$ and $h^* = 2.5$.

3.4.2 Inter-Model Comparison and Validation

Figure 3.7 shows a comparison between the drag, lift, and moment coefficients obtained from the physical experiments and numerical simulations for a scaled Tx-28 bridge with an 8-m deck at $Fr = 0.2$ as a function of h^*. The root mean square error (RMSE) of the difference between physical and numerical modeling results for OpenFOAM and ANSYS Fluent is given in Table 3.8.

For the drag coefficient, the ANSYS Fluent results agree with the physical modeling results at lower h^* but do not closely follow the experimental results at $h^* > 1.5$, resulting

Table 3.6. Summary of flow parameters for 2%, 1%, and 0.2% AEP flood events in Harris County watersheds.

	Velocity (ft/s)	Flow Depth (ft)	Froude #	Water Depth above Low Chord (ft)
			2% AEP	
Min	6.1	18.5	0.4	3.1
Avg	8.8	28.4	0.5	7.7
Max	14.5	48.3	0.6	15.8
			1% AEP	
Min	6.0	15.0	0.2	2.3
Avg	9.6	30.8	0.6	8.9
Max	15.1	51.3	0.7	17.2
			0.2% AEP	
Min	6.5	22.1	0.3	5.2
Avg	9.9	33.8	0.5	12.2
Max	17.4	56.8	0.7	20.0

Table 3.7. Summary of flow parameters for 2%, 1%, and 0.2% AEP flood events in Travis County watersheds.

	Velocity (ft/s)	Flow Depth (ft)	Froude #	Water Depth above Low Chord (ft)
			2% AEP	
Min	5.6	8.1	0.3	-2.3
Avg	13.4	18.7	0.8	6.0
Max	20.2	34.6	1.0	15.4
			1% AEP	
Min	5.7	8.3	0.3	-0.9
Avg	14.2	19.9	0.8	7.1
Max	21.3	37.8	1.0	18.0
			0.2% AEP	
Min	4.1	8.6	0.3	0.7
Avg	15.5	22.8	0.8	8.7
Max	26.9	44.8	1.0	23.9

Table 3.8. Comparison between physical and numerical modeling results.

	RMSE		
Model	$\mathbf{C_D}$	$\mathbf{C_L}$	$\mathbf{C_M}$
Fluent	0.59	0.42	0.10
OpenFOAM	0.44	0.68	0.06

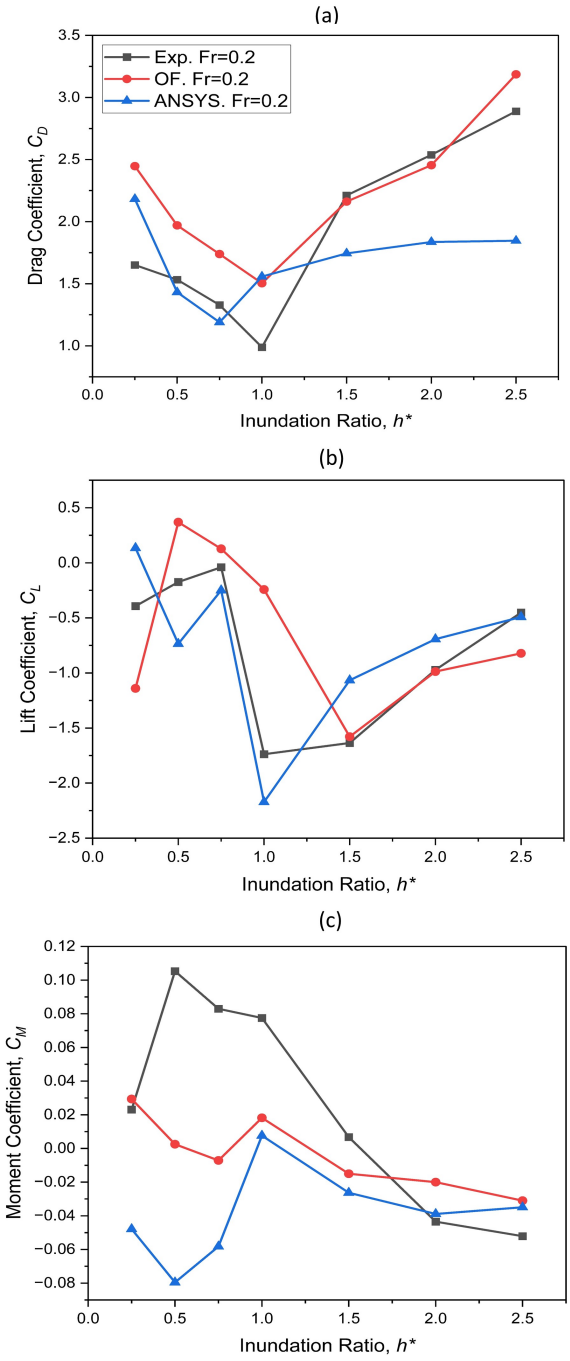

Fig. 3.7. Comparison of (a) drag, (b) lift, and (c) moment coefficients determined from physical and numerical modeling for a Tx-28 bridge with 8-m deck.

in a RMSE of 0.59. The OpenFOAM drag coefficient results show reasonable agreement with the physical modeling results for both higher and lower h^* and follow a similar trend to the physical modeling (RMSE = 0.44). The ANSYS Fluent lift coefficients agree with the physical modeling results in most simulations at higher and lower h^* (RMSE = 0.42). However, the OpenFOAM lift coefficients show reasonable agreement only at higher h^* (RMSE = 0.68). The moment coefficients produced by the CFD solvers do not closely match the results of the physical experiments. This lack of agreement was also described by [17, 13, 14], who performed numerical simulations using ANSYS Fluent, STAR-CD, and OpenFOAM CFD solvers, respectively.

In the literature, drag coefficients are often given more consideration in hydrodynamic loading on bridges in riverine areas because of their significant impact on the stability of the bridge [17, 84]. This is particularly true for bridges subjected to high flow velocities or located in areas with strong currents. As a result, when modeling the hydrodynamic forces on bridges in Texas, it was determined that OpenFOAM would be the most suitable software due to its ability to more accurately reflect the drag coefficients measured by the physical modeling, particularly at higher inundation ratios similar to the critical conditions evaluated in this study (h^* = 2.5).

3.4.3 Scaling Effects

Figure 3.8 compares hydrodynamic force and moment coefficients for the full-scale and scaled Tx-28 bridge with an 8-m deck at Fr = 0.5. Differences between the scaled and full-scale results for the drag, lift, and moment coefficients are minimal (<12%), indicating that there are no noticeable impacts due to scaling.

3.4.4 Effects of Bridge Geometry

Using the validated OpenFOAM model, the effects of bridge geometry on force and moment coefficients were examined. Figure 3.9 shows the drag, lift, and moment

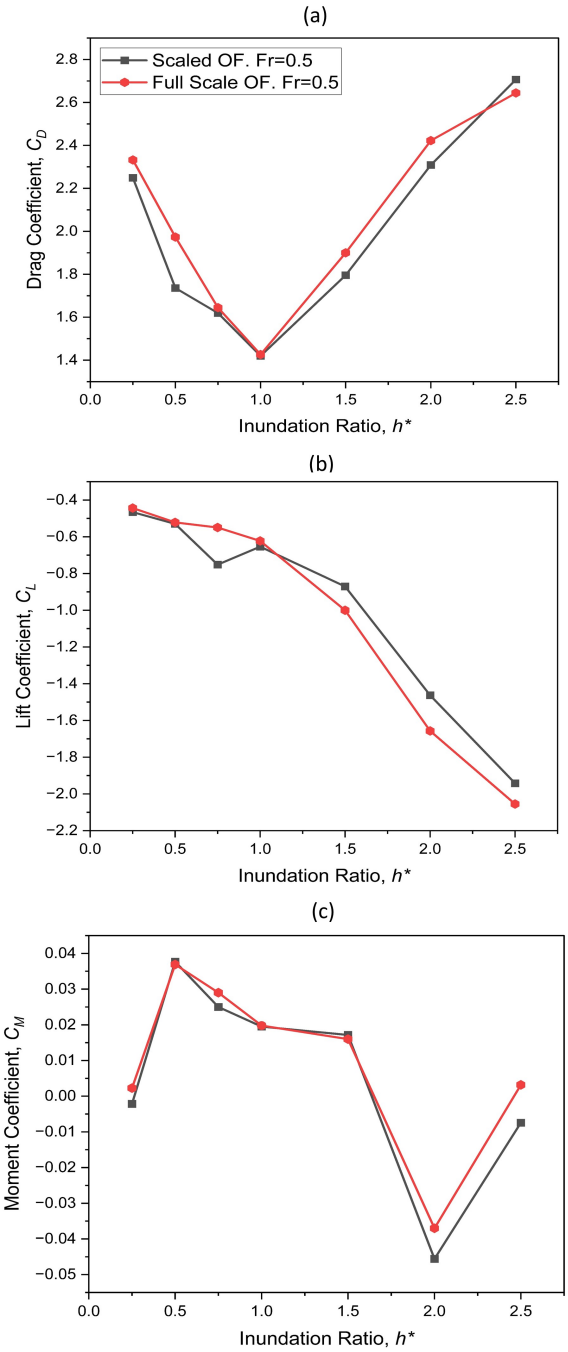

Fig. 3.8. Comparison of (a) drag, (b) lift, and (c) moment coefficients for scaled and full-scale models.

coefficients computed for Fr = 0.2 as a function of h^* for I-girder (Tx-28 and Tx-54), box-beam (5B-28), and slab-beam (5SB-15) bridge decks. The I-girder bridge decks have

larger drag and lift coefficients than box- and slab-beam bridge decks. Specifically, the Tx-54 bridge deck has the highest drag and lift coefficient magnitude due to its larger height and flow blockage area. However, the moment coefficient of I-girders is slightly smaller than the box- and slab-beams, although the differences are minor.

Figure 3.10 shows the velocity contours and flow vectors around the bridge geometries. The velocity contours show an increase in velocity above the bridge deck due to flow separation. The velocity under the bridge deck increases due to area contraction. The velocity flow field also shows that bridge deck attachments such as railings and girders significantly disturb the boundary layer. Flow separates from the bridge's leading-edge corner from the point known as the stagnation point, where the local velocity is zero. When the flow separates, adverse velocity gradients emerge in the boundary layers, and the flow is reattached near the trailing edge. Due to adverse pressure gradients, many vortices occur at various scales along the bridge deck surface. The three bridge deck types show noticeable differences in the flow field. The I-girder bridge deck produced the largest vortex zones between the girders and a larger wake than the box- and slab-beam bridge decks, causing a greater disturbance on top of the deck and producing larger lift and drag forces.

Figure 3.11 shows the pressure contours on the bridge deck surface, demonstrating that pressure has a higher magnitude on the upstream side where the water strikes the bridge deck and a lower magnitude on the downstream side. The pressure difference could cause instability or failure of the bridge. All bridge geometries respond differently due to variations in flow patterns in the wake zone above and below the bridge decks, which indicate differences in energy loss and vortex distribution over the bridge deck surface.

3.4.5 Full-Scale Modeling

The results of the full-scale modeling for Fr = 0.9 and h^* = 2.5 are shown in Table 3.9. The shape, size, and presence of debris influence the drag force on the bridges. A

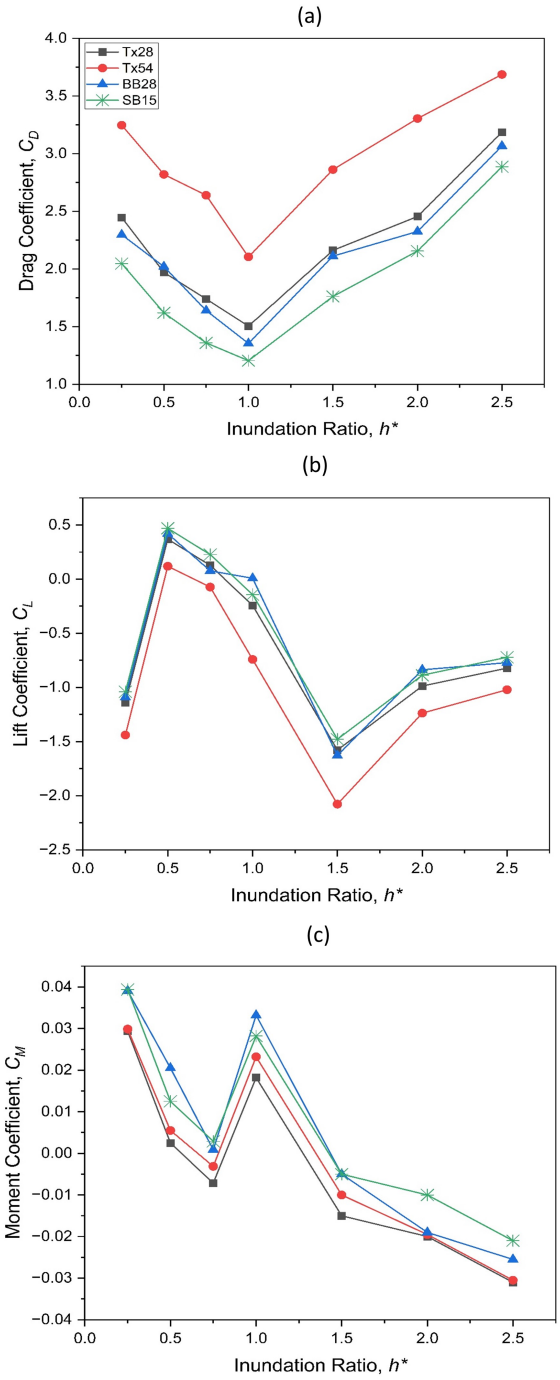

Fig. 3.9. Comparison of (a) drag, (b) lift, and (c) moment coefficients across bridge geometries.

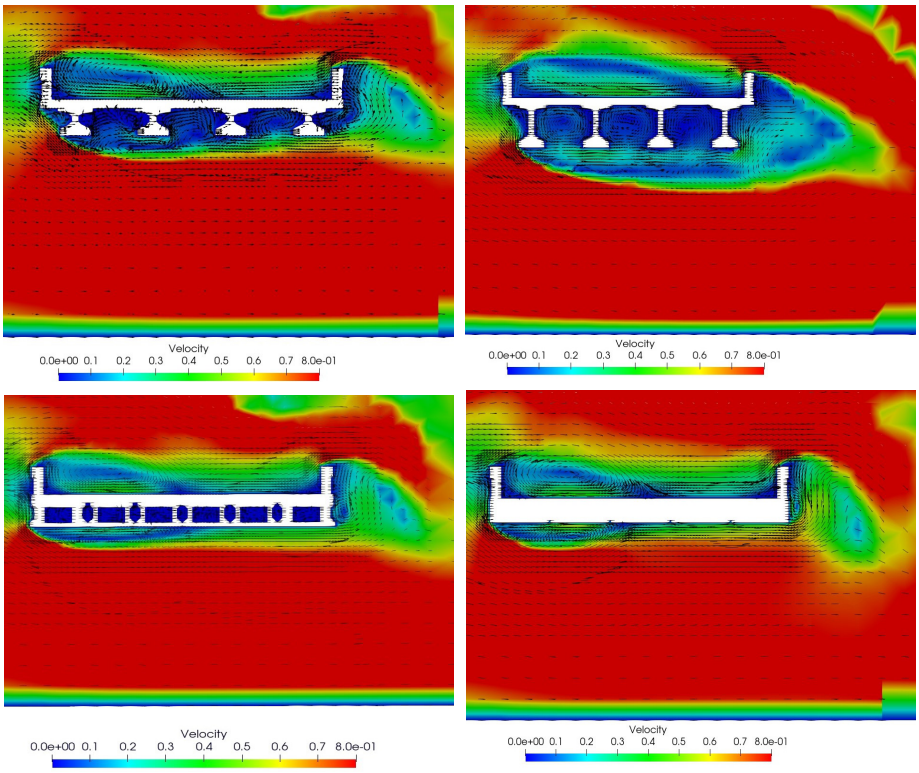

Fig. 3.10. Velocity flow fields around bridges with $Fr = 0.2$ and $h^* = 2.5$.

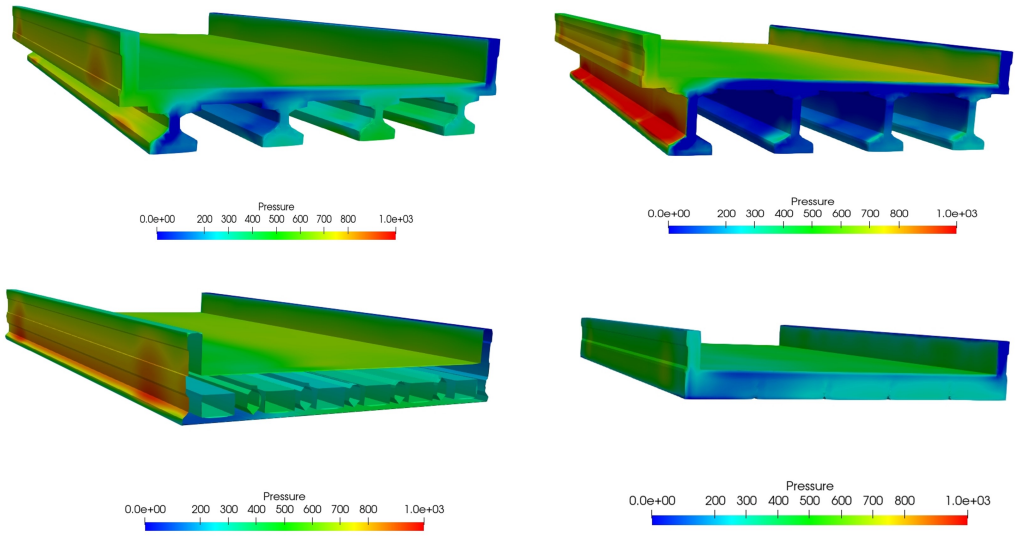

Fig. 3.11. Pressure contours on the surface of bridges with $Fr = 0.2$ and $h^* = 2.5$.

longer span length and wider deck increase the surface area exposed to fluid flow, leading to a higher drag force. Debris can alter the flow of fluid around the bridge, increasing the drag force. Flat plate debris is particularly effective at increasing the drag force due to its large surface area. The bridge with the combined longest span length (38 m), widest deck (14 m), and presence of flat plate debris experiences the highest drag force among the scenarios tested.

Table 3.9. Drag forces calculated for full-scale bridge models with Fr = 0.9 and h^* = 2.5.

Bridge Type	**Deck Width (m)**	**Span Length (m)**	**Drag Force** (kN)
Tx-28	8	15	1,370
Tx-28	14	15	1,477
Tx-54	8	15	2,914
Tx-54	14	15	3,109
Tx-54	8	38	6,806
Tx-54	14	38	7,162
Tx-54 (Debris - Flat Plate)	14	15	4,488
Tx-54 (Debris - Wedge)	14	15	2,100
Tx-54 (Debris - Flat Plate)	14	38	10,409
Tx-54 (Debris - Wedge)	14	38	4,515
Box-Beam	8	15	1,410
Slab-Beam	8	15	979

3.5 Discussion

Comparing numerical modeling results from OpenFOAM and ANSYS Fluent with physical modeling results from [95] shows that ANSYS Fluent underestimates the drag coefficients at higher h^*. In contrast, OpenFOAM drag coefficients reasonably agree with the physical modeling results, especially at higher h^*. In the case of lift and moment coefficients, OpenFOAM shows reasonable agreement only at higher h^*. One reason for the difference in ANSYS Fluent and OpenFOAM results could be the chosen mesh type, as this was the only difference between the CFD solvers. For subsequent modeling of a range

of bridge geometries and flow conditions, OpenFOAM was chosen over ANSYS Fluent because of its enhanced ability to capture trends in the drag coefficient observed through the physical modeling, particularly at higher h^*.

When considering the potential for scaling effects, maintaining appropriate similitude is critical. In general, gravity forces govern in free surface flow, while viscous forces govern in wall-bounded flow [17, 107]. Maintaining Fr similitude is sufficient to prevent scaling effects if the flow is turbulent. However, if the flow is not turbulent and viscous effects are present, fulfillment of solely the Fr similitude criteria would not be sufficient to prevent scaling effects. Because the flow in the numerical domain in this study is free surface and turbulent ($Re > 10^5$), the viscous forces can be neglected, so only Fr similitude is needed. This is highlighted by the modeling results, which demonstrate that scaling up the model to full scale has no significant effect on the magnitudes of the force and moment coefficients. Thus, measurements made during laboratory tests or results from scaled numerical modeling can be used to assess forces on full-scale bridge structures if Fr similarity is maintained.

The results of CFD modeling suggest that the drag coefficient of a bridge tends to increase with increasing h^*, but there is a dip in the drag coefficient at $h^* = 1$. This dip may be caused by the transition of the water depth from being below the top of the girders to overtopping the bridge deck, which can lead to changes in the fluid flow around the bridge and a temporary reduction in the drag coefficient. One possible explanation for this dip is the formation of a separation bubble on the upstream side of the bridge deck, which can reduce the drag coefficient by decreasing the amount of fluid in contact with the bridge's surface. However, the specific cause of this dip in drag coefficient is not fully understood and requires further investigation. The fact that the drag coefficients are more significant at higher inundation ratios suggests that the fluid flow exerts a stronger force on the bridge

at these levels. This increased force can increase the likelihood of sliding failure, as the drag force can cause the bridge deck to move horizontally along its foundation.

The lift coefficient of a bridge is negative for all h^*, indicating that the fluid flow is applying a downward force on the bridge. This downward force varies due to the bridge's shape and the way the fluid flows interact with it. A bridge with a more streamlined shape typically experiences a lower downward force than a bridge with a more bluff or block-like shape. This is because the streamlined shape allows the water flow to pass more smoothly over the bridge, creating less turbulence and drag. On the other hand, a bluff or block-like shape can create more turbulence in the flow, leading to a greater downward force. As the bridge is fully submerged, the lift coefficient becomes more negative before gradually returning to near zero as h^* increases. The downward lift force may have implications for the stability of the bridge, particularly if it causes oscillations or swaying, and may also be beneficial in terms of resisting uplifting forces.

The moment coefficients are nearly zero for every h^*, which means that the moments (or rotational forces) acting on the bridge due to the hydrodynamic loading are very small. One possible implication of this outcome is that the bridge may be more resistant to lateral or torsional instability due to hydrodynamic loading. Second, the bridge may be less likely to experience lateral or torsional deformations, which could potentially lead to structural failure. Hence, it may be possible to use a smaller or more lightweight structural system, which could potentially result in cost savings and a more efficient design.

To increase the stability of riverine bridges subjected to extreme flow conditions, countermeasures that reduce the drag and buoyant forces may be needed. This could involve making modifications to the bridge itself (e.g., changing the shape or increasing the structural stiffness) or changing the flow in the vicinity of the bridge (e.g., by using flow-control devices or debris removal strategies) [108, 109]. By reducing the drag and

buoyant forces experienced by the bridge, these countermeasures could increase the bridge's stability and reduce the risk of sliding or uplift failure.

Although the numerical modeling results show reasonable agreement with the physical modeling results, some discrepancies are notable, particularly for the moment coefficient. Similar discrepancies have been observed in other studies as well [17, 82, 14]. Further advancements in the numerical modeling approach could potentially provide improved results and could be the focus of future research efforts. For example, using a Reynolds-Averaged Navier-Stokes (RANS) model in this research introduces simplifications, as it involves decomposing instantaneous quantities into time-averaged and fluctuating components to solve the Navier-Stokes equations [98]. Because of these assumptions, the numerical model may not correctly resolve the small details in the physics (e.g., small eddies), which could contribute to the force coefficients [17]. Using more accurate modeling approaches (e.g., large eddy simulation and direct numerical simulation) or conducting formal comparisons with PIV data collected in the lab could provide additional enhancements to the modeling presented here. In addition, the $K\omega$-SST turbulence model, a second-order turbulence model, was used to close the RANS equations in these simulations. Using higher-order turbulence models, such as the Reynolds Stress Model, can improve the accuracy of the results [110]. Furthermore, the standard wall functions in turbulence models were used. The primary purpose of the standard wall function is to resolve the very small length scales near the bridge to capture the viscous drag. Using enhanced wall functions in the turbulence model can increase the accuracy [17]. It is important to note that all of these enhancements require additional computational power and would thus increase the time and resources needed to conduct the numerical modeling studies.

Hydrodynamic loading on bridges can significantly impact their structural performance and safety. The use of CFD modeling can provide a more accurate and reliable assessment of these loads compared to traditional methods that rely on simplifying as-

sumptions. For example, the American Association of State Highway and Transportation Officials (AASHTO) provides design specifications for bridges through its Load and Resistance Factor Design (LRFD) approach, but these guidelines assume that the force and moment coefficients resulting from hydrodynamic loading are constant regardless of the flow conditions. As a result, bridges may not be designed adequately to capture the complex and variable nature of real-world loading conditions. By using CFD modeling, it is possible to more accurately predict the hydrodynamic loads on a bridge based on the specific flow conditions and geometries involved, providing a more realistic assessment of the structural performance and safety of the bridge.

3.6 Conclusion

Numerical modeling of hydrodynamic forces on bridge decks using CFD solvers displayed a reasonable potential for assessing the impacts on submerged bridge decks. Although the numerical models did not capture the entire range of behavior shown in the physical modeling results conducted by [95], the estimation of hydrodynamic forces exhibited sufficient similarity to quantify the impacts of flood forces on bridge structures. Furthermore, the CFD modeling approach allows for flexibility in simulating various flow and inundation scenarios, thus complementing physical modeling. The numerical simulations conducted across a range of scales suggest that if Froude number similitude is maintained, scaling effects are not significant. Thus, the hydrodynamic forces obtained using scaled physical and numerical models can be used to predict the behavior of full-scale bridge structures.

The results of the CFD modeling are expected to be more reliable than the parameters specified in AASHTO's LRFD bridge design specifications, which assume a constant value for the force and moment coefficients irrespective of flow conditions. The results of this study were also used to inform an analysis of structural countermeasures conducted by the

structural modeling team at UTA as a part of TxDOT RTI 0-7068 Task 5 [96]. Overall, the CFD modeling results provide a wealth of information on the potential hydrodynamic forces experienced by partially or fully inundated bridges to inform more detailed design criteria for riverine bridges.

CHAPTER 4

Development of a Probabilistic Modeling Framework for Improved Risk Assessment of Coastal Bridges Subjected to Hydrodynamic Loading

4.1 Abstract

Storm surges and high waves caused by hurricanes can exert large forces on bridge decks in coastal areas. When accompanied by an increase in water level, the energy carried by waves during these storm events is partially transferred to the bridge structure and can cause damage or failure. Decision-makers are increasingly concerned about the vulnerability and loss of bridges during storm events, as the performance of bridges vulnerable to storm surges and waves is crucial to the resilience of coastal regions. The formulation of design guidelines, which entails simulating the wave forces exerted on bridges, is an important part of reducing bridge vulnerability to coastal storms. This study aims to support improved design guidelines for coastal bridges by developing a modeling framework that allows for coupled simulation of wave forces, structural response, and uncertainty in hazard and bridge parameters to assess failure risk for coastal bridges subjected to surge and wave loading. The framework is applied to evaluate the performance of a typical Texas bridge geometry subjected to surge and wave conditions observed during Hurricane Ike. The findings demonstrate that waves with long wavelengths cause the most significant impacts to bridge stability. Bridge response is most sensitive to uncertainties in the concrete density in the case of vertical stability and uncertainties in the lateral stiffness of the bearings in the case of horizontal stability. The proposed framework will improve the quantification of the failure probability of coastal bridges, which could inform the

prioritization of maintenance and retrofitting efforts for transportation systems in coastal regions.

4.2 Introduction

Low-lying coastal areas are prone to flooding from storm surges and waves, which can be disastrous for communities and critical infrastructure assets [111]. In the U.S. alone, there are more than 36,000 bridges within 15 miles of the coast [112]. These bridges are likely to experience more frequent and severe disruptions from flood events in the future due to rising sea levels and local land subsidence [113, 114, 115]. Given the important role that bridges play in the local and regional transportation systems in coastal areas, it is critical to understand their performance under extreme hydrodynamic loading conditions to inform the prioritization of mitigation activities and the allocation of resources following severe storms [7].

Storm surge and wave loads on bridge superstructures have caused significant damage in the past [22]. For example, Hurricane Katrina destroyed two bridges on US-90 over St. Louis Bay and Biloxi Bay in Mississippi and one on Interstate 10 (I-10) over Lake Pontchartrain in Louisiana in 2005 [22, 116, 17]. The Rollover Pass Bridge on the Bolivar Peninsula in Galveston collapsed during Hurricane Ike in 2008 due to a 15-ft storm surge and 5-ft waves [23]. It is projected that it will cost more than $1 billion to rebuild all of the coastal bridges damaged by Hurricanes Katrina (2005) and Ivan (2004) [117]. Thus, in order to effectively repair damaged bridges and protect vulnerable coastal bridges in hurricane-prone areas, it is important to have a thorough understanding of the extreme hydrodynamic conditions that can occur during storms and their impact on the structural integrity of bridges. This knowledge can inform the design and maintenance of bridges to ensure that they are able to withstand extreme conditions and remain safe and functional [118, 110, 119].

Substantial work has been conducted, both in laboratory settings [120, 121, 122, 123, 124, 125, 116, 119] and through numerical modeling [126, 127, 128, 129, 18, 119, 130, 131, 18], to evaluate the interactions between coastal surge/waves and built structures, including bridges. However, many gaps still exist that, if addressed, could provide critical insight into the response and reliability of bridge structures during coastal storm events. Physical and numerical modeling studies have applied regular waves with varying water depths, wave periods, and heights to measure resultant loading on a range of bridge deck configurations. The results are then used to develop empirical formulas to translate surge/wave conditions into forces and, in some cases, failure probabilities [18]. Most empirical formulas, however, give maximum horizontal and vertical forces acting on coastal bridge decks [12]. Although this information is useful for assessing initial risk, detailed time histories of wave loads are required for dynamic structural analysis of coastal bridges. In addition, most numerical modeling studies have considered bridge decks as fixed, ignoring the impact of dynamic bridge responses. Because the stiffness at the contact between the superstructure and the substructure allows the bridge deck system to move [12], the resulting structural responses cannot be captured completely by fixed models. As a result, a detailed assessment of the wave loading acting on submerged and sub-aerial bridge decks by considering dynamic responses is required to better constrain the failure processes of bridge decks under extreme hydrodynamic conditions.

Uncertainties in hydrodynamic loading conditions and structural and material properties can influence the structural response of bridges and affect the ability to predict failure potential [6, 7]. A study of hurricane-induced wave loads on bridges by [6] found that potential variations in wave characteristics have the greatest effect on the bridge's response. This study also demonstrated that the deck mass is the most important structural variable when determining bridge response, followed by the friction coefficient and the stiffness of the elastomeric pads. Another study by [7] developed fragility curves for maximum

hurricane wind speeds by considering the uncertainty in concrete density and bridge deck thickness. However, this study did not include uncertainty in the friction factor, the stiffness of the elastomeric bearing pads, or the modulus of elasticity, which can also influence bridge response [7]. Limited reliability analyses have been conducted for bridges subjected to surge and wave loads using finite element models (FEM) [132, 133], but these studies lack precise uncertainty quantification in their hydrodynamic and structural modeling, thus limiting their capacity to anticipate bridge response to coastal storm events.

This chapter develops a modeling framework to facilitate coupled simulation of hydrodynamic forces, structural response, and probabilistic failure risk for coastal bridges subjected to surge and wave loading. The framework is applied to quantify the hydrodynamic loading on a typical coastal bridge structure during Hurricane Ike to assess its vulnerability to hurricane-induced flood hazards. The presented approach advances past research by accounting for time-varying wave histories, simulating dynamic structural response, and including uncertainties in material properties (i.e., concrete density, friction factor, and modulus of elasticity).

4.3 Methods

This study was conducted through the application of a probabilistic bridge vulnerability framework that integrated several models, as shown in Figure 4.1. First, observed storm surge and wave parameters from Hurricane Ike were used as boundary conditions in a computational fluid dynamics (CFD) model to quantify local hydrodynamic forces around a bridge structure. The CFD simulation results were then used in a finite element model (FEM) to evaluate deterministic bridge response under different loading conditions. The probabilistic bridge response was computed by incorporating uncertainties in material properties. Based on the reliability analysis, fragility curves under different hazard scenar-

ios were then calculated, which can help assess long-term damage loss. Additional details about each step are provided in the following sections.

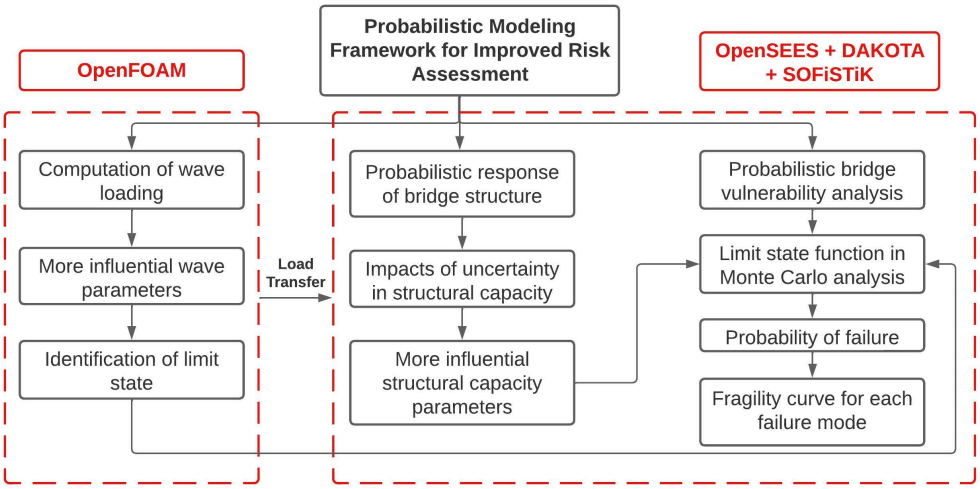

Fig. 4.1. Probabilistic framework for improved bridge vulnerability assessment.

4.3.1 Identification of Storm Parameters

Wave parameters from Hurricane Ike, which damaged 53 bridges in and around Galveston, Texas, in 2008 [23], were used to examine the impacts of extreme wave loading on coastal bridges. Time series of significant wave height (H_s) and peak wave period (T_p) predicted by [2] (Figure 4.2) were extracted at 10-hour intervals from the 90-hour data set and were utilized to run CFD models to predict loading on the representative bridge structure throughout the storm.

4.3.2 Modeling of Wave Forces

CFD models were set up using OpenFOAM following the steps outlined in Chapter 3. Figure 4.3 shows the boundary conditions of the CFD wave modeling. Cnoidal wave theory [134] was used to model the waves observed during Ike, which were relatively long and possessed larger energy, due to its ability to describe surface gravity waves with

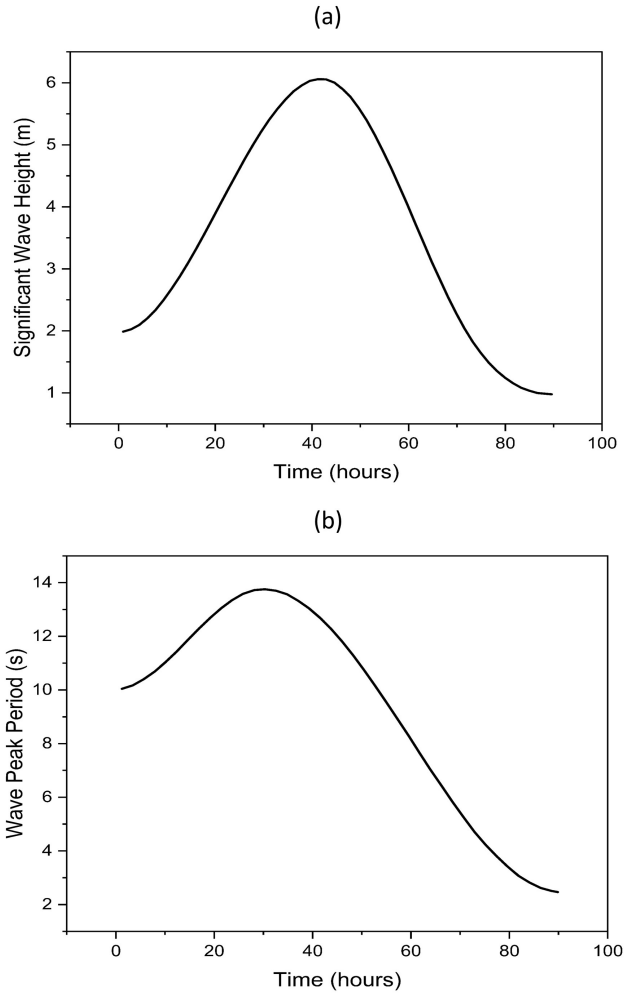

Fig. 4.2. Time series of (a) significant wave height and (b) peak period during Hurricane Ike. Source: [2].

long wavelength compared to the water depth [135]. The simulations were completed using the volume of fluid (VOF) multiphase model and $K\omega$-SST turbulence model. A wave absorption boundary condition was defined in the region near the outlet to prevent numerical reflections from propagating upstream.

The wave properties used in as boundary conditions in the numerical modeling are shown in Table 4.1. The water depth (d) in all simulations was 9.69 m. The wavelength (λ), H_{s}, and T_{p} considered during the numerical simulations are also presented in the table.

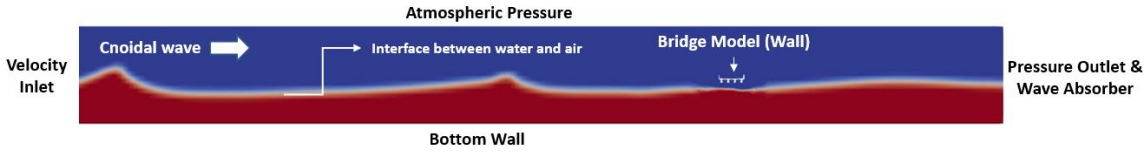

Fig. 4.3. Boundary conditions for numerical simulations of wave loading.

Wave breaking occurs when H_s/d is greater than 0.78 [136]. Throughout the storm, H_s/d is less than 0.78, indicating that waves are not breaking. The waves are considered deep water waves if $d > \lambda/2$, transitional waves if $\lambda/20 < d < \lambda/2$, and shallow water waves if $d < \lambda/20$ [135]. Since d throughout the storm is between $\lambda/2$ and $\lambda/20$, all waves are transitional.

Table 4.1. Wave properties for numerical modeling.

Time (hours)	H_s (m)	T_p (s)	H_s/d	λ (m)	$\lambda/20$ (m)	$\lambda/2$ (m)
0	2.00	10.00	0.21	97.50	4.87	48.75
10	2.59	11.00	0.27	107.20	5.36	53.62
20	3.95	12.80	0.41	124.80	6.24	62.40
30	5.30	13.70	0.55	133.60	6.68	66.79
40	6.04	12.80	0.62	124.80	6.24	62.40
50	5.50	10.80	0.57	105.30	5.26	52.65
60	4.00	8.00	0.41	78.00	3.90	39.00
70	2.10	5.00	0.22	48.70	2.44	24.37
80	1.20	3.30	0.12	32.20	1.61	16.09
90	0.98	2.47	0.10	24.10	1.20	12.04

Submergence depths and elevations were selected such that the bridge deck model was fully elevated (Z_1), partially submerged (Z_2), and fully submerged (Z_3) with respect to the stillwater level (SWL) (Figure 4.4). The different submergence values were chosen to assess how the magnitude of hurricane storm surge would influence the bridge's sensitivity to wave loading. To accurately calculate the structural responses, the spatial distribution of wave forces and moments along the span length was computed at ten different locations, as

indicated by the red circles in Figure 4.4. All simulations were run for 200 s, and the time series of the last 50 s was used in the FEM. To ensure the efficient and timely completion of simulations with high computational complexity, the models were run on the University of Texas at Arlington's high performance computing facility.

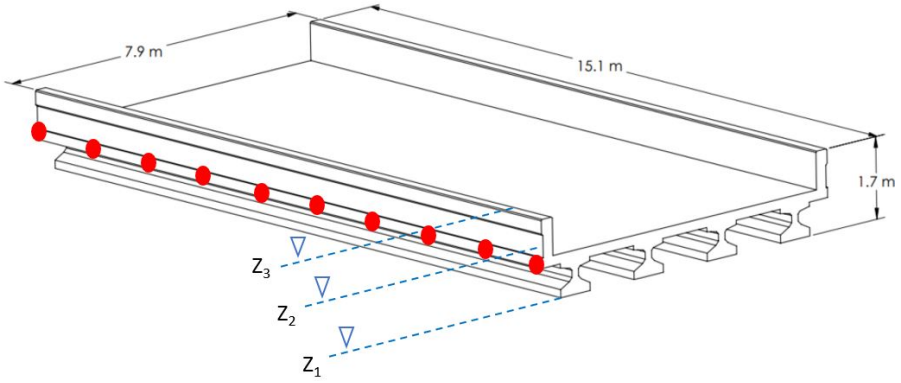

Fig. 4.4. Bridge model segmentation to calculate wave forces.

Coastal bridge deck failure can be caused by horizontal and vertical wave forces and overturning moments. Although these forces and moments combine to drive failure, they are investigated separately for the preliminary structural analysis. Tracing wave loading time histories revealed several significant points that may have an impact on bridge stability, including (1) maximum vertical force $F_{\text{v-max}}$, which could exceed the weight of the bridge deck and cause the deck to lift (uplift failure); (2) maximum horizontal force $F_{\text{h-max}}$, which could produce transverse displacement by exceeding the friction force between the superstructure and substructure (sliding failure); and (3) maximum moment M_{max}, which could topple the deck (overturning failure). This analysis identifies key surge and wave parameters that substantially impact wave loads during the storm. A representative full-scale I-girder (Tx-28) bridge with an 8-m deck width was chosen for the CFD analysis to demonstrate the potential behavior of critical hydrodynamic parameters. The method

described here, however, can be utilized to evaluate the sensitivity of various bridge geometries.

4.3.3 Modeling of Bridge Response

OpenSEES [137], an open-source FEM, was used to examine the structural performance and capacity of the modeled bridge under various storm conditions. Wave forces and moments from the CFD model for the worst-case scenario of higher forces and moments were transferred to the FEM to evaluate bridge response. Bearing constraints were used at the bottom of each beam, as shown in Figure 4.5. The lateral stiffness of the bearing constraints was also defined in the FEM.

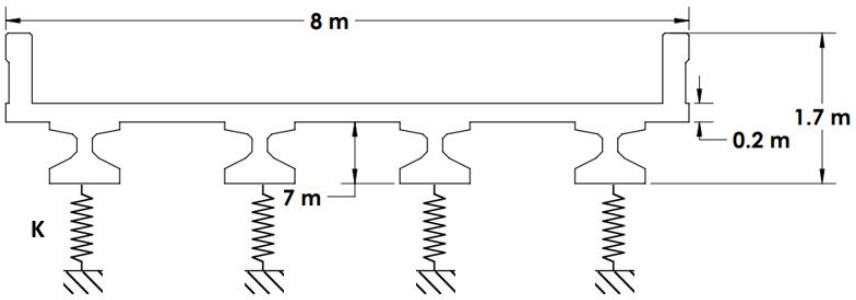

Fig. 4.5. Bridge model with bearing constraints.

The nodal configuration of the FEM is shown in Figure 4.6. Beams were represented as line elements, whereas slabs and railings were represented as shell elements. The material used in all bridge components is elastic isotropic, meaning its properties do not vary with direction. Wave loads and moments extracted from the last 50 s of wave loading were applied on the front beam (Beam-1) nodes, and the bridge response time histories due to wave and gravity loads were recorded at a representative node (N-B1-6).

The structural and material properties used in the FEM are shown in Table 4.2. The Tx-28 girder and beam properties were extracted from the Texas Department of

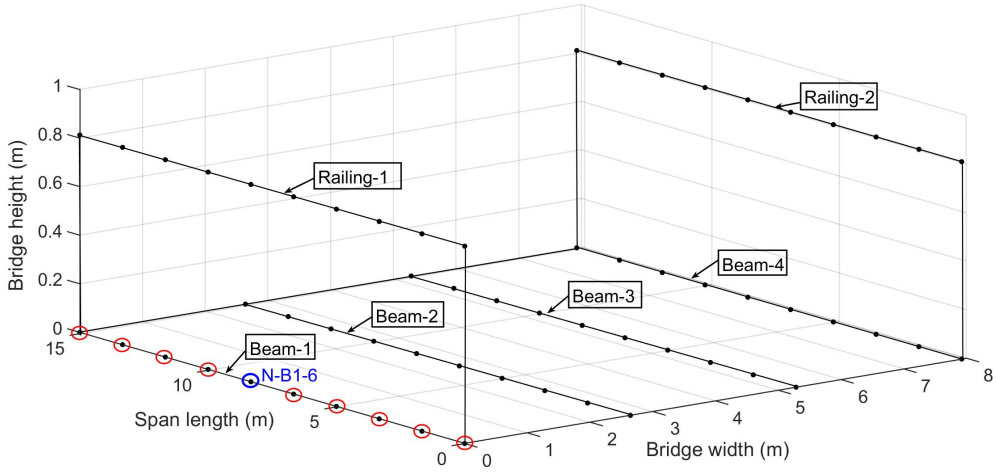

Fig. 4.6. Node configuration of the finite element model.

Transportation's (TxDOT) Bridge Design Manual [138]. TxDOT recommends using a modulus of elasticity of 5,000 ksi for the deck, railing, and girders. The concrete density and lateral stiffness of the bearings were determined from past research on bridge structural response [139, 140].

Table 4.2. Structural properties of modeled bridge.

Parameters	**Values**	**Units**
Cross-sectional area of beam (A_b)	585	in^2
Modulus of elasticity (E)	5,000	ksi
Beam shear modulus (G_b)	2,142	in^4
Beam polar moment of inertia (J_b)	16,986	in^4
Beam moment of inertia along vertical axis (I_{yb})	40,559	in^4
Beam moment of inertia along horizontal axis (I_{xb})	52,772	in^4
Concrete density (γ)	$8.68e^{-5}$	k/in^3
Lateral stiffness of bearings (K_L)	$1e^3$	k/in

Bridges undergo displacement and acceleration due to wave loading [141]. The accelerations associated with excess bridge vibrations can deteriorate bridge components. Furthermore, hydraulic loading may cause vertical and transverse displacements, which

may adversely influence structural elements [6]. Hence, for this study, the transverse and vertical displacements (δ_t and δ_v) and transverse and vertical accelerations (A_t and A_v) were examined to quantify the impacts on bridge performance [142, 7, 143].

4.3.3.1 Uncertainty Analysis

Uncertainties related to material parameters should be considered when examining dynamic bridge response in real-world conditions and identifying potential sources of uncertainty in probabilistic bridge vulnerability modeling. For example, reinforced concrete density may fluctuate from specified values, affecting the bridge's overall capacity [133, 6]. Probabilistic bridge response was computed by incorporating uncertainties in material properties using quoFEM, an open-source research application currently being developed at the University of California Berkeley SimCenter that provides uncertainty quantification methods (i.e., forward, inverse, sensitivity, parameter estimation, and surrogate modeling) to researchers in natural hazards. quoFEM uses the software toolkit Dakota for quantifying uncertainty and performing global sensitivity analysis [144, 145]. Dakota provides a range of methods and algorithms for characterizing uncertainty and identifying the most influential input parameters in complex systems and models [146].

The uncertainty impacts of material parameters were explored using values summarized in Table 4.3. Concrete density, modulus of elasticity, and lateral stiffness of the bearing were chosen based on previous research on bridge modeling parameters [147, 6, 7, 148]. According to [147], the density of reinforced concrete follows a normal distribution with a mean of $8.68e^{-5}$ k/in and a standard deviation of $3.47e^{-6}$ k/in. The probability distributions of modulus of elasticity E and lateral stiffness of bearing K_L were assigned based on a literature review [6, 7]. These material parameter probability distributions were then used as input to run OpenSEES 100 times. Each OpenSEES run yielded maximum values of displacement and acceleration, which were then processed by Dakota to build the structural

response distributions. The response at a representative node (N-B1-6) was utilized for the uncertainty analysis. A global sensitivity was also carried out to assess the most sensitive material parameters to be considered as random variables in the reliability analysis. Sobol sensitivity indices (SSI) were estimated with these random variables. SSI estimates how much each parameter contributes to the variation in the structural response. Figure 4.4 shows the steps used to evaluate the impacts of uncertainty on bridge response.

Table 4.3. Variables for uncertainty analysis with probability distributions and values. Source: [6, 7].

Parameters	**Distribution**	**Values**	**Units**
Modulus of elasticity (E)	Normal	N(5000,500)	ksi
Concrete density (γ)	Normal	N($8.68e^{-5}$,$3.47e^{-6}$)	k/in^3
Lateral stiffness of bearings (K_L)	LogNormal	LN(0.4,0.048)	k/in

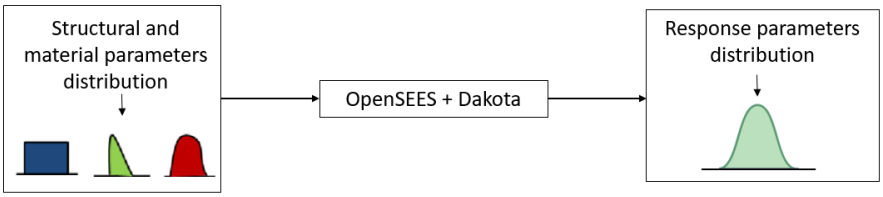

Fig. 4.7. Approach for uncertainty analysis of structural response.

4.3.3.2 Probabilistic Bridge Vulnerability Analysis

A probabilistic bridge vulnerability analysis was conducted using SOFiSTik software to examine the coastal bridge's structural performance and capacity under extreme surge and wave loading. SOFiSTik is a software tool used in the construction industry to analyze and design structures, including buildings and bridges. It offers a range of features for structural analysis, design, and detailing and contains a module called RELY that evaluates

the reliability of engineering structures modeled using finite elements [149]. Monte Carlo simulation (MCS), a third-order reliability method, was used to compute the probability of failures corresponding to each failure mode (i.e., uplift, sliding, and overturning). MCS generates random load and resistance parameter samples and substitutes these samples in the limit state function to compute the probability of failure. MCS was chosen because it is a powerful tool that is simple to deploy and capable of tackling a wide range of reliability problems [150, 151]. The main aim of this task is to determine how the probability of exceeding structural capacity varies based on the given hydrodynamic loading. The probability distribution of structural resistance parameters, including concrete density (γ) and friction factor (μ), were determined using existing literature [147, 6] and are shown in Table 4.4.

Table 4.4. Variables for reliability analysis with probability distributions and values.

Parameters	**Distribution**	**Values**	**Units**
Concrete density (γ)	Normal	N(8.68e^{-5},3.47e^{-6})	k/in^3
Friction factor (μ)	LogNormal	LN(0.4,0.008)	–

In general, the limit state function (Z) of the bridge failure model can be assessed by considering the resistance (R) and the loads (F) [152, 153]:

$$Z = R - F \tag{4.1}$$

Failure occurs when $R < F$. The probability of failure (P_f) is given by:

$$P_{\mathrm{f}} = P[Z < 0] = P[F > R] \tag{4.2}$$

The method for finding the probability of failure using MCS in shown in Figure 4.8.

For uplift failure, the resistance R against $F_{\text{v-max}}$ is mainly provided by the deck weight (W_{d}). The weight of the bridge deck is a function of bridge dimensions, including

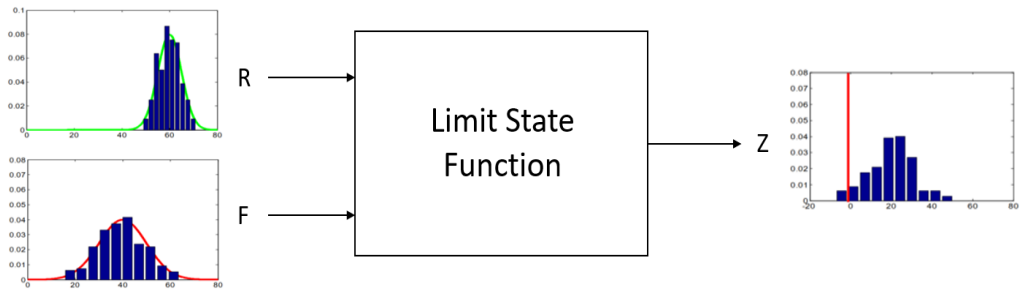

Fig. 4.8. Approach for Monte Carlo simulation.

the deck thickness (d_t), width (b), span length (l), cross-sectional area of the girder (A_g), number of girders (n_g), cross-sectional area of the railing (A_r), and unit weight of reinforced concrete (γ). Z_{uplift} can be calculated as:

$$Z_{\text{uplift}} = W_d - F_{\text{v-max}} \tag{4.3}$$

$$Z_{\text{uplift}} = (d_t b + A_b n_b + A_r n_r)\gamma l - F_{\text{v-max}} \tag{4.4}$$

For sliding failure, the resistance R against $F_{\text{h-max}}$ is provided by the friction force F_f between the bridge deck and bearings. Z_{sliding} can be calculated as:

$$Z_{\text{sliding}} = F_f - F_{\text{h-max}} \tag{4.5}$$

$$Z_{\text{sliding}} = W_d \mu - F_{\text{h-max}} \tag{4.6}$$

For overturning failure, the resistance R against M_{max} is a function of resisting moment M_R due to the W_d. $Z_{\text{overturning}}$ can be calculated as:

$$Z_{\text{overturning}} = M_R - M_{\text{max}} \tag{4.7}$$

In the reliability analysis, the loads were considered deterministic. For the resistance parameters considered here (i.e., μ and γ), 100,000 random numbers were generated based on the probability distributions. The generated random numbers were then put into the limit state function for each failure mode. P_f was calculated by dividing the number of

failed samples (where the load is greater than resistance) by the total number of samples generated. By varying the deterministic load with this approach, fragility curves for each failure mechanism were developed for the coastal bridge.

4.4 Results

4.4.1 Wave Induced Forces and Moments

Figure 4.9 shows the wave force and moment time histories for an example scenario (i.e., at the 30th hour of the storm) with H_s = 5.3 m and T_p = 13.7 s when SWL is at Z_1 (panel a), Z_2 (panel b), and Z_3 (panel c). The vertical and horizontal wave forces and moments rise to a peak and then decrease as the wave crest passes over the bridge. The peak $F_{\text{v-max}}$ is significantly greater than the peak $F_{\text{h-max}}$. The largest magnitude of wave forces and moments are observed when SWL is at Z_1. The sharp peaks in wave forces observed under these conditions indicate the impulsive or slamming forces and wave impacts experienced by the girders. Comparing the time histories of wave loading reveals various notable occurrences that might affect structural stability, as discussed in the next section.

4.4.2 Bridge Deck Failure Mechanisms

Figure 4.10 shows the peak values of $F_{\text{h-max}}$, $F_{\text{v-max}}$, M_{max} extracted from the wave loading time series at each 10-hr interval during the storm. Values are shown separately for each of the three bridge deck elevations. The dashed line in each graph indicates the limit of structural resistance (i.e., F_f = 55.6 kN for horizontal forces, W_d = 139 kN for vertical forces, and M_R = 545 kN-m for overturning moments). W_d was computed using a standard γ of 2,400 kg/m^3, and F_f was estimated using μ = 0.4.

During the storm, the wave forces experienced by the bridge vary significantly depending on the water level and the characteristics of the storm. The largest values of $F_{\text{h-max}}$ and M_{max} are observed at the 30th hour of the storm, when T_p and λ have the highest

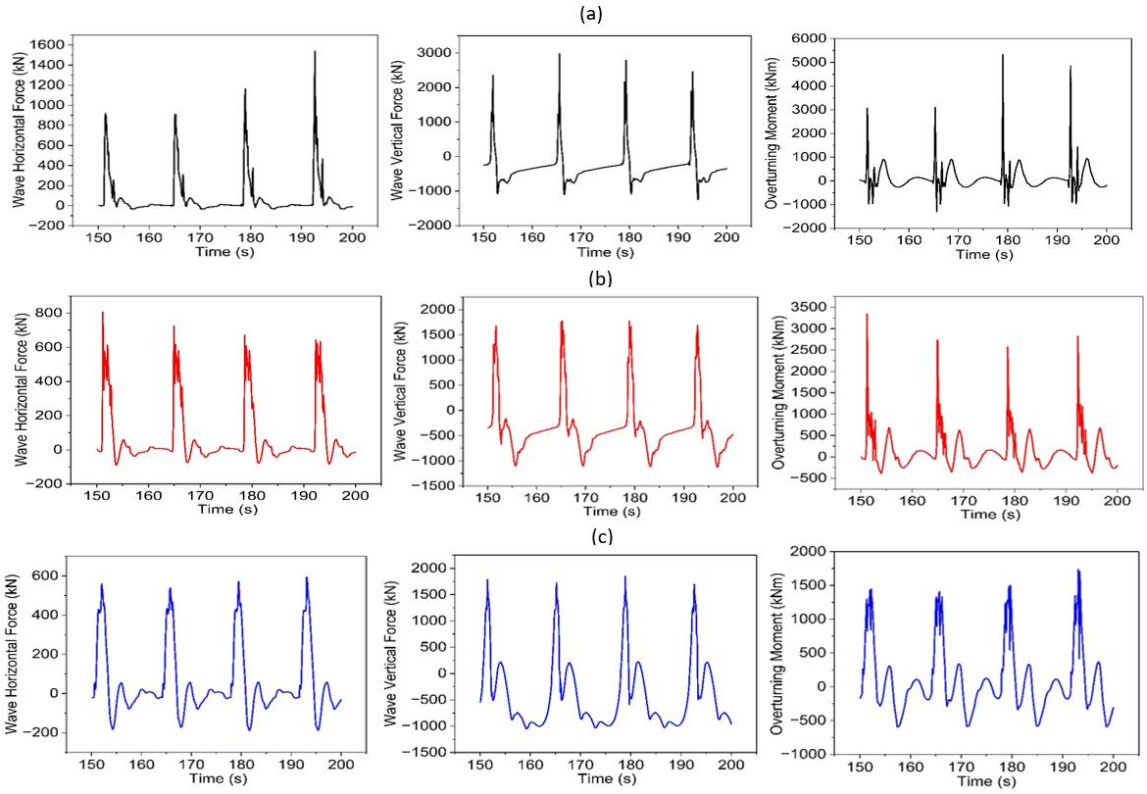

Fig. 4.9. Time history of wave loading at the 30th hour of the storm when stillwater level is at (a) Z_1, (b) Z_2, and (c) Z_3.

values. This pattern is consistent across all bridge deck elevation scenarios, with the worst case loading occurring when the bridge superstructure is placed above the SWL (Z_1). The Z_1 scenario results in an $F_{\text{h-max}}$ value that is 22% greater than for Z_2 and 45% greater than for Z_3. Similarly, the M_{max} value for Z_1 is 65% greater than for Z_2 and 100% greater than for Z_3. When the bridge is partially (Z_2) or fully (Z_3) inundated, the maximum $F_{\text{v-max}}$ is observed at the 40th hour of the storm, when the wave has the highest H_{s}. However, when the bridge is fully elevated above the SWL (Z_1), the maximum $F_{\text{v-max}}$ is observed at the 20th hour of the storm. The $F_{\text{v-max}}$ value experienced by the bridge at Z_1 is 10% greater than for Z_2 and 19% greater than for Z_3.

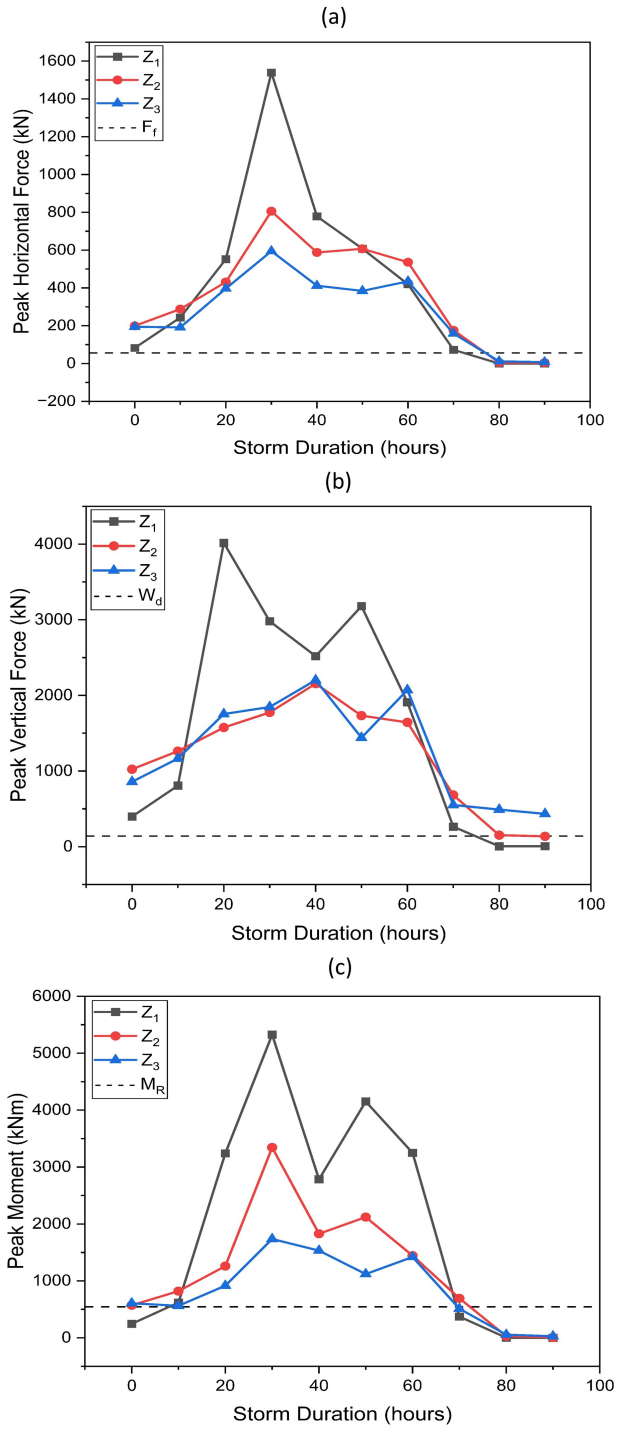

Fig. 4.10. Peak (a) horizontal forces, (b) vertical forces, and (c) overturning moments across stillwater level scenarios.

4.4.3 Structural Response

Figure 4.11 shows the displacement and acceleration time histories at representative node N-B1-6 for the worst scenario identified in CFD modeling (i.e., at the 30th hour of the storm) at different bridge deck elevations. The transverse and vertical displacement time series are in phase with the transverse and vertical wave loading on the bridge deck. Following the wave response time series, the maximum transverse and vertical displacements occur when the bridge is fully elevated over SWL (Z_1). The peak transverse and vertical displacements are 0.056 in and 0.12 in, respectively. The American Association of State Highway and Transportation Officials (AASHTO) load-and-resistance factor design (LRFD) guidelines define a live load deflection limit criterion of $l/1000$ for pedestrian and traffic bridges with span length l. For the bridge considered here, this limit criterion equals 0.59 in. Vertical displacement due to wave loads is only 21% of the overall deflection limit, while transverse displacement is only 10%.

The maximum transverse and vertical accelerations also occur when the bridge is fully elevated over SWL (Z_1). The peak transverse and vertical accelerations are 157 in/s^2 and 210 in/s^2, respectively. The Federal Highway Administration (FHWA) LRFD for highway bridge superstructures proposed an acceleration limit of 100 in/s^2 [154] based on research done by [155]. Eurocode provides a bridge deck acceleration limit of 138 in/s^2 [156] for railway and highway bridges. Hence, the peak transverse and vertical accelerations exceed the proposed limit of the standards, suggesting that the most extreme wave loading conditions during Hurricane Ike can damage the representative coastal bridge deck due to high-intensity vibrations.

4.4.4 Uncertainty in Structural Response

The spectral parameters of the structural response distribution are shown in Table 4.5. Figure 4.12 shows the probability density and cumulative probability of transverse

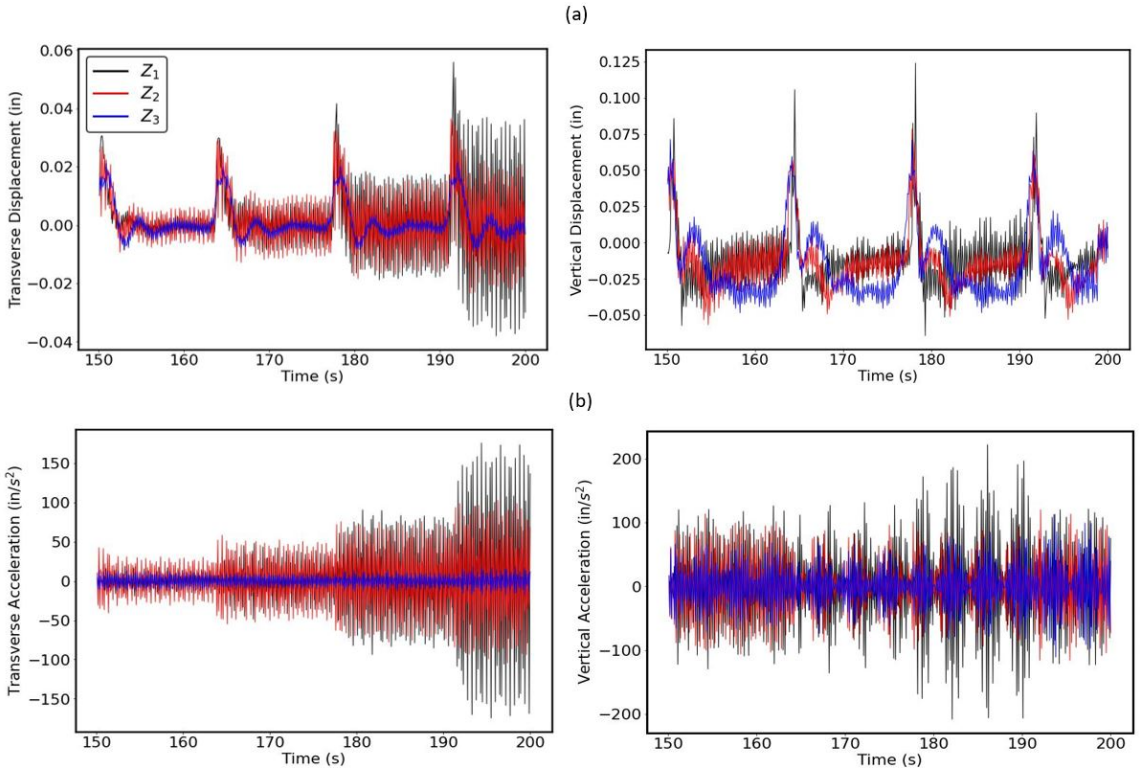

Fig. 4.11. Time history of (a) transverse and vertical displacements and (b) transverse and vertical accelerations at node N-B1-6.

and vertical displacements when uncertainties in the material properties are considered. The uncertainty analysis yields a mean of 0.053 in with a standard deviation of 0.0064 in for transverse displacement and a mean of 0.127 in with a standard deviation of 0.031 in for vertical displacement.

Table 4.5. Spectral parameters of structural response distributions for transverse displacement (δ_t), vertical displacement (δ_v), transverse acceleration (A_t), and transverse acceleration (A_v).

Parameters	**Mean**	**Standard deviation**	**Skewness**	**Kurtosis**
δ_t (in)	0.13	0.03	0.90	4.05
δ_v (in)	0.05	0.001	0.17	2.75
A_t (in/s^2)	99.64	37.87	0.80	2.50
A_v (in/s^2)	301.31	125.15	0.80	2.82

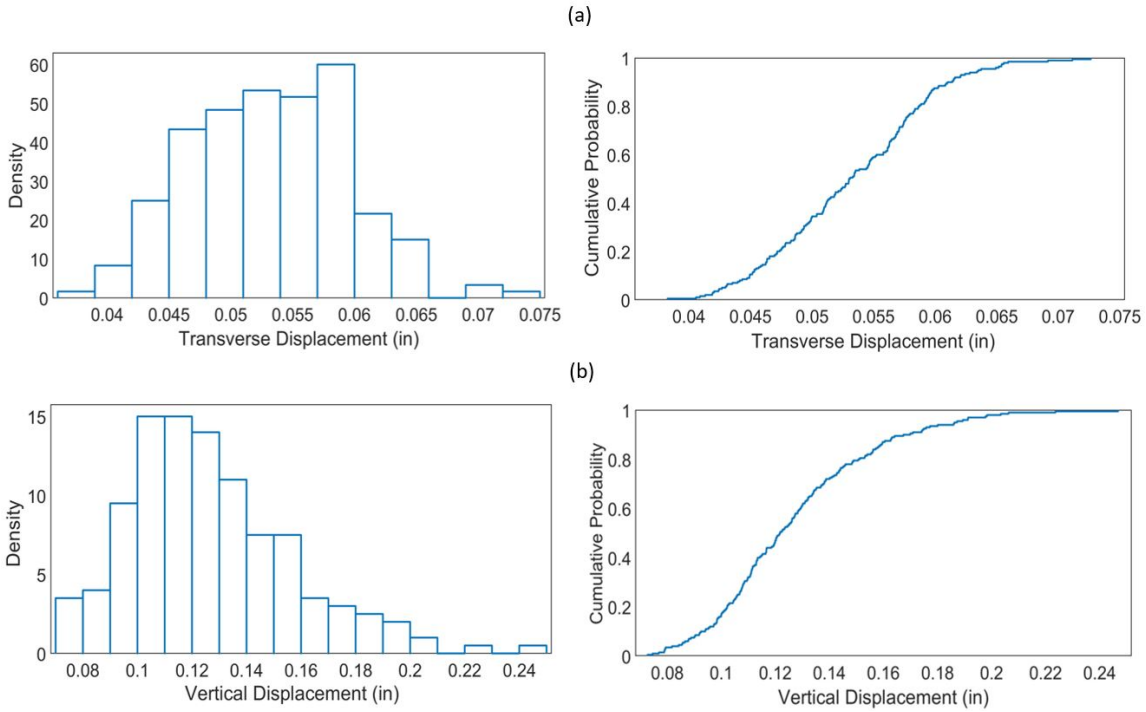

Fig. 4.12. Density and cumulative probability of (a) transverse and (b) vertical displacements.

Figure 4.13 shows the probability density and cumulative probability of transverse and vertical accelerations. The uncertainty analysis yields a mean of 99.6 in/s^2 with a standard deviation of 37.9 in/s^2 for transverse acceleration and a mean of 301.3 in/s^2 with a standard deviation of 125.2 in/s^2 for vertical acceleration.

4.4.5 Sensitivity Analysis

Sensitivity analysis provides information about the contribution of each input random variable to the uncertainty in bridge response and reveals the impacts of potential variations in material properties on the dynamic response of bridges. After running the OpenSEES FEM 100 times, the total SSI for the bridge's transverse and vertical displacements and transverse and vertical accelerations was calculated (Table 4.6). Concrete density has the highest SSI for vertical displacement (0.632) and vertical acceleration (0.675). The

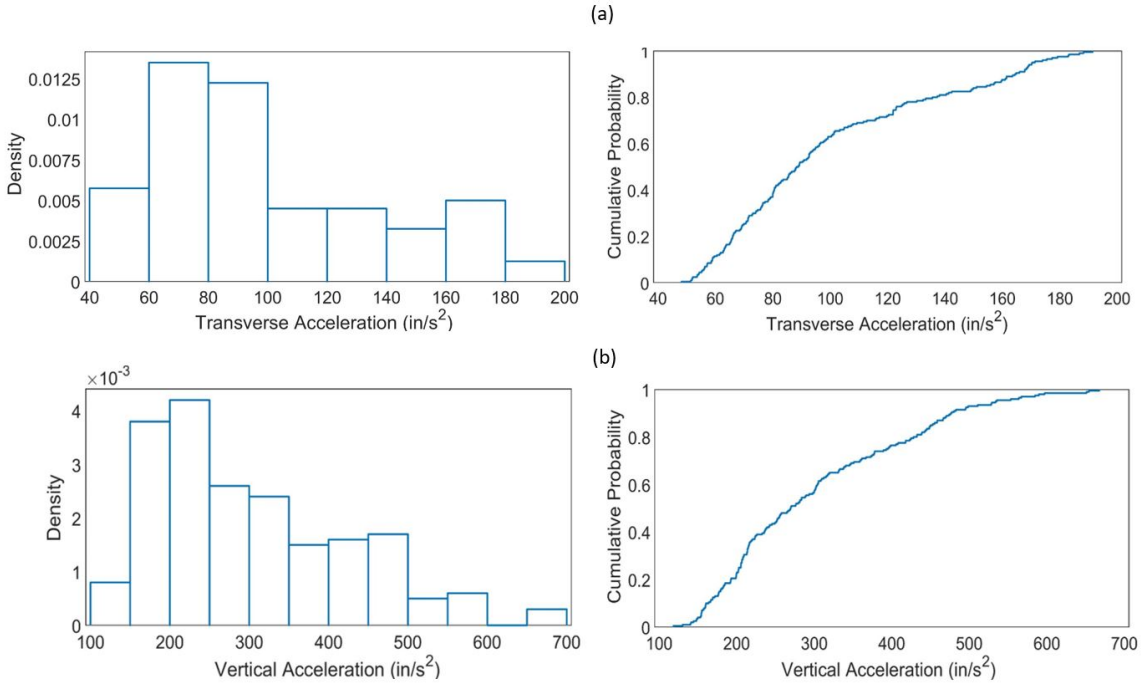

Fig. 4.13. Density and cumulative probability of (a) transverse and (b) vertical accelerations.

lateral stiffness of bearings significantly impacts horizontal response, with the highest SSI for transverse displacement (0.567) and transverse acceleration (0.505). The modulus of elasticity has a smaller impact on bridge response, mostly strongly affecting transverse displacement (SSI = 0.172) and acceleration (SSI = 0.189) and having a negligible effect on vertical acceleration.

Table 4.6. Sobol sensitivity indices for bridge parameters.

Random Variable	**SSI (δ_t)**	**SSI (δ_v)**	**SSI (A_t)**	**SSI (A_v)**
Modulus of elasticity (E)	0.172	0.13	0.189	0.015
Concrete density (γ)	0.262	0.632	0.306	0.675
Lateral stiffness of bearings (K_L)	0.567	0.238	0.505	0.311

4.4.6 Probabilistic Bridge Vulnerability Analysis

The probability of a bridge failing under a particular load is shown in Figure 4.14. In general, the failure probability increases with increasing wave loading, and the impact of small wave loads on the bridge is small, consistent with past studies [7]. In the fragility curves, $P_f = 0$ corresponds to no damage, meaning the structure is fully reliable. $P_f = 1$ denotes a 100% probability of failure. Previous studies suggested the need for retrofitting bridges if $P_f \geq 0.5$ and indicated that bridges should only be operational if $P_f < 0.5$ [157, 158]. Hence, $0.5 \leq P_f \leq 1$ is the critical zone for the bridge structure. From the fragility curves, this zone is 38–60 kN for horizontal stability, 95–120 kN for vertical stability, and 375–450 kNm for overturning moment. During Hurricane Ike, the bridge is subjected to wave forces that surpass its resistance to sliding and uplifting for a large portion of the storm (80% and 93% of the storm's duration, respectively). The bridge's resistance to overturning is also exceeded for 73% of the storm duration.

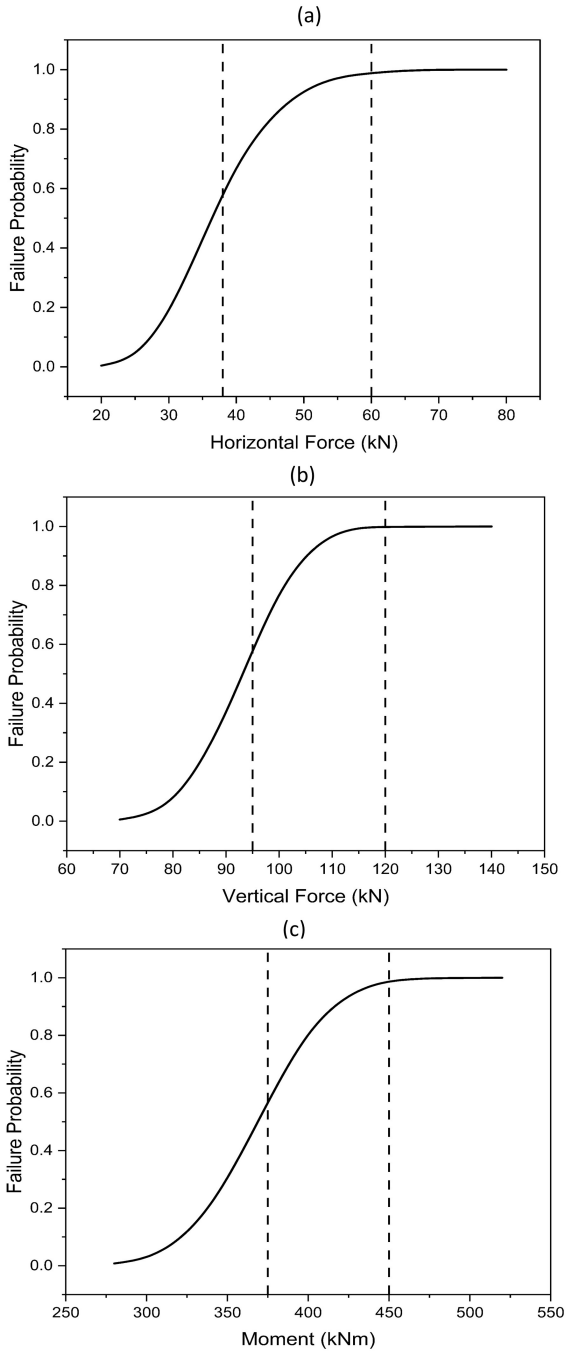

Fig. 4.14. Fragility curves for (a) sliding, (b) uplifting, and (c) overturning of the coastal bridge.

4.5 Discussion

The results of this study indicate that waves with the highest peak periods and longest wavelengths are the main contributing factors to bridge instability. This suggests that these types of waves may be more likely to cause significant structural damage or failure, especially if a bridge is not designed to withstand such loads. The vertical wave forces modeled for Hurricane Ike are almost twice as large as the horizontal wave forces. The larger vertical wave forces can reduce the vertical stability of the bridge and can result in vertical displacements or uplifting, which could affect the stability and integrity of the bridge. Throughout Hurricane Ike, the extreme wave loading exceeds the bridge resistance in more than 70% of the time history for every failure mode, indicating the need for a more sophisticated bridge design to more effectively resist wave loading. Overall, this analysis reflects the maximum magnitude of wave loading a bridge may encounter during a hurricane hazard and helps define limit states for the investigated failure modes (i.e., sliding, uplifting, and overturning).

The modeled bridge exhibits the largest structural response when fully elevated over SWL, as this scenario creates impulsive loads characterized by large magnitude and short duration that directly impact the superstructure. For the fully elevated condition, the bridge's horizontal and transverse displacements are well within the upper deflection limit specified by AASHTO LRFD. Thus, wave-induced deflections are not a primary concern for the representative bridge during Hurricane Ike. In contrast, the transverse and horizontal accelerations exceed the limit proposed by the design standards considered here (i.e., FHWA LRFD and Eurocode). In fact, the peak vertical acceleration is more than twice the FHWA LRFD limit. This high acceleration can lead to damage to the bridge deck due to high-intensity vibrations. It is thus recommended to pay particular attention to structural accelerations in the design of coastal bridges. The acceleration data from this

analysis can be translated into the frequency domain to determine peak amplitudes and corresponding frequencies to support bridge design [159].

The sensitivity analysis of material parameters reveals that concrete density is the most sensitive parameter in the case of vertical stability of the bridge deck, as it is directly related to the bridge's weight, which is the sole parameter that opposes the vertical load. Hence, it may be necessary to carefully consider the density of concrete used in the bridge design to ensure adequate vertical stability. In the case of horizontal stability, the lateral stiffness of the bearing is the most sensitive parameter, and it may be essential to optimize the lateral stiffness of the bridge to ensure adequate horizontal stability. The findings about the most sensitive parameters can be used to identify potential designs or countermeasures that can be implemented to improve the stability of a bridge. For example, since concrete density is determined as a critical parameter for vertical stability, it may be necessary to adopt measures such as increasing the thickness of the concrete deck or using higher-density concrete to improve the vertical stability of the bridge. Furthermore, the most sensitive parameters can also help identify potential maintenance issues that may need to be addressed to maintain the stability and performance of a bridge. To maintain adequate horizontal stability, it may be necessary to conduct regular inspections of the bearing system to verify its condition and ensure that it is capable of providing adequate lateral stiffness. For vertical stability, it may be important to carefully assess the condition of the concrete deck during inspections to ensure that deterioration or loss of capacity has not occurred. This study's sensitivity analysis results can thus guide the focus of bridge inspections and evaluations.

The probabilistic vulnerability model developed in this study aims to address gaps in understanding the failure mechanisms of coastal bridges subjected to hurricane wave impacts by considering uncertainty in both the structural demand and capacity and by quantifying the effects of wave forces and overturning moments. The fragility curves

developed using this model suggest that significant wave heights greater than 2 meters and wave peak periods greater than 5 seconds produce wave forces and moments for which the probability of failure is 1. These findings can be useful for risk assessment, management, maintenance, and design of coastal bridges. The fragility curves can also be used to assess the long-term damage loss of coastal bridges by providing the conditional probability of failure.

Finally, the study recommends further investigation into the performance of potential countermeasures to improve the resilience of coastal bridge decks against wave loading. Several potential countermeasures can be considered to reduce accelerations and displacements resulting from wave loading on bridges. Structural strengthening measures can be used to improve the capacity of a bridge to resist wave loading. This could involve using advanced materials, such as fiber-reinforced composites or high-strength concrete [148, 109]. Furthermore, dynamic damping systems can be used to reduce vibrations or oscillations caused by wave loading on a bridge. These systems can be passive (e.g., tuned mass dampers) or active (e.g., piezoelectric dampers) and can help reduce the bridge's dynamic response and improve its performance [12, 108, 160].

The probabilistic framework presented here provides an important step in addressing the recognized need for more detailed and comprehensive bridge vulnerability models that consider material uncertainty [161, 148]. However, there are several limitations that can be addressed in future work. While this study focused on modeling hydrodynamic loading using regular waves, simulating irregular waves would provide a more accurate depiction of the expected loading on bridge decks. In the structural modeling, a single degree of freedom system was used to simulate the structure's reaction to wave loading. Including multiple degrees of freedom would provide a more precise prediction of a bridge deck's motion when a wave strikes it. Furthermore, the failure model used here evaluates all failure modes individually. Compared to the combined failure modes, this approach may

underestimate the hurricane-induced risk to coastal bridges. This study also does not discuss the impacts of entrapped air on wave loading, which can increase buoyancy forces and impact the bridge's vertical stability [12].

4.6 Conclusion

Recent hurricane disasters have emphasized the vulnerability of coastal bridges to surge and wave loads. As a result, it is necessary to establish a reliable approach for probabilistic assessment of the susceptibility of existing coastal bridge inventories to hurricane-induced loading. This research presents a framework for analyzing the probabilistic vulnerability of coastal bridges subjected to hurricane hazards using CFD, FEM, and probabilistic numerical simulations. For the failure mechanisms examined (i.e., uplift, sliding, and overturning), limit states are established. The uncertainty caused by the properties of the structural materials is examined, and a sensitivity study of a coastal bridge's response under probable variations in bridge material parameters is conducted. Fragility curves are computed using reliability analysis approaches, which can be used for long-term damage assessment.

Simulations of wave-deck interactions demonstrate that waves with the highest peak periods and longest wavelengths were the main cause of bridge instability. During Hurricane Ike, extreme wave loading exceeded the bridge resistance for more than 70% of the simulation period for every failure mode. Furthermore, although the bridge's transverse and vertical displacements are within the range specified by AASHTO LRFD, its transverse and vertical accelerations exceed the limits proposed by the FHWA LRFD and Eurocode design standards. This research thus provides critical information on the potential for bridge failure during storm events and can inform bridge safety and vulnerability assessments. Other types of highway bridges and the consequences of changing climate will be examined in future research. Although this probabilistic framework was developed for

coastal bridges, the approach can also be used for riverine bridge risk assessment (Chapter 3).

CHAPTER 5

Conclusions

This dissertation advances the transportation community's research needs by developing validated computational frameworks to improve the assessment of hydrodynamic impacts on bridges in riverine and coastal areas. In particular, the presented research (a) investigates the effects of climate change and urbanization on peak discharges, flow velocity, and bridge freeboard encroachment in 19 watersheds of Harris County, Texas, to support regional transportation asset management; (b) quantifies hydrodynamic loading conditions on a range of bridge superstructures to inform the design of failure countermeasures and evaluates the feasibility of using scaled-model experiments to predict conditions at full-scale bridges using similitude theory, and (c) develops a modeling framework that allows for seamless simulation of surge and wave forces and structural response to assess failure risk for coastal bridges. The bridge vulnerability assessment approaches presented in this study can assist decision-makers in identifying potentially vulnerable bridges and prioritizing maintenance, retrofitting, or replacement efforts that reduce susceptibility to extreme flood events.

Chapter 2 of this study presents a regional screening tool to assess the impacts of climate change and urbanization on stream-crossing bridges in Harris County, Texas. The framework improves upon previous studies by applying hydrologic and hydraulic models to simulate local flow conditions at bridge locations based on meteorological inputs and land use in the contributing watersheds. The findings suggest that projected changes in precipitation have a more significant impact on peak flows than projected changes in urbanization. In addition, bridge vulnerability to loss of freeboard or increased flow velocity

due to higher peak flows is observed across all 19 watersheds studied. Increases in peak flows and resulting impacts to bridges are projected to be greater from 2010 to 2050 than from 2050 to 2100, highlighting the importance of incorporating climate non-stationarity and changes in urbanization into current bridge design and hydraulic analysis guidelines to address potential impacts by mid-century. Overall, outputs from the presented bridge vulnerability assessment approach can assist decision-makers in identifying potentially vulnerable bridges and prioritizing investments that reduce the impacts of expected climate change and urbanization.

Chapter 3 quantifies the magnitude of hydrodynamic forces on bridge decks under a range of flow conditions using computational fluid dynamics (CFD) modeling. The CFD results show that hydrodynamic force and moment coefficients can vary substantially based on flow characteristics, bridge geometries, and debris configurations, highlighting the need for more detailed hydrodynamic loading guidelines that account for such variations. Although the numerical models used in the study do not capture the entire range of behavior observed in corresponding physical modeling experiments, the estimation of hydrodynamic forces is similar enough to be useful in understanding the impacts of flood forces on bridge structures. The CFD results performed across a range of scaling ratios indicate that maintaining Froude number similitude is sufficient to prevent scaling effects, thus allowing results from scaled physical and numerical modeling approaches to be applied to quantify loading on full-scale bridge structures.

Chapter 4 assesses probabilistic failure risk for coastal bridges subjected to surge and wave loading through an integrated modeling framework that couples hydrodynamic modeling of coastal water levels and velocities, CFD modeling of resulting forces, finite element modeling of structural response, and uncertainty quantification. Based on wave conditions from Hurricane Ike, the results suggest that the waves with the highest peak period and longest wavelength are the leading causes of bridge instability. Furthermore,

although simulated bridge displacements are within the limits specified in bridge design standards, peak accelerations exceed the limits, suggesting the need to carefully consider wave-induced accelerations when assessing the safety and reliability of coastal bridges. The fragility curves developed in this study indicate that the bridge experiences damage or failure in all three failure modes (i.e., horizontal stability, vertical stability, and overturning moment) during Hurricane Ike due to extreme wave loading. Although this probabilistic framework was developed for coastal bridges, the approach can also be used for riverine bridge risk assessment.

Overall, the results of this dissertation can be used to improve the safety, reliability, and resilience of bridges during extreme weather events, such as floods and hurricanes. The study's focus on the impacts of climate change and urbanization on peak flood discharges and their associated uncertainties can be used in the development of design guidelines that account for variations in force and moment coefficients across a range of flow conditions and are thus more responsive to the specific hydrodynamic loading conditions that bridges may be subjected to during extreme weather events. Additionally, the fragility curves developed in this study can be used to assess the likelihood of a bridge experiencing damage or failure under different hydrodynamic loading conditions and can inform the design of new bridges and the decision of whether to repair or retrofit existing bridges. Future work will focus on extending the proposed frameworks to account for irregular wave and unsteady flow conditions, to improve the complexity of the structural behavior modeling, and to expand the application of the frameworks to a broader study area to access their transferability.

APPENDIX A

Effects of Climate Change and Urbanization on Bridge Flood Vulnerability: A Regional Assessment for Harris County, Texas

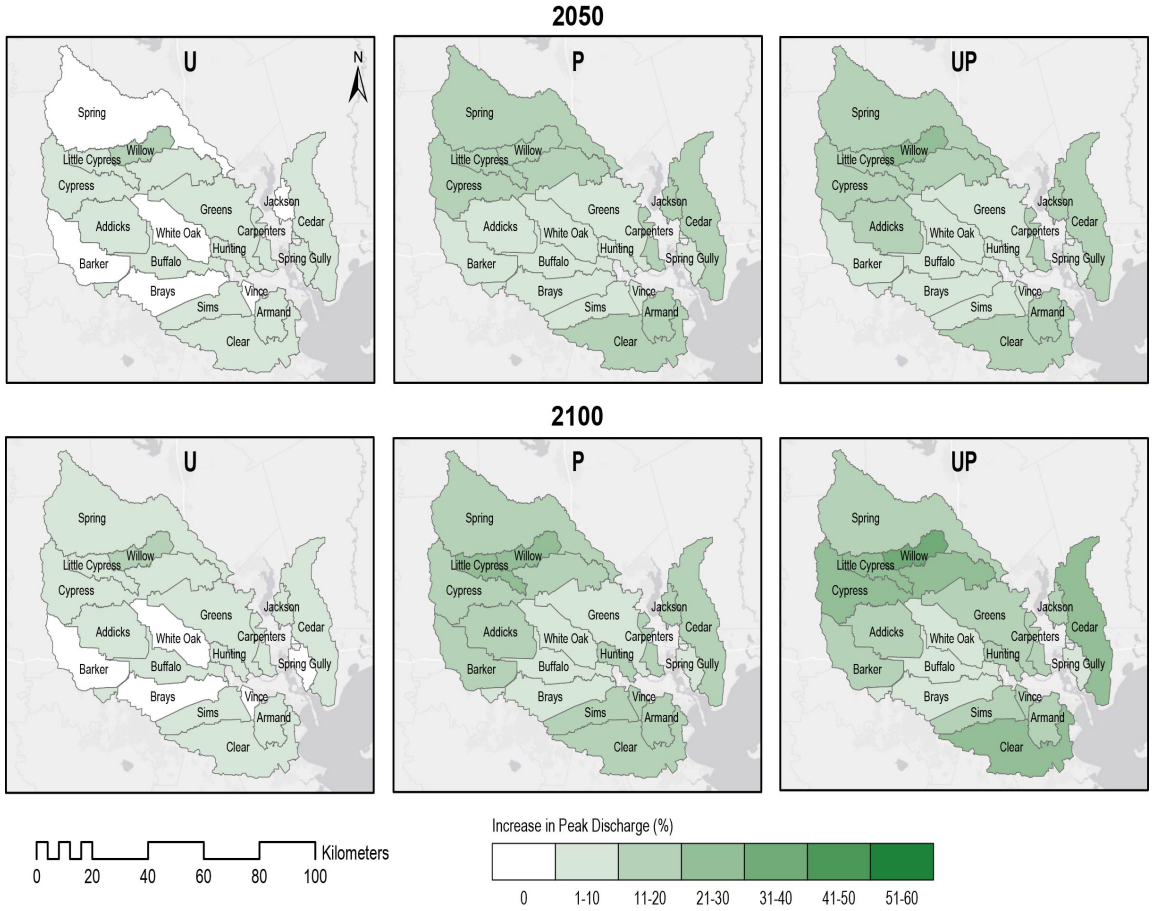

Fig. A.1. Increase in peak discharge for 1% AEP event.

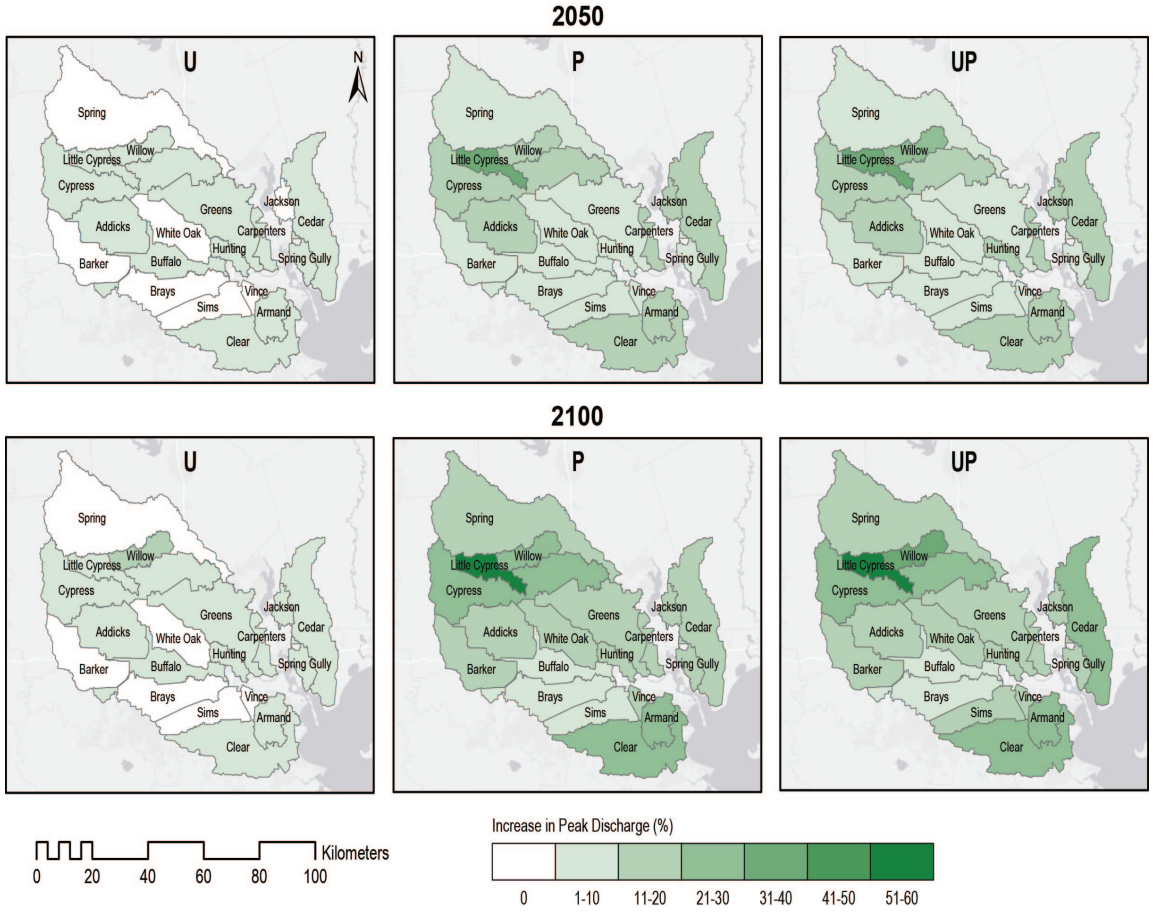

Fig. A.2. Increase in peak discharge for 0.2% AEP event.

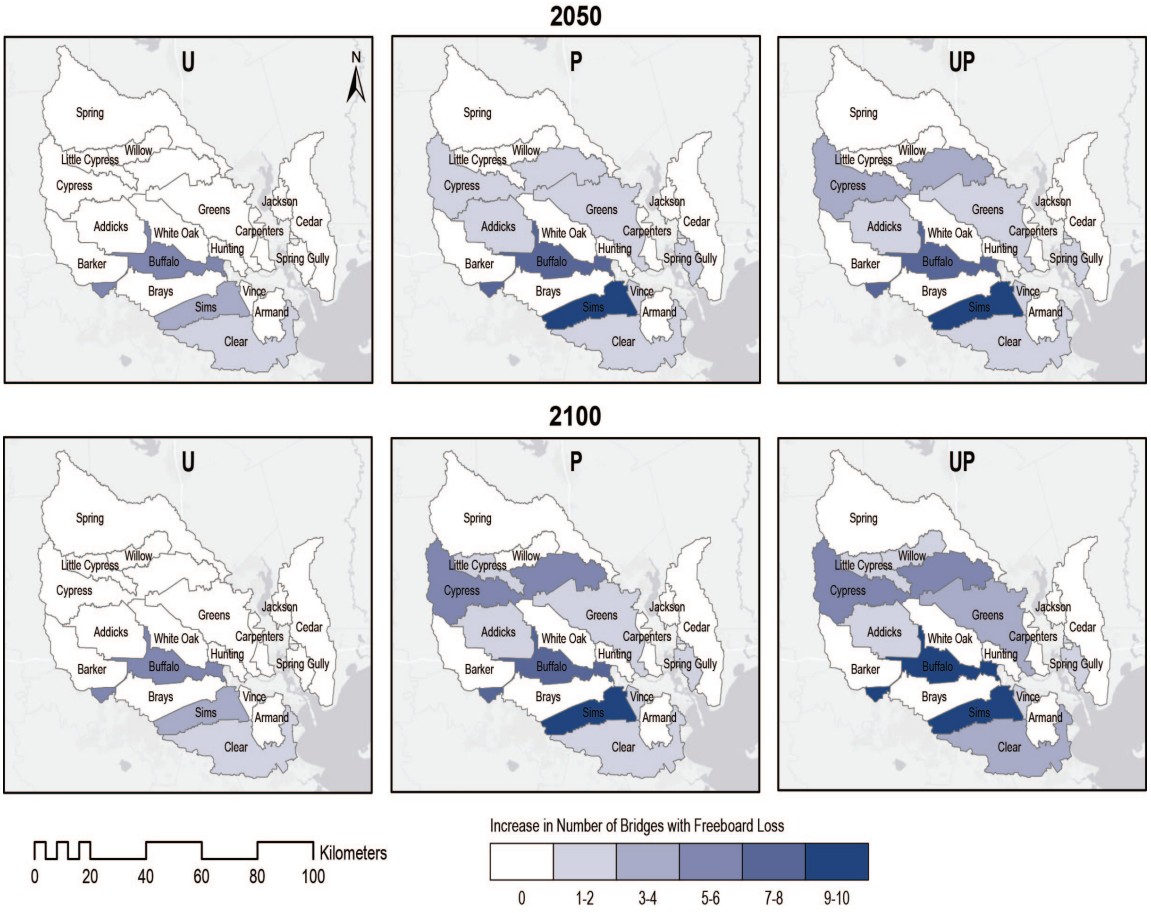

Fig. A.3. Increase in number of bridges with freeboard loss for 1% AEP event.

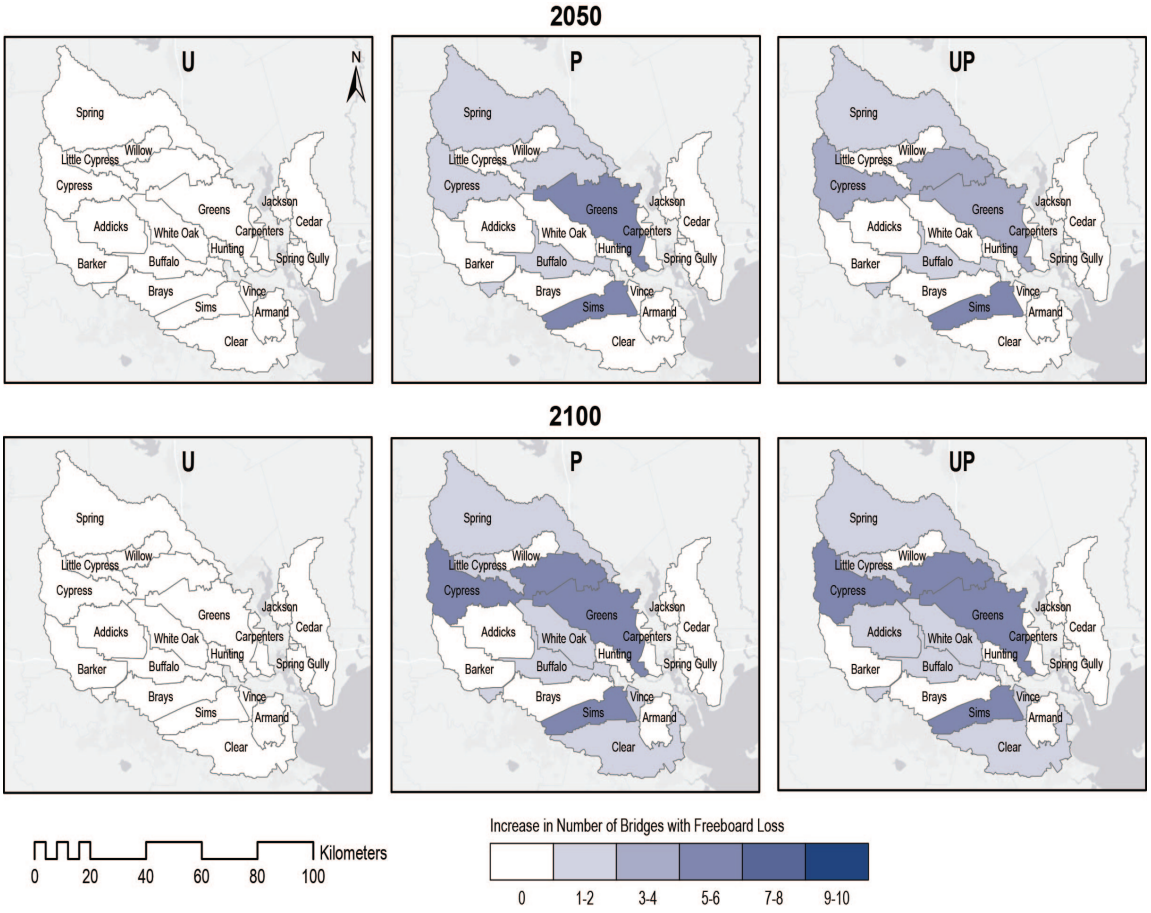

Fig. A.4. Increase in number of bridges with freeboard loss for 0.2% AEP event.

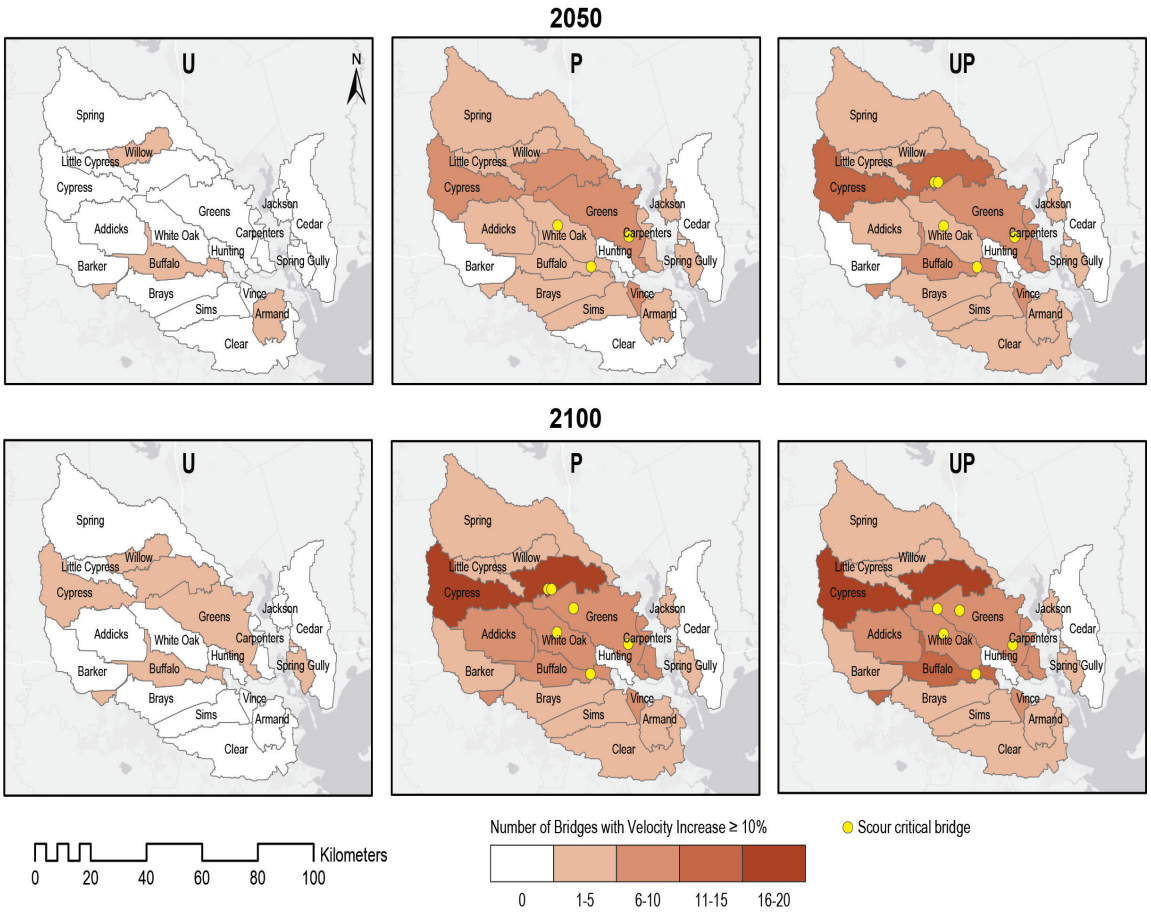

Fig. A.5. Number of bridges with velocity increase ≥10% for 1% AEP event.

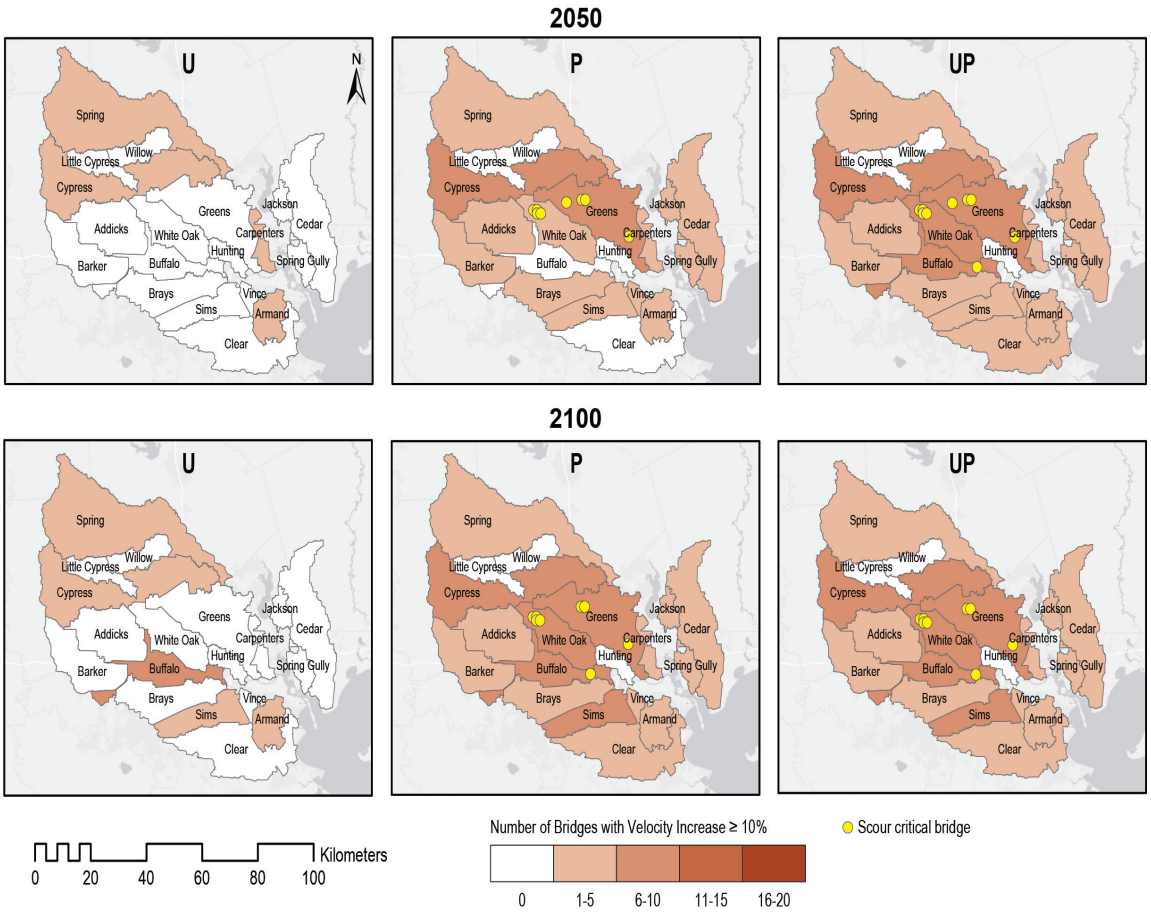

Fig. A.6. Number of bridges with velocity increase ≥10% for 0.2% AEP event.

References

[1] T. L. Sohl, K. L. Sayler, M. A. Bouchard, R. R. Reker, A. M. Friesz, S. L. Bennett, B. M. Sleeter, R. R. Sleeter, T. Wilson, C. Soulard, *et al.*, "Spatially explicit modeling of 1992–2100 land cover and forest stand age for the conterminous united states," *Ecological Applications*, vol. 24, no. 5, pp. 1015–1036, 2014.

[2] J. Muller, J. Figlus, and S. De Vries, "Xbeach simulation of hybrid coastal protection: a galveston seawall test case," *Coastal Engineering Proceedings*, no. 36, pp. 100–100, 2018.

[3] Harris County Flood Control District, "Model and Map Management System," 2021. [Online]. Available: https://www.hcfcd.org/Resources/Interactive-Mapping-Tools/Model-and-Map-Management-M3-System

[4] U.S. Census Bureau, "County Population Totals," 2021. [Online]. Available: https://www.census.gov/data/tables/time-series/demo/popest/2020s-counties-total.html

[5] Texas Department of Transportation, "Bridge Design Manual," 2020. [Online]. Available: https://www.txdot.gov/

[6] N. Ataei and J. E. Padgett, "Probabilistic modeling of bridge deck unseating during hurricane events," *Journal of Bridge Engineering*, vol. 18, no. 4, pp. 275–286, 2013.

[7] D. Zhu, Y. Li, Y. Dong, and P. Yuan, "Long-term loss assessment of coastal bridges from hurricanes incorporating overturning failure mode," *Advances in Bridge Engineering*, vol. 2, no. 1, pp. 1–15, 2021.

[8] M. J. Hammond, A. S. Chen, S. Djordjević, D. Butler, and O. Mark, "Urban flood impact assessment: A state-of-the-art review," *Urban Water Journal*, vol. 12, no. 1, pp. 14–29, 2015.

[9] T. McAllister and T. McAllister, *Developing guidelines and standards for disaster resilience of the built environment: A research needs assessment*. US Department of Commerce, National Institute of Standards and Technology . . . , 2013.

[10] National Oceanic and Atmospheric Administration, "Billion-dollar weather and climate disasters," 2022. [Online]. Available: https://www.ncdc.noaa.gov/billions/summary-stats#temporal-comparison-div

[11] M. Pregnolato, "Bridge safety is not for granted–a novel approach to bridge management," *Engineering Structures*, vol. 196, p. 109193, 2019.

[12] X. Chen, Z. Chen, G. Xu, X. Zhuo, and Q. Deng, "Review of wave forces on bridge decks with experimental and numerical methods," *Advances in Bridge Engineering*, vol. 2, no. 1, pp. 1–24, 2021.

[13] K. Kerenyi, T. Sofu, and J. Guo, "Hydrodynamic forces on inundated bridge decks," 2009.

[14] J. D. Bricker, K. Kawashima, and A. Nakayama, "Cfd analysis of bridge deck failure due to tsunami," in *Proceedings of the international symposium on engineering lessons learned from the 2011 Great East Japan Earthquake*, 2012, pp. 1–4.

[15] Rob Jordan, "When bridges collapse: Stanford researchers study whether we're underestimating the risk," 2017. [Online]. Available: https://news.stanford.edu/press-releases/2017/04/28/bridges-collapserestimating-risk/

[16] Federal Highway Administration, "Bridges and Structures," 2022. [Online]. Available: https://www.fhwa.dot.gov/bridge/

[17] N. Naderi, "Numerical simulation of hydrodynamic forces on bridge decks," 2018.

[18] M. Hayatdavoodi, R. C. Ertekin, I. N. Robertson, and H. R. Riggs, "Vulnerability assessment of coastal bridges on oahu impacted by storm surge and waves," *Natural Hazards*, vol. 79, no. 2, pp. 1133–1157, 2015.

[19] S. Kara, T. Stoesser, T. W. Sturm, and S. Mulahasan, "Flow dynamics through a submerged bridge opening with overtopping," *Journal of Hydraulic Research*, vol. 53, no. 2, pp. 186–195, 2015.

[20] T. C. Stamey, "Floods in central and southwestern georgia in july 1994." Georgia Institute of Technology, 1995.

[21] J. Padgett, R. DesRoches, B. Nielson, M. Yashinsky, O.-S. Kwon, N. Burdette, and E. Tavera, "Bridge damage and repair costs from hurricane katrina," *Journal of Bridge Engineering*, vol. 13, no. 1, pp. 6–14, 2008.

[22] D. M. Sheppard, J. Marin, *et al.*, "Wave loading on bridge decks: final report, december 2009." 2009.

[23] M. Stearns and J. E. Padgett, "Impact of 2008 hurricane ike on bridge infrastructure in the houston/galveston region," *Journal of Performance of Constructed Facilities*, vol. 26, no. 4, pp. 441–452, 2012.

[24] C. Furl, H. Sharif, J. W. Zeitler, A. El Hassan, and J. Joseph, "Hydrometeorology of the catastrophic Blanco River flood in South Texas, May 2015," *Journal of Hydrology: Regional Studies*, vol. 15, pp. 90–104, 2018.

[25] Texas Department of transportation, "RM 2900 Bridge Replacement in Kingsland," 2018. [Online]. Available: https://www.txdot.gov/projects/projects-studies/austin/rm2900-kingsland-bridge-replacement.html

[26] Victoria Mananan, "Post Road Bridge opens years after it was washed away in floods," 2017. [Online]. Available: https://spectrumlocalnews.com/tx/austin/news/2017/12/21/post-road-bridge-opens-years-after-it-was-washed-away-in-flood

[27] R. Nasouri, A. Matamoros, A. Montoya, and F. Testik, "Vulnerability of coastal bridges under extreme hurricane conditions," *Bridge Structures*, vol. 15, no. 3, pp. 89–101, 2019.

[28] F. Pervaiz, "Evaluation of ice loads on beitstadsundet bridge by deterministic and probabilistic approaches." Master's thesis, NTNU, 2019.

[29] M. Mirza, "Climate change, flooding in south asia and implications," *Regional environmental change*, vol. 11, no. 1, pp. 95–107, 2011.

[30] D. Swain, O. E. Wing, P. D. Bates, J. Done, K. Johnson, and D. Cameron, "Increased flood exposure due to climate change and population growth in the united states," *Earth's Future*, vol. 8, no. 11, p. e2020EF001778, 2020.

[31] M. Golian, A. Saffarzadeh, H. Katibeh, M. Mahdad, H. Saadat, M. Khazaei, E. Sametzadeh, A. Ahmadi, E. Sharifi Teshnizi, M. Samadi Darafshani, *et al.*, "Consequences of groundwater overexploitation on land subsidence in fars province of iran and its mitigation management programme," *Water and Environment Journal*, vol. 35, no. 3, pp. 975–985, 2021.

[32] K. E. Trenberth, "Changes in precipitation with climate change," *Climate research*, vol. 47, no. 1-2, pp. 123–138, 2011.

[33] K. E. Trenberth, A. Dai, R. M. Rasmussen, and D. B. Parsons, "The changing character of precipitation," *Bulletin of the American Meteorological Society*, vol. 84, no. 9, pp. 1205–1218, 2003.

[34] D. R. Easterling, K. E. Kunkel, J. R. Arnold, T. Knutson, A. N. LeGrande, L. R. Leung, R. S. Vose, D. E. Waliser, and M. F. Wehner, "Precipitation change in the United States," in *Climate Science Special Report: Fourth National Climate Assessment, Volume I*, D. J. Wuebbles, D. W. Fahey, K. A. Hibbard, D. J. Dokken, B. C. Stewart, and T. K. Maycock, Eds. U.S. Global Change Research Program, 2017.

[35] H. E. Willoughby, "Forecasting hurricane intensity and impacts," *Science*, vol. 315, no. 5816, pp. 1232–1233, 2007.

[36] K. Emanuel, "Assessing the present and future probability of hurricane harvey's rainfall," *Proceedings of the National Academy of Sciences*, vol. 114, no. 48, pp. 12 681–12 684, 2017.

[37] B. E. Montz, "The generation of flood hazards and disasters by urban development of floodplains," *Floods*, vol. 1, pp. 116–127, 2000.

[38] B. Feng, Y. Zhang, and R. Bourke, "Urbanization impacts on flood risks based on urban growth data and coupled flood models," *Natural Hazards*, vol. 106, no. 1, pp. 613–627, 2021.

[39] G. Zhao, H. Gao, and L. Cuo, "Effects of urbanization and climate change on peak flows over the san antonio river basin, texas," *Journal of Hydrometeorology*, vol. 17, no. 9, pp. 2371–2389, 2016.

[40] C. Pyke, M. P. Warren, T. Johnson, J. LaGro Jr, J. Scharfenberg, P. Groth, R. Freed, W. Schroeer, and E. Main, "Assessment of low impact development for managing stormwater with changing precipitation due to climate change," *Landscape and Urban Planning*, vol. 103, no. 2, pp. 166–173, 2011.

[41] F. Kong, Y. Ban, H. Yin, P. James, and I. Dronova, "Modeling stormwater management at the city district level in response to changes in land use and low impact development," *Environmental Modelling & Software*, vol. 95, pp. 132–142, 2017.

[42] G. A. Meehl, T. F. Stocker, W. D. Collins, P. Friedlingstein, A. T. Gaye, J. M. Gregory, A. Kitoh, R. Knutti, J. M. Murphy, A. Noda, S. C. Raper, I. G. Watterson, A. J. Weaver, and Z. C. Zhao, "Global climate projections. Chapter 10," in *Climate Change 2007: The Physical Science Basis. Contribution of Working Group I to the Fourth Assessment Report of the Intergovernmental Panel on Climate Change*, S. Solomon, D. Qin, M. Manning, Z. Chen, M. Marquis, K. Averyt, M. Tignor, and H. Miller, Eds. Cambridge University Press, 2007.

[43] S. Westra, H. J. Fowler, J. P. Evans, L. V. Alexander, P. Berg, F. Johnson, E. J. Kendon, G. Lenderink, and N. Roberts, "Future changes to the intensity and frequency of short-duration extreme rainfall," *Reviews of Geophysics*, vol. 52, no. 3, pp. 522–555, 2014.

[44] J. L. Rainey, S. D. Brody, G. E. Galloway, and W. E. Highfield, "Assessment of the growing threat of urban flooding: A case study of a national survey," *Urban Water Journal*, vol. 18, no. 5, pp. 375–381, 2021.

[45] A. Mondoro, D. M. Frangopol, and M. Soliman, "Optimal risk-based management of coastal bridges vulnerable to hurricanes," *Journal of Infrastructure Systems*, vol. 23, no. 3, p. 04016046, 2017.

[46] E. Batchabani, E. Sormain, and M. Fuamba, "Potential impacts of projected climate change on flooding in the Riviere des Prairies basin, Quebec, Canada: One-dimensional and two-dimensional simulation-based approach," *Journal of Hydrologic Engineering*, vol. 21, no. 12, p. 05016032, 2016.

[47] M. Pregnolato, A. O. Winter, D. Mascarenas, A. D. Sen, P. Bates, and M. R. Motley, "Assessing flooding impact to riverine bridges: an integrated analysis," *Natural Hazards and Earth System Sciences*, vol. 22, no. 5, pp. 1559–1576, 2022.

[48] A. Nasr, I. Björnsson, D. Honfi, O. Larsson Ivanov, J. Johansson, and E. Kjellström, "A review of the potential impacts of climate change on the safety and performance of bridges," *Sustainable and Resilient Infrastructure*, vol. 6, no. 3-4, pp. 192–212, 2021.

[49] A. Alipour, "Enhancing resilience of bridges to extreme events by rapid damage assessment and response strategies," *Transportation Research Record*, vol. 2604, no. 1, pp. 54–62, 2017.

[50] M. M. Flint, O. Fringer, S. L. Billington, D. Freyberg, and N. S. Diffenbaugh, "Historical analysis of hydraulic bridge collapses in the continental united states," *Journal of Infrastructure Systems*, vol. 23, no. 3, p. 04017005, 2017.

[51] L. Wright, P. Chinowsky, K. Strzepek, R. Jones, R. Streeter, J. B. Smith, J.-M. Mayotte, A. Powell, L. Jantarasami, and W. Perkins, "Estimated effects of climate change on flood vulnerability of us bridges," *Mitigation and Adaptation Strategies for Global Change*, vol. 17, no. 8, pp. 939–955, 2012.

[52] R. Bhatkoti, G. E. Moglen, P. M. Murray-Tuite, and K. P. Triantis, "Changes to bridge flood risk under climate change," *Journal of Hydrologic Engineering*, vol. 21, no. 12, p. 04016045, 2016.

[53] J. E. Neumann, J. Price, P. Chinowsky, L. Wright, L. Ludwig, R. Streeter, R. Jones, J. B. Smith, W. Perkins, L. Jantarasami, *et al.*, "Climate change risks to us infrastructure: impacts on roads, bridges, coastal development, and urban drainage," *Climatic Change*, vol. 131, no. 1, pp. 97–109, 2015.

[54] A. Khelifa, L. A. Garrow, M. J. Higgins, and M. D. Meyer, "Impacts of Climate Change on Scour-Vulnerable Bridges: Assessment Based on HYRISK," *Journal of Infrastructure Systems*, vol. 19, no. 2, pp. 138–146, 2013.

[55] Harris County, Texas, "Population Report, February 2018," 2018. [Online]. Available: https://budget.harriscountytx.gov/doc/Budget/fy2019/FY19_Population_Report.pdf

[56] Federal Emergency Management Agency, "Flood Insurance Study: Harris County, Texas and Incorporated Areas. FIS Number 48201CV001G," 2019. [Online]. Available: https://www.fema.gov/glossary/flood-insurance-study-fis

[57] G. J. Van Oldenborgh, K. Van Der Wiel, A. Sebastian, R. Singh, J. Arrighi, F. Otto, K. Haustein, S. Li, G. Vecchi, and H. Cullen, "Attribution of extreme rainfall from

Hurricane Harvey, August 2017," *Environmental Research Letters*, vol. 12, no. 12, p. 124009, 2017.

[58] A. Kiaghadi, A. Govindarajan, R. S. Sobel, and H. S. Rifai, "Environmental damage associated with severe hydrologic events: a LiDAR-based geospatial modeling approach," *Natural Hazards*, vol. 103, no. 3, pp. 2711–2729, 2020.

[59] M. Rusca, G. Messori, and G. Di Baldassarre, "Scenarios of human responses to unprecedented social-environmental extreme events," *Earth's Future*, vol. 9, no. 4, p. e2020EF001911, 2021.

[60] J. Nielsen-Gammon, J. Escobedo, C. Ott, J. Dedrick, and A. Van Fleet, "Assessment of historic and future trends of extreme weather in Texas, 1900-2036," 2020. [Online]. Available: https://oaktrust.library.tamu.edu/handle/1969.1/188618

[61] Cambridge Systamatics, *Central Texas Extreme Weather and Climate Change Vulnerability Assessment of Regional Transportation Infrastructure*. Austin, TX: Capital Area Metropolitan Planning Organization, 2015.

[62] Intergovernmental Panel on Climate Change, "IPCC Special Report: Emissions Scenarios, Summary for Policymakers," 2000. [Online]. Available: https://www.ipcc.ch/site/assets/uploads/2018/03/sres-en.pdf

[63] D. W. Pierce, D. R. Cayan, and B. L. Thrasher, "Statistical downscaling using localized constructed analogs (LOCA)," *Journal of Hydrometeorology*, vol. 15, no. 6, pp. 2558–2585, 2014.

[64] USACE, *HEC-HMS User's Manual Version 4.2*. Davis, CA: US Army Corps of Engineers, Hydrologic Engineering Center, 2016.

[65] W. H. Green and G. Ampt, "Studies on soil phyics." *The Journal of Agricultural Science*, vol. 4, no. 1, pp. 1–24, 1911.

[66] C. Clark, "Storage and the unit hydrograph," *Transactions of the American Society of Civil Engineers*, vol. 110, no. 1, pp. 1419–1446, 1945.

[67] V. Chow, *Handbook of Applied Hydrology*. New York: McGraw Hill, 1959.

[68] F. M. Henderson, *Open Channel Flow*. New York: Macmillan, 1996.

[69] USACE, *HEC-RAS User's Manual Version 5.0*. Davis, CA: US Army Corps of Engineers, Hydrologic Engineering Center, 2016.

[70] Federal Highway Administration, "Evaluating Scour at Bridges: Fifth Edition," Tech. Rep., 2012. [Online]. Available: https://www.fhwa.dot.gov/engineering/hydraulics/pubs/hif12003.pdf

[71] Texas Department of Transportation, "Scour Evaluation Guide," 2020. [Online]. Available: https://ftp.txdot.gov/pub/txdot-info/library/pubs/bus/bridge/scour-guide.pdf

[72] Federal Highway Administration, "National Bridge Inventory," 2022. [Online]. Available: https://www.fhwa.dot.gov/bridge/nbi.cfm

[73] D. Istrati, A. Hasanpour, and I. Buckle, "Numerical investigation of tsunami-borne debris damming loads on a coastal bridge," in *Proceedings of the 17 World Conference on Earthquake Engineering, Sendai, Japan*, vol. 27, 2020.

[74] F. Pervaiz and M. Hummel, "Evaluation of climate change and urbanization impacts on bridges in harris county, texas," in *World Environmental and Water Resources Congress 2022*, 2022, pp. 499–507.

[75] K. Oudenbroek, "Experimental research on hydrodynamic failure of river bridges on spread footings," 2018.

[76] A. Hasanpour, D. Istrati, and I. Buckle, "Coupled sph–fem modeling of tsunami-borne large debris flow and impact on coastal structures," *Journal of Marine Science and Engineering*, vol. 9, no. 10, p. 1068, 2021.

[77] F. Ashraf, H. Tyralis, and G. Papacharalampous, "Explaining the flood behavior for the bridge collapse sites," *Journal of Marine Science and Engineering*, vol. 10, no. 9, p. 1241, 2022.

[78] K. Wardhana and F. C. Hadipriono, "Analysis of recent bridge failures in the united states," *Journal of performance of constructed facilities*, vol. 17, no. 3, pp. 144–150, 2003.

[79] G. C. Lee, S. Mohan, C. Huang, and B. N. Fard, *A study of US bridge failures (1980-2012)*. MCEER Buffalo, NY, 2013.

[80] C. Montalvo, W. Cook, and T. Keeney, "Retrospective analysis of hydraulic bridge collapse," *Journal of Performance of Constructed Facilities*, vol. 34, no. 1, p. 04019111, 2020.

[81] S. Malavasi and A. Guadagnini, "Hydrodynamic loading on river bridges," *Journal of Hydraulic Engineering*, vol. 129, no. 11, pp. 854–861, 2003.

[82] J. Guo, D. M. Admiraal, and T. C. Zhang, "Computational design tool for bridge hydrodynamic loading in inundated flows of midwest rivers," 2010.

[83] C.-R. Chu, C.-H. Chung, T.-R. Wu, and C.-Y. Wang, "Numerical analysis of free surface flow over a submerged rectangular bridge deck," *Journal of Hydraulic Engineering*, vol. 142, no. 12, p. 04016060, 2016.

[84] K. Oudenbroek, N. Naderi, J. D. Bricker, Y. Yang, C. Van der Veen, W. Uijttewaal, S. Moriguchi, and S. N. Jonkman, "Hydrodynamic and debris-damming failure of bridge decks and piers in steady flow," *Geosciences*, vol. 8, no. 11, p. 409, 2018.

[85] H. Chanson, "Turbulent air–water flows in hydraulic structures: dynamic similarity and scale effects," *Environmental fluid mechanics*, vol. 9, no. 2, pp. 125–142, 2009.

[86] W. Anderson, P. Huber, and A. Sonin, "Small scale modeling of hydrodynamic forces in pressure suppression systems. final report.[bwr]," Massachusetts Inst. of Tech., Cambridge (USA). Dept. of Mechanical Engineering, Tech. Rep., 1977.

[87] G. Vaz, D. Hally, T. Huuva, N. Bulten, P. Muller, P. Becchi, J. Herrer, S. Whitworth, R. Macé, and A. Korsström, "Cavitating flow calculations for the e779a propeller in open water and behind conditions: code comparison and solution validation," in

Proceedings of the 4th International Symposium on Marine Propulsors, Austin, TX, USA, vol. 31, 2015.

[88] K. Matsuda, K. Cooper, H. Tanaka, M. Tokushige, and T. Iwasaki, "An investigation of reynolds number effects on the steady and unsteady aerodynamic forces on a 1: 10 scale bridge deck section model," *Journal of Wind Engineering and Industrial Aerodynamics*, vol. 89, no. 7-8, pp. 619–632, 2001.

[89] American Association of State Highway and Transportation Officials, "AASHTO LRFD Bridge Design Specifications," 2017. [Online]. Available: https://www.transportation.org/

[90] M. M. Lwin, W. P. Yen, and J. J. Shen, "Effects of hurricane katrina on the performance of us highway bridges," *Journal of Performance of Constructed Facilities*, vol. 28, no. 1, pp. 40–48, 2014.

[91] M. Bozorgnia, *Computational fluid dynamic analysis of highway bridge superstructures exposed to hurricane waves*. University of Southern California, 2012.

[92] G. Zhang, J.-i. Hoshikuma, and T. Usui, "An experimental study on countermeasure for mitigating tsunami effect on highway bridge," 2012.

[93] G. Chen, E. C. Witt III, D. Hoffman, R. Luna, and A. Sevi, "Analysis of the interstate 10 twin bridge's collapse during hurricane katrina," *Science and the Storms: The USGS Response to the Hurricanes of*, pp. 35–42, 2005.

[94] City of Austin, "Model and Map Management System," 2019. [Online]. Available: https://www.austintexas.gov/page/floodplain-regulations

[95] S. M. I. Kabir, H. Ahmari, and M. Dean, "Experimental study to investigate the effects of bridge geometry and flow condition on hydrodynamic forces," *Journal of Fluids and Structures*, vol. 113, p. 103688, 2022.

[96] H. Ahmari, M. Hummel, S.-H. S. Chao, S. M. I. Kabir, F. Pervaiz, B. R. Acharya, M. Dean, and Q. A. Mowla, "Identify and analyze inundated bridge superstructures in high velocity flood events," Tech. Rep., 2021.

[97] H. Medina, A. Beechook, J. Saul, S. Porter, S. Aleksandrova, and S. Benjamin, "Open source computational fluid dynamics using openfoam," in *Royal Aeronautical Society, General Aviation Conference, London*, 2015.

[98] U. Manual, "Ansys fluent 21.0," *Theory Guide*, 2021.

[99] W. F. Noh and P. Woodward, "Slic (simple line interface calculation)," in *Proceedings of the fifth international conference on numerical methods in fluid dynamics June 28–July 2, 1976 Twente University, Enschede*. Springer, 1976, pp. 330–340.

[100] B. Nichols, C. Hirt, and R. Hotchkiss, "Volume of fluid (vof) method for the dynamics of free boundaries," *J. Comput. Phys*, vol. 39, pp. 201–225, 1981.

[101] D. C. Wilcox, "Formulation of the kw turbulence model revisited," *AIAA journal*, vol. 46, no. 11, pp. 2823–2838, 2008.

[102] N. D. Katopodes, "Volume of fluid method," *Free-Surface Flow*, pp. 766–802, 2019.

[103] A. Califano and S. Steen, "Numerical simulations of a fully submerged propeller subject to ventilation," *Ocean engineering*, vol. 38, no. 14-15, pp. 1582–1599, 2011.

[104] S.-C. Xue, N. Phan-Thien, and R. Tanner, "Three dimensional numerical simulations of viscoelastic flows through planar contractions," *Journal of Non-Newtonian Fluid Mechanics*, vol. 74, no. 1-3, pp. 195–245, 1998.

[105] A. K. Runchal, "Brian spalding: Cfd & reality," in *Proceedings of CHT-08 ICHMT International Symposium on Advances in Computational Heat Transfer*. Begel House Inc., 2008.

[106] R. Courant, E. Isaacson, and M. Rees, "On the solution of nonlinear hyperbolic differential equations by finite differences," *Communications on pure and applied mathematics*, vol. 5, no. 3, pp. 243–255, 1952.

[107] A. Fluent, "18.0 ansys fluent theory guide 18.0," *Ansys Inc*, 2017.

[108] C. Zhang, G. Gholipour, and A. A. Mousavi, "State-of-the-art review on responses of rc structures subjected to lateral impact loads," *Archives of Computational Methods in Engineering*, vol. 28, no. 4, pp. 2477–2507, 2021.

[109] N. Ataei, *Vulnerability assessment of coastal bridges subjected to hurricane events*. Rice University, 2013.

[110] A. Guo, Q. Fang, X. Bai, and H. Li, "Hydrodynamic experiment of the wave force acting on the superstructures of coastal bridges," *Journal of Bridge Engineering*, vol. 20, no. 12, p. 04015012, 2015.

[111] M.-M. Dickey, *Wave forces on bridges*. Mississippi State University, 2008.

[112] S. L. Douglass, B. M. Webb, R. Kilgore, and C. Keenan, "Highways in the coastal environment: Assessing extreme events," United States. Federal Highway Administration, Tech. Rep., 2014.

[113] M. Shirzaei and R. Bürgmann, "Global climate change and local land subsidence exacerbate inundation risk to the san francisco bay area," *Science advances*, vol. 4, no. 3, p. eaap9234, 2018.

[114] R. J. Nicholls and A. Cazenave, "Sea-level rise and its impact on coastal zones," *science*, vol. 328, no. 5985, pp. 1517–1520, 2010.

[115] S. Lim, D. Popov, N. Raza, F. Pervaiz, and M. Al-Qadi, "Feasibility study of submerged floating crossing," 2018.

[116] S. L. Douglass, S. Hughes, S. Rogers, and Q. Chen, "The impact of hurricane ivan on the coastal roads of florida and alabama: A preliminary report," *Rep. to Coastal Transportation Engineering Research and Education Center, Univ. of South Alabama, Mobile, Ala*, pp. 1–19, 2004.

[117] W. Nickas, R. Renna, N. Sheppard, and D. Mertz, "Hurricane-based wave attacks," *Florida Dept. of Transportation, Tallahassee, Fla*, 2005.

[118] B. R. Seiffert, *Tsunami and storm wave impacts on coastal bridges*. University of Hawai'i at Manoa, 2014.

[119] Q. Chen, L. Wang, and H. Zhao, "Hydrodynamic investigation of coastal bridge collapse during hurricane katrina," *Journal of Hydraulic Engineering*, vol. 135, no. 3, pp. 175–186, 2009.

[120] T. Schumacher, C. Higgins, C. Bradner, D. Cox, and S. C. Yim, "Large-scale wave flume experiments on highway bridge superstructures exposed to hurricane wave forces," in *Sixth National Seismic Conference on Bridges and HighwaysMultidisciplinary Center for Earthquake Engineering ResearchSouth Carolina Department of TransportationFederal Highway AdministrationTransportation Research Board*, 2008.

[121] R. L. McPherson, "Hurricane induced wave and surge forces on bridge decks," Ph.D. dissertation, Texas A & M University, 2010.

[122] M. Hayatdavoodi, B. Seiffert, and R. C. Ertekin, "Experiments and computations of solitary-wave forces on a coastal-bridge deck. part ii: Deck with girders," *Coastal Engineering*, vol. 88, pp. 210–228, 2014.

[123] B. Huang, B. Zhu, S. Cui, L. Duan, and J. Zhang, "Experimental and numerical modelling of wave forces on coastal bridge superstructures with box girders, part i: Regular waves," *Ocean Engineering*, vol. 149, pp. 53–77, 2018.

[124] Q. Fang, R. Hong, A. Guo, and H. Li, "Experimental investigation of wave forces on coastal bridge decks subjected to oblique wave attack," *Journal of Bridge Engineering*, vol. 24, no. 4, p. 04019011, 2019.

[125] D. Zhu and Y. Dong, "Experimental and 3d numerical investigation of solitary wave forces on coastal bridges," *Ocean Engineering*, vol. 209, p. 107499, 2020.

[126] B. Meng, *Calculation of extreme wave loads on coastal highway bridges*. Texas A&M University, 2008.

[127] S. An and O. M. Faltinsen, "Linear free-surface effects on a horizontally submerged and perforated 2d thin plate in finite and infinite water depths," *Applied Ocean Research*, vol. 37, pp. 220–234, 2012.

[128] R. C. Ertekin, M. Hayatdavoodi, and J. W. Kim, "On some solitary and cnoidal wave diffraction solutions of the green–naghdi equations," *Applied Ocean Research*, vol. 47, pp. 125–137, 2014.

[129] B. R. Seiffert, M. Hayatdavoodi, and R. C. Ertekin, "Experiments and calculations of cnoidal wave loads on a coastal-bridge deck with girders," *European Journal of Mechanics-B/Fluids*, vol. 52, pp. 191–205, 2015.

[130] K. A. Anarde, S. Kameshwar, J. N. Irza, J. A. Nittrouer, J. Lorenzo-Trueba, J. E. Padgett, A. Sebastian, and P. B. Bedient, "Impacts of hurricane storm surge on infrastructure vulnerability for an evolving coastal landscape," *Natural Hazards Review*, vol. 19, no. 1, p. 04017020, 2018.

[131] A. Montoya, A. Matamoros, F. Testik, A. Shahriar, R. Nasouri, A. Majlesi, *et al.*, "Structural vulnerability of coastal bridges under extreme hurricane conditions," Transportation Consortium of South-Central States, Tech. Rep., 2019.

[132] G. P. Balomenos, S. Kameshwar, and J. E. Padgett, "Parameterized fragility models for multi-bridge classes subjected to hurricane loads," *Engineering Structures*, vol. 208, p. 110213, 2020.

[133] D. Zhu, Y. Li, and Y. Dong, "Reliability-based retrofit assessment of coastal bridges subjected to wave forces using 3d cfd simulation and metamodeling," *Civil Engineering and Environmental Systems*, vol. 38, no. 1, pp. 59–83, 2021.

[134] J. W. Miles, "The korteweg-de vries equation: a historical essay," *Journal of fluid mechanics*, vol. 106, pp. 131–147, 1981.

[135] J. Bosboom and M. J. Stive, "Coastal dynamics," 2021.

[136] Y.-J. Jeong, M.-S. Park, J. Kim, and S.-H. Song, "Wave force characteristics of large-sized offshore wind support structures to sea levels and wave conditions," *Applied Sciences*, vol. 9, no. 9, p. 1855, 2019.

[137] F. McKenna, G. Fenves, F. Filippou, S. Mazzoni, M. Scott, A. Elgamal, Z. Yang, J. Lu, P. Arduino, and P. McKenzie, "Opensees," *University of California, Berkeley: nd*, 2010.

[138] L. TxDOT, "Bridge design manual," 2021.

[139] J. D. Sipple and M. Sanayei, "Full-scale bridge finite-element model calibration using measured frequency-response functions," *Journal of Bridge Engineering*, vol. 20, no. 9, p. 04014103, 2015.

[140] N. Ataei, M. Stearns, and J. E. Padgett, "Response sensitivity for probabilistic damage assessment of coastal bridges under surge and wave loading," *Transportation Research Record*, vol. 2202, no. 1, pp. 93–101, 2010.

[141] T. Huff, *LRFD Bridge Design: Fundamentals and Applications*. CRC Press, 2022.

[142] M. Yuan, "Lateral displacement of reinforced concrete frame buildings," Ph.D. dissertation, The Ohio State University, 2014.

[143] G. A. Tutuianu, "Peak vertical floor accelerations of tall steel structures," Ph.D. dissertation, University of New Hampshire, 2019.

[144] Frank McKenna, Sang-ri Yi, Aakash Bangalore Satish, Adam Zsarnoczay, Michael Gardner, Kuanshi Zhong, Wael Elhaddad, "NHERI-SimCenter/quoFEM: Version 3.0.0 (v3.0.0). Zenodo: DOI: 10.5281/zenodo.6404498," 2022. [Online]. Available: https://simcenter.designsafe-ci.org/research-tools/quofem-application/

[145] Gregory G. Deierlein, Frank McKenna, Adam Zsarnóczay, Tracy Kijewski-Correa, Ahsan Kareem, Wael Elhaddad, Laura Lowes, Matt J. Schoettler, and Sanjay Govindjee, "A Cloud-Enabled Application Framework for Simulating Regional-Scale Impacts of Natural Hazards on the Built

Environment." 2020. [Online]. Available: FrontiersintheBuiltEnvironment.6: 558706.DOI:10.3389/fbuil.2020.558706

[146] B. Adams, W. Bohnhoff, K. Dalbey, M. Ebeida, J. Eddy, M. Eldred, R. Hooper, P. Hough, K. Hu, J. Jakeman, *et al.*, "Dakota, a multilevel parallel object-oriented framework for design optimization, parameter estimation, uncertainty quantification, and sensitivity analysis: Version 6.13 user's manual." Sandia National Lab.(SNL-NM), Albuquerque, NM (United States), Tech. Rep., 2020.

[147] J. Jcss, "Probabilistic model code: Joint committee on structural safety," *JCSS, Japan*, 2001.

[148] S. Kameshwar and J. E. Padgett, "Multi-hazard risk assessment of highway bridges subjected to earthquake and hurricane hazards," *Engineering Structures*, vol. 78, pp. 154–166, 2014.

[149] A. Sofistik, "Sofistik manual," 2017.

[150] M. Gordini, M. Habibi, M. Tavana, M. TahamouliRoudsari, and M. Amiri, "Reliability analysis of space structures using monte-carlo simulation method," in *Structures*, vol. 14. Elsevier, 2018, pp. 209–219.

[151] J. B. Cardoso, J. R. de Almeida, J. M. Dias, and P. G. Coelho, "Structural reliability analysis using monte carlo simulation and neural networks," *Advances in Engineering Software*, vol. 39, no. 6, pp. 505–513, 2008.

[152] S. Jonkman, R. Steenbergen, O. Morales-Nápoles, A. Vrouwenvelder, and J. Vrijling, "Probabilistic design: risk and reliability analysis in civil engineering," *Collegedictaat CIE4130*, 2015.

[153] O. Aladegboye, D. Opeyemi, O. Atoyebi, S. Akingbonmire, and E. Ibitogbe, "Reliability analysis of reinforced concrete beam using varying properties," in *IOP Conference Series: Earth and Environmental Science*, vol. 445, no. 1. IOP Publishing, 2020, p. 012031.

[154] M. A. Grubb, K. E. Wilson, C. D. White, W. N. Nickas, *et al.*, "Load and resistance factor design (lrfd) for highway bridge superstructures-reference manual," National Highway Institute (US), Tech. Rep., 2015.

[155] R. N. Wright and W. H. Walker, "Criteria for the deflection of steel bridges," 1971.

[156] E. Cen, "1: Actions on structures-part 2: Traffic loads on bridges," *Nen-en*, vol. 30, pp. 1991–2, 2003.

[157] F. Nateghi and V. L. Shahsavar, "Development of fragility and reliability curves for seismic evaluation of a major prestressed concrete bridge," in *The 13th World Conference on Earthquake Engineering, Paper*, no. 1351, 2004.

[158] M. Shinozuka, M. Grigoriu, A. R. Ingraffea, S. L. Billington, P. Feenstra, T. T. Soong, A. M. Reinhorn, and E. Maragakis, "Development of fragility information for structures and nonstructural components," *MCCER2000*, 2000.

[159] L. Liu, X. Yang, B. Yan, and S. Miao, "Dynamic responses of rc girder bridge under heavy truck and seismic loads combined," *Sustainability*, vol. 14, no. 15, p. 9263, 2022.

[160] I. Qeshta, "Fragility and resilience of bridges subjected to extreme wave-induced forces," Ph.D. dissertation, RMIT University, 2019.

[161] A. Saeidpour, M. G. Chorzepa, J. Christian, and S. Durham, "Probabilistic hurricane risk analysis of coastal bridges incorporating extreme wave statistics," *Engineering Structures*, vol. 182, pp. 379–390, 2019.